Non-equilibrium Disordering Processes in Binary Systems due to an Active Agent

Wannapong Triampo

Dissertation submitted to the Faculty of the Virginia Polytechnic Institute and State University in partial fulfillment of the requirements for the degree of

DOCTOR OF PHILOSOPHY
in
PHYSICS

APPROVED:

B. Schmittmann, Chair

R.K.P. Zia

A. L. Ritter

R. Heflin

U. Tauber

April, 2001
Blacksburg, Virginia

Keywords: Ising model, Random walk, Non-equilibrium processes, Brownian motion, Vacancy-mediated dynamics, Disordering processes, Mean-field theory, Dynamic scaling, Monte Carlo, Data corruption.

Non-equilibrium Disordering Processes in Binary Systems due to an Active Agent

Wannapong Triampo

(ABSTRACT)

In this thesis, we study the kinetic disordering of systems interacting with an agent or a walker. Our studies divide naturally into two classes: for the first, the dynamics of the walker conserves the total magnetization of the system, for the second, it does not. These distinct dynamics are investigated in part I and II respectively.

In part I, we investigate the disordering of an initially phase-segregated binary alloy due to a highly mobile vacancy which exchanges with the alloy atoms. This dynamics clearly conserves the total magnetization. We distinguish three versions of dynamic rules for the vacancy motion, namely a pure random walk , an "active" and a biased walk. For the random walk case, we review and reproduce earlier work by Z. Toroczkai et. al., [9] which will serve as our base-line. To test the robustness of these findings and to make our model more accessible to experimental studies, we investigated the effects of finite temperatures ("active walks") as well as external fields (biased walks). To monitor the disordering process, we define a suitable disorder parameter, namely the number of broken bonds, which we study as a function of time, system size and vacancy number. Using Monte Carlo simulations and a coarse-grained field theory, we observe that the disordering process exhibits three well separated temporal regimes. We show that the later stages exhibit dynamic scaling, characterized by a set of exponents and scaling functions. For the random and the biased case, these exponents and scaling functions are computed analytically in excellent agreement with the simulation results. The exponents are remarkably universal. We conclude this part with some comments on the early stage, the interfacial roughness and other related features.

In part II, we introduce a model of binary data corruption induced by a Brownian agent or random walker. Here, the magnetization is not conserved, being related to the density of corrupted bits ρ. Using both continuum theory and computer simulations, we study the average density of corrupted bits, and the associated density-density correlation function, as well as several other related quantities. In the second half, we extend our investigations in three main directions which allow us to make closer contact with real binary systems. These are i) a detailed analysis of two dimensions, ii) the case of competing agents, and iii) the cases of asymmetric and quenched random couplings. Our analytic results are in good agreement with simulation results. The remarkable finding of this study is the robustness of the phenomenological model which provides us with the tool, continuum theory, to understand the nature of such a simple model.

In loving memory of
Patcharee (Ann) Hensirisak
You are always in my heart and soul.

Acknowledgment

When it came down to the final stage of writing this dissertation, I came to realize that this part is the most valuable part for me and the part that I would like to write the most because it would come out from my heart, not my head like the rest. The best of all is that it gives me an opportunity to say thanks and express my appreciation to the people who are behind this work.

My warmest thanks go to my fianceé, Patcharee (Ann) Hensirisak who supported and encouraged my work and my ownself from the beginning when we met ten years ago until the moment she passed away. I sadly dedicate this work to her who instilled in me the desire to better myself through learning. She did everything she could to complete me and always gave me her unwavering love. Especially, I am grateful so much to her for always being there for me, both enjoying the ups and helping to endure the downs. It is her love and her heart that always kept me going.

I am especially grateful to my thesis advisor Prof. Beate Schmittmann for introducing and teaching me non-equilibrium statistical physics, as well as for her guidance, inspiration, and invaluable contributions throughout this research project. Her expert advice has helped me considerably to improve my physics skills to become a better scientist, and her scholarly influence on my professional career certainly extends beyond this Ph.D. dissertation.

I am thankful to Prof. R.K.P. Zia with whom I had fruitful discussions when we had the chance to talk physics. He also helped me through difficult stages, especially when I first started my research and my advisor was on sabbatical leave.

I am indebted to other members of my committee, Prof. R. Heflin whose valuable graduate course on quantum electronics I was fortunate to attend, Prof. A.L. Ritter with whom I had a very joyful time working as a TA of the solid state course, and Prof. U. Tauber who helped to open up my physics world constantly by asking interesting questions in seminars.

I would like to thank a great friend and colleague of mine, Prof. T.J. Newman. He patiently baby-sat me through the second and third years of my research. He has earned my special thanks for inspiring me to love research. He maintains a level of vigor and excitement in physics which always lifted up my physics spirits. With him, tomorrow has always an adventure for me.

I deeply appreciate Chris Thomas, physics department's secretary, who has helped me with graduate student matters, and who supported me in going through many difficult times of my life. She deserves a lot of credit for helping me to understand the value of the human being. She has played a role in my life which goes beyond the duties of her position.

I am thankful for Robert Astalos, a very good friend and much more. Because of him, helping to raise funds for my fianceé to get the cancer treatment, it helped me greatly to have more time to stay with her which I consider one of the best gift, I ever received and it inspired me greatly.

I thank Timo Aspelmeier, a good friend and colleague with whom I had very fruitful discussions and who also kindly read the first part of this dissertation and made some good comments.

There are some post-docs and physics graduate fellows who contributed to my understanding in physics through long discussions. Those who deserve special note are Irina Mazilu, Zoltan Toroczkai, Will Loinaz as well as, Martin Howard.

I owe and acknowledge the opportunity provided and financial support of the Royal Thai government and Thai citizens. With the training and experience I received here, I definitely will return to them all the knowledge and know-how as much as I can.

I thank Roger Link for managing to keep us on-line and for helping me solve the computer-related problems from time to time.

I thank many other members of physics Department for providing a pleasant and educational environment for my graduate studies.

I would like to express my appreciation to my former teachers and friends in Thailand who helped me to start graduate studies and showed interest in my development while I was away.

And finally again, I deeply thanks the most important person in my life, my fianceé, for her endless love and care-giving. She always wished for me to be the best human being that i could be and had such a big impact on my life. Without her, I would not have come this far. I wish and believe that she is looking down to me from heaven and still is and will be my guardian angel for ever.

Contents

Chapter 1

Introduction

Brownian motion is one of the fundamental processes in Nature. It was originally observed in the irregular motion of pollen grains by the botanist Brown [1], and cast into the language of the diffusion equation by Einstein [2]. It has been applied to an enormous variety of processes in the mathematical framework of random walks [3]. A very rich field of research has been built around the behavior of a random walk coupled to a disordered environment [4], a good example being the anomalous diffusion of electrons in a disordered medium [5]. Also, one can consider a random walker, i.e. some type of defect, *being* the disordering agent in its environment. Applications of the latter include the tagged diffusion of atoms in a crystal [6, 7, 8], magnetic disordering mediated by wandering vacancies [9].

Motivated by the important role of such processes for real systems, we shall study some specific models for the interactions between the walker and its environment, namely how a system disorders when its kinetics is mediated by different kinds of walkers: Brownian random walkers as well as their "cousins" including biased and active walkers (the latter being controlled by energetic "feedback" from the environment). We should stress, of course, that our studies touch on just a few of the myriad of systems in which a walker interacts in some way with its environment. Depending on the dynamics which we implement, our models either respect or violate the conservation of total magnetization (CTM). We use this terminology intentionally, in analogy to the classification of dynamic critical phenomena. In this thesis we shall study two classes of systems, with and without CTM, which shall be considered in part I and II respectively.

In the first part, we investigate the disordering of an initially phase-segregated interacting binary alloy, due to a highly mobile vacancy. The kinetics of binary alloys, undergoing mixing or segregation processes, represents a venerable problem in the physics and materials science communities. A very rich field of research has resulted, studying this problem extensively [10]. Much attention has been drawn to the dynamics of phase ordering and domain growth, as a system is rapidly quenched below its ordering temperature or the coexistence curve. Starting from an initial non-equilibrium configuration, the system evolves towards its final equilibrium state, giving rise to fundamental questions: Crucial to metallurgy, the domain morphology is intimately linked to structural stability, while statistical physics focuses on the universal, self-similar aspects of its temporal evolution, manifested in characteristic growth exponents and dynamic scaling.

Specifically, the temporal growth of ordered domains, as measured, e.g., via a time-dependent structure factor, exhibits universal features, such as characteristic growth exponents and dynamic scaling, in remarkable analogy to critical phenomena.

A key ingredient in the study of these processes is the mechanism by which two particles exchange positions. From the viewpoint of modeling and simulation purposes, *direct* particle-particle exchanges obviously lead to the simplest codes and coarse-grained equations. Moreover, invoking universality, it is expected that the details of the microscopic mechanisms do not affect large-wavelength, long-time properties, such as growth exponents and universal scaling functions. In this spirit, Kawasaki dynamics and the Cahn-Hilliard equation have been extensively used to describe phase ordering in binary alloys. However, in most real solids, microscopic atom-atom exchanges can be mediated by a variety of processes [11], with direct exchanges playing a rather small role since steric hindrance tends to create large energy barriers. It is much more common for atoms to move through the lattice by jumping to vacant or interstitial sites, i.e., these mechanisms involve exchanges with defects. Since the vacancies are located at the sites of the underlying lattice and are always present with a given (temperature-dependent) concentration, binary alloys have often been modeled by three-state models [12]. Two problems in particular have attracted considerable attention: first, the effect of vacancies on phase separation and domain growth [13, 14], and second, their role in atomic interdiffusion [15, 16]. A number of studies have also addressed vacancy-mediated ordering in a variety of *antiferromagnetic* alloys [17], as well as surface modes of unstable droplets in a stable vapor phase [18].

Here, we will describe a third aspect of defect-mediated dynamics, namely, the "inverse" of the phase ordering problem. Instead of studying the growth of order in response to a sudden temperature decrease (a "quench"), we focus on the *disordering* of a finite system, following a rapid *increase* in temperature. In the spirit of domain growth studies, we will seek to identify any universal features in the time evolution of the system, such as dynamic scaling controlled by characteristic exponents. Starting with a zero-temperature ferromagnetic configuration, i.e., a perfectly phase-segregated system with sharp interfaces, we monitor how interfaces "roughen" and how particles of one species are transported into regions dominated by the other species. The evolution process terminates when the system reaches its final state, characterized by a much higher degree of disorder than the initial one.

The complete or partial mixing of two materials at an interface plays a key role in many physical processes, such as corrosion or erosion phenomena [19]. We mention just two applications with huge technological potential for device fabrication. The first concerns nanowire etching by electron beam lithography [21]: If a thin film of platinum is deposited on a silicon wafer, interdiffusion of Pt and Si produces a mixing layer. If this layer is heated locally by, e.g., exposure to a conventional electron beam, silicides, such as Pt_2Si and PtSi, form. The unexposed platinum can subsequently be etched away, leaving conducting nanoscale structures behind. The second example concerns mesoscopic superlattice structures, consisting of alternating magnetic and non-magnetic metallic layers. If adjacent magnetic layers couple antiferromagnetically, the application of a large uniform magnetic field to these layered structures results in giant magnetoresistance [22]. However, the performance of these devices requires precisely engineered layer thicknesses and interfaces, and can be significantly affected by disorder [23], including interdiffusion or interfacial fluctuations.

In the second part, we consider a class of dynamics which violates CTM. Again, a Brownian agent (BA) diffuses through a binary medium; however, in contrast to the studies reported in part 1, encounters of the agent with a background element *change* the state of the latter. Although this model is interesting in its own right, we also believe it will have useful applications. Hence we can consider the environment to be composed of binary data (our favored realization), magnetic spins, chemical species A and B, and so on. As the BA wanders through the environment it has a certain probability to switch the value of an element in its immediate vicinity and it is not affected by the environment in any way. Thus, if we start with a system in which all elements exist in the same state ('up' say), and introduce the BA at the origin, then after some time, there will be a region around the origin in which the elements will be found in a mixture of 'up' and 'down' states. We once again want to emphasize that here the total number of 'up' and 'down' are not conserved. Naturally, the linear size of the region will grow on average as $\sqrt{t}$. The more subtle question concerns the degree of disordering which exists for elements within this region, and also their spatial correlations. As we shall see, the statistics of the disordered elements are very rich. This is most convincingly demonstrated by the dominance of extreme fluctuations; for instance, the distribution of disordered elements is log-normal. Thus, typical and average events are quite distinct, and become more so as time proceeds.

We would like to end this section with a few words about the potential relevance of this system to data corruption. With the advent of semiconductor memories (for dynamic random access memories (DRAM's) and various types of read only memories (ROM's)), there has been a tremendous drive within the semiconductor industry to produce ever-smaller memory devices [40, 41]. There are many properties (*e.g.* stability, power consumption, volatility, and cost) which must be balanced in the design of such devices. These factors determine the type of material used, and the geometry, dimension and architecture of the device. (For instance, three dimensional arrays have a very efficient address structure, and are stable against interference from bombarding alpha particles, but are very expensive to produce [40].) One of the main issues is the stability, or reliability, of the device. In semiconductor memories, there are many physical effects which can create hard errors (destruction or corruption of the device itself) or soft errors (corruption of the data stored in the device). In the latter category, the most common problems originate from electron clouds caused by alpha particles, but soft errors may also arise from electromigration and charge diffusion [42]. The key point is that different corruption mechanisms operate on different time scales (leading to the famous bath-tub curve of device reliability [41]). It is therefore important to know on what time-scales one should expect significant corruption from a given process. The model we propose here (namely data corruption via a BA) is probably not relevant for today's semiconductor devices, since there are so many 'mesoscopic' processes occurring on the level of a flip-flop, that subtle correlations due to a BA will be washed out. However, we can look ahead to the new generation of (quantum) storage devices, in which a single electron (controlled in a gate via coulomb blockade) can store one bit of data. In this case, a microscopic BA may indeed play an important role in data corruption, and it will be necessary to understand its time-scales and efficacy of operation, so that we can minimize its influence. This work constitutes a first step towards gaining such an understanding.

Part I

The System with Conservation of Total Magnetization

Chapter 2

Introduction and Outline

In this part, we describe our studies of systems satisfying CTM. [1]. We focus on the *disordering* of a finite system, starting with a zero-temperature ferromagnetic - i.e., perfectly phase-segregated - configuration. Several questions emerge quite naturally: Are there characteristic time scales on which the disordering takes place, and how do they depend on system size, temperature and other control parameters? How do local density profiles and correlation functions evolve with time? Are there any scaling regimes, and what are the appropriate scaling variables? How do these features respond to changes in the relative concentrations of vacancies and alloy components?

In the following, we address some of these questions in simple models for defect-mediated interface destruction and bulk disordering. We consider a symmetric (Ising-like) binary alloy of A and B atoms which is diluted by a very small number of vacancies (defects), reflecting the minute vacancy concentrations (of the order of 10^{-5}) found in most real systems. Following an up-quench from *zero* to a *higher* temperature T, the vacancies act as "catalysts" for the disordering process, exchanging with neighboring particles according to the usual energetics of the (dilute) Ising model. The particles themselves form a passive background whose dynamics is slaved to the defect motion. Thus, this system corresponds to a real material in which the characteristic time scale for vacancy diffusion is much faster than the ordinary bulk diffusion time. While vacancies are typically distributed uniformly in the bulk, certain defects may prefer to accumulate at the interfaces. Thus, the number of defects is not necessarily extensive in system size.

While we allow for some variation in the vacancy number, we consider equal concentrations of A and B atoms. Thus, our work forms a natural complement to the only other study [20] of vacancy-mediated disordering in the literature. There, the alloy composition is chosen to be highly asymmetric: 95% of A atoms versus only 5% for the B species, with a single vacancy. Thus, the A atoms form a *matrix* for a B-*precipitate*. The alloy is first equilibrated at a very low temperature, so that small clusters of B atoms are present. It is then rapidly heated to a higher temperature, and the number and size of B clusters are monitored. Three different scenarios are observed, depending on whether the final temperature is below the miscibility gap, above the miscibility gap but below T_c, or above T_c. In the first case, the precipitates remain compact. They dissolve

[1] The work in this part has been done in collaboration with B. Schmittmann, R.K.P. Zia and T. Aspelmeier

partially at first, but then equilibrate again by coarsening. In the second case, the precipitates also remain compact but eventually dissolve completely, mostly through "evaporation" from their surfaces. In the third case, the clusters decompose rapidly ("explode") into a large number of small fragments which then disappear diffusively.

While motivated by potential applications to the next generation of nano-devices, our study can only form a baseline here, for further work on more realistic models. However, it also has some rather fundamental implications. First, it serves as a testing ground for a basic problem in statistical physics, namely, how a system approaches its final steady state, starting from an initial *non-stationary* configuration. A second view of our study addresses the effect of a random walker (the vacancy) on its background medium. The vacancy explores a lattice filled with particles of two species, labelled as "black" and "white", or "up" and "down" spins, and each of its moves rearranges the background atoms slightly, leaving a trail behind like a child running across a sandy beach. In the simplest case, the walker is purely Brownian. In our language, this corresponds to an upquench to infinite temperature, $T = \infty$, where energy barriers are completely irrelevant. In this case, there is no feedback from the background to the local motion of the vacancy. Nevertheless, each displaced atom displays its own intriguing dynamics [7, 24, 9]. The key results for this simplest case [9], which will be briefly reviewed in chapter 3, form the basis for our studies: Starting from a perfectly phase-segregated state, three distinct temporal regimes are observed, separated by two crossover times. During the late stages of this process, the number of broken bonds exhibits dynamic scaling, characterized by a set of exponents and a scaling function. A mean-field theory allows for the analytic calculation of these features, in excellent agreement with simulations [9]. Rigorous continuum calculations are also performed in Ref.[8]. Also, the structure factors of this model have been studied in [25].

In order to make the above model more realistic, we extend these investigations to a system heated to *finite* temperature, as detailed in chapter 3. Since the background affects the vacancy through the local energetics associated with the next move, only approximate solutions of the mean-field equations can be found [51]. Here, we will report progress relying on simulations. Again, we observe *three* distinct temporal regimes, separated by two crossover times, provided the final temperature is not too close to T_c. The *intermediate and late* stages of the disordering process exhibit dynamic scaling. Characteristic exponents are measured by computer simulations and scaling functions are conjectured. For the system sizes considered here, a clear breakdown of these scaling forms is observed for temperatures within about 10% of T_c. We argue that this occurs when the correlation length becomes comparable to the system size.

In chapter 4, we test the range of universality of this model further by extending our studies to the case of a *biased* random walker. The vacancy or defect hops preferentially along one of the lattice directions, as if subject to gravity or an electric field. In the language of electrostatics, the defect is charged, disordering an initial configuration of neutral atoms in the presence of an electric field. We note that this is completely equivalent to having a neutral (or less massive) vacancy in a background of particles, all of which carry the *same* charge (or larger mass). Returning to upquenches to infinite temperature, we do not allow for any *feedback* from the background to the defect, i.e., the motion of the vacancy is independent of the local background configuration. However, the choice of boundary conditions along the direction of the field now becomes important: we will consider two cases, one in which spatial inhomogeneities persist in the long-time limit,

and another which approaches a homogeneous steady state. Intriguingly, in both cases the three temporal regimes noted before are still clearly observable. Our key goal is to explore to what extent scaling functions and exponents are *universal*, i.e., independent of boundary conditions and bias. Employing exact results, a mean-field theory and Monte Carlo simulations, we find that the scaling *exponents* are completely *universal*, but that the scaling *functions* can depend sensitively on the boundary conditions, through a new scaling variable which involves the bias.

Chapter 3

Dynamic Scaling in vacancy-mediated disordering: the effect of temperatures

3.1 The Model

In this section, we describe the dilute Ising model underlying our Monte Carlo simulations. It is defined on a two-dimensional ($d = 2$) square lattice of dimension $L \times L$, with sites denoted by a pair of integers, $\mathbf{r} \equiv (x, y)$. The boundary conditions are fully periodic in all directions. To model the two species of particles, black ("spin up") and white ("spin down", displayed as gray in the figures), and the vacancies, we introduce a spin variable $\sigma_{\mathbf{r}}$ at each site which can take three values: $+1$ (-1) if the site is occupied by a black (white) particle, and $\sigma_{\mathbf{r}} = 0$ if it is empty. Multiple occupancy is forbidden. Thus, the configurations of our system can be characterized by a set $\{\sigma_{\mathbf{r}}\}$ of spin variables. The numbers of black (N^+) and white (N^-) particles are conserved and differ by at most 1. The number of vacancies, M, is much smaller: $M \ll N^+$. In fact, most of our simulations will be restricted to $M = 1$, to model the minute vacancy concentrations in real systems. In the analytic work [9], we will also consider a more general case, where M is allowed to vary with system size according to $M \propto L^\gamma$. Different values of this *vacancy number* exponent $\gamma \in [0, d]$ will be discussed. Clearly, the single vacancy case corresponds to $\gamma = 0$.

The particles and vacancies interact with one another according to a dilute Ising model:

$$\mathcal{H}[\{\sigma_{\mathbf{r}}\}] = -J \sum_{\langle \mathbf{r}, \mathbf{r}' \rangle} \sigma_{\mathbf{r}} \sigma_{\mathbf{r}'} \tag{3.1}$$

with a ferromagnetic, nearest-neighbor coupling $J > 0$. Since the dilution is so small, the behavior of the system is that of the ordinary (non-dilute) two-dimensional Ising model. Thus, it has a phase transition, from a disordered to a phase-segregated phase, at the Onsager critical temperature, $T_c = 2.267...J/k_B$ [26]. The ground state is doubly degenerate. It consists of a strip of black and a strip of white particles, each filling half the system, separated by two planar interfaces

running parallel to a lattice axis. Since the particle-particle interactions are ferromagnetic, the few vacancies accumulate at the interfaces.

Next, we turn to the dynamics of the model. It is defined in terms of $W[\{\sigma_{\mathbf{r}}\}|\{\sigma'_{\mathbf{r}}\}]$, denoting the transition rate, per unit time, from configuration $\{\sigma_{\mathbf{r}}\}$ into a new configuration $\{\sigma'_{\mathbf{r}}\}$. Here, only particle-hole exchanges are allowed, and we choose W to be the usual Metropolis [27] rate: $\min\{1, \exp(-\beta\Delta\mathcal{H})\}$, where $\Delta\mathcal{H}$ is the energy difference of the system after and before the jump, and $\beta = 1/(k_B T)$ is the inverse temperature. The initial configuration of the system is perfectly phase-segregated, with the two interfaces chosen to lie along the x-axis. The vacancies are located at random positions along one of the interfaces. As time proceeds, the vacancies disorder the interfaces and, if $T > T_c$, dissolve them completely.

An exact solution of our model would correspond to the knowledge of the full time-dependent distributions, $P(\{\sigma_{\mathbf{r}}\}, t)$, for the probability of finding configuration $\{\sigma_{\mathbf{r}}\}$ at time t, given our initial condition. This requires finding *all* eigenvalues and eigenvectors of the underlying master equation:

$$\partial_t P(\{\sigma_{\mathbf{r}}\}, t) = \sum_{\{\sigma'_{\mathbf{r}}\}} \{W[\{\sigma'_{\mathbf{r}}\}|\{\sigma_{\mathbf{r}}\}]P(\{\sigma'_{\mathbf{r}}\}, t) - W[\{\sigma_{\mathbf{r}}\}|\{\sigma'_{\mathbf{r}}\}]P(\{\sigma_{\mathbf{r}}\}, t)\} \tag{3.2}$$

Even though Eqn. (3.2) is only linear in the probabilities, a complete solution is usually feasible only for systems which are either very small ($L \leq 3$) or restricted to one dimension. Both cases are only of limited interest here. However, it is often possible to determine a particular eigenvector, namely the one associated with the (non-degenerate) eigenvalue zero: this provides us with the *stationary limits*, $P_o(\{\sigma_{\mathbf{r}}\}) \equiv \lim_{t\to\infty} P(\{\sigma_{\mathbf{r}}\}, t)$, of the full distributions. In our case, the final steady state is clearly an equilibrium state of the usual two-dimensional Ising model: $P_o(\{\sigma_{\mathbf{r}}\}) \propto \exp[-\beta\mathcal{H}]$. Therefore, many of its properties are exactly known [28].

In our simulations, the system sizes range from $L = 30$ to 60. The final temperature T, measured in units of the Onsager temperature T_c, varies between $1.1T_c$ and infinity. Our data are averages over 10^2 to 10^4 realizations (or runs) depending on the desired quality of the data. The time unit is one Monte Carlo step (MCS) which corresponds to M attempted particle-hole exchanges. All systems investigated equilibrate after about 10^8 MCS.

To monitor the evolution of the system, we measure a "disorder parameter", defined as the average number of black and white nearest-neighbor pairs (broken bonds), $\mathcal{A}(L, t)$, as a function of (Monte Carlo) time t. This quantity is easily related to the Ising energy,

$$\mathcal{A}(L, t) = \frac{d}{2}L^d + \frac{1}{2J}\langle\mathcal{H}\rangle + O(L^\gamma) \tag{3.3}$$

where $\langle\cdot\rangle$ denotes the configurational average over runs. The correction is due to the vacancies and remains much smaller than the two leading terms. More detailed information is carried by the local hole and magnetization densities, defined respectively as

$$\begin{aligned} \phi(\mathbf{r}, t) &\equiv \langle\delta_{\sigma_{\mathbf{r}},0}\rangle \\ \psi(\mathbf{r}, t) &\equiv \langle\sigma_{\mathbf{r}}\rangle \end{aligned} \tag{3.4}$$

using coarse-grained version. The Kronecker-δ ensures that lattice site $\mathbf{r}$ is occupied by the vacancy. Non-zero values of $\psi(\mathbf{r}, t)$ indicate an *excess* of white or black particles at lattice site

r, which is obviously a sensitive measure of the disordering process. The full time dependence of these densities can in general only be computed within a mean-field approach. However, their stationary forms are easily found from exactly known properties of the two-dimensional Ising model.

3.2 Brownian Vacancies: $T = \infty$

In this Section, we review the simplest case, namely, upquenches to infinite temperature [9], which sets the reference frame for our further studies. Clearly, the nearest-neighbor coupling J plays no role here at all, and all attempted particle-hole exchanges are executed with unit rate. Thus, the vacancies perform a Brownian random walk, regardless of their local environment. We first summarize the simulation results which suggest the key to the mean-field analysis, namely, a separation of time scales. We then introduce a suitable set of exponents and scaling forms and show that the late stages of the disordering process display dynamic scaling. Finally, we turn to a mean-field theory and compute these exponents and scaling functions analytically.

3.2.1 Simulation Results

To illustrate the gradual destruction of the interfaces and the disordering of the bulk, Fig. 3.1 shows the evolution of a typical configuration, in a 60×60 system with a single vacancy (represented by a white square in the figures). At $t = 0$, the vacancy is located at the interface in the center. For short times $t > 0$, this interface begins to break up slowly. Eventually, the second interface also becomes affected, as more and more particles are transported into regions of opposite color, until the system finally disorders completely. For later reference, we note that the *last two* configurations, at 10^7 and 10^8 MCS, are both already fully random. The disordering process is clearly reflected in the number of broken bonds, denoted by $\mathcal{A}(L,t)$. For our system, $\mathcal{A}(60,t)$ is shown in Fig. 3.2: It increases from its minimum of $O(L)$ for the initial configuration at $t = 0$, to $O(L^2)$ for the fully equilibrated system at $t = 10^7$. One clearly distinguishes three regimes, shown schematically in the inset: an *early* regime (I), the *intermediate*, or *scaling*, regime (II), and finally a *late* or *saturation* regime (III) in which the system has effectively reached the steady state. Tracking the motion of the vacancy, the physical origin of these three regimes is easily identified. For *early* times (regime I), the vacancy is still localized in the vicinity of its starting point, far from the boundaries of the system. After a time of $O(L^2)$, however, the vacancy has explored the whole system and is effectively equilibrated. This marks the onset of the *intermediate* regime. The particle distribution is still strongly inhomogeneous here and does not equilibrate until the system enters the *saturation* regime. We emphasize that the second and third regimes emerge only in a *finite* system. In an infinite system, regime I persists for all times. Some aspects will be briefly summarized in the concluding remarks.

Our key observation [9] is that, independent of dimension, Regimes II and III exhibit *dynamic scaling*. To characterize this behavior, a set of exponents is introduced: First, the saturation value of $\mathcal{A}$ scales with system size according to $\lim_{t\to\infty} \mathcal{A}(L,t) \equiv \mathcal{A}_{sat}(L) \sim L^{\alpha}$. Second, in the intermediate regime, $\mathcal{A}(L,t)$ grows as $\mathcal{A}(L,t) \sim L^{\sigma} t^{\beta}$. Finally, the two crossover times ("early"

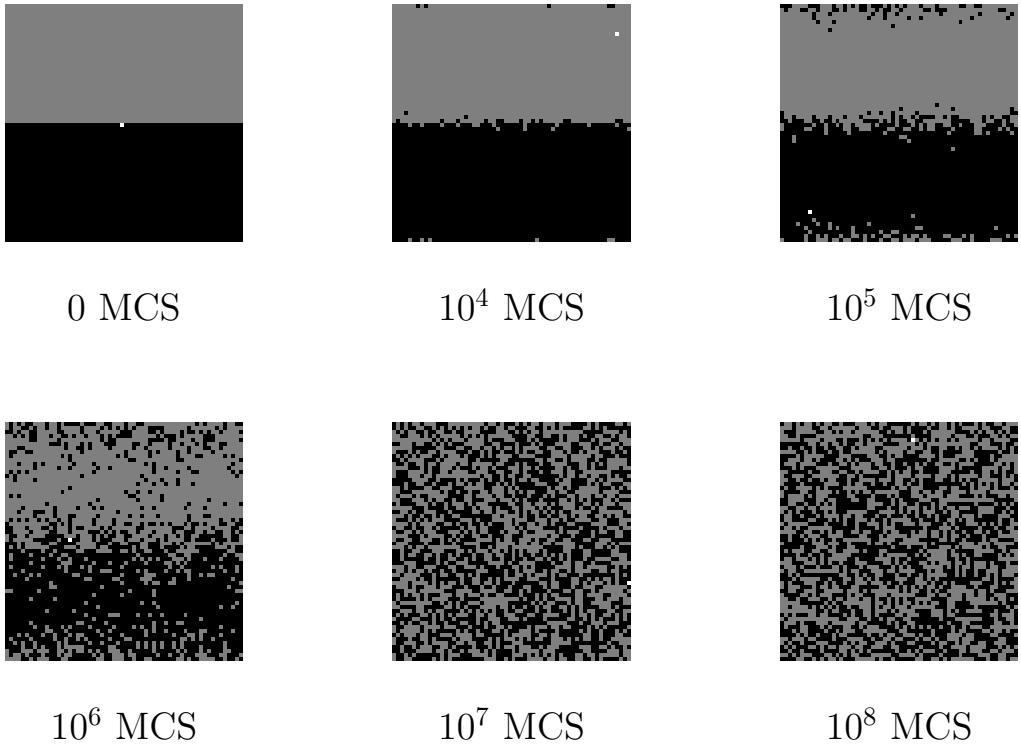

Figure 3.1: *Sequence of snapshots showing the disordering process of a* 60×60 *system with* $T = \infty$. *The black and gray squares represent the two types of particles(*$\sigma = \pm 1$*) and the white square denotes the vacancy(*$\sigma = 0$*). The configurations were recorded after* $0, 10^4, 10^5, 10^6, 10^7$ *and* 10^8 *MCS.*

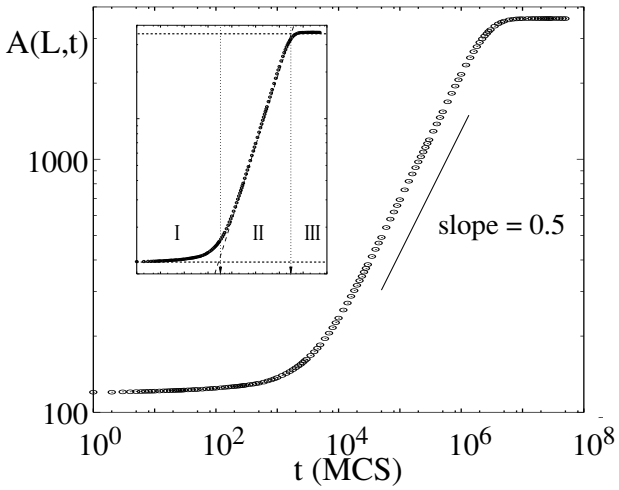

Figure 3.2: *Plot of the total number of broken bonds, $A(L,t)$ vs t, for $L = 60$ and $T = \infty$. It shows the emergence of an* early *regime (I), an* intermediate, *or* scaling, *regime (II), and a* late *or* saturation *regime (III). The straight reference line has slope* 0.5.

and "late") scale as $t_e \sim L^{z_e}$, and $t_l \sim L^{z_l}$. Thus, the intermediate-to-late time crossover can be summarized by the scaling form

$$\mathcal{A}(L,t) \sim L^{\alpha} f\left(t/t_l\right) \tag{3.5}$$

with a scaling function f which satisfies $f(x) \simeq const$ for $x \gg 1$, and $f(x) \sim x^{\beta}$ for $x \ll 1$ (but x large enough to fall within Regime II). The consistency condition $\mathcal{A}(L,t_l) \simeq \mathcal{A}_{sat}(L)$ yields the scaling law

$$\sigma + z_l \beta = \alpha. \tag{3.6}$$

Due to the presence of the novel exponent σ, (3.6) *differs* from the familiar $z\beta = \alpha$ which controls surface growth in, e.g., the Edwards-Wilkinson [29] or KPZ [30] models.

We first consider a single vacancy, in $d = 2$. For this case, the data give $\alpha = 2 \pm 0.1$, $\beta = 0.5 \pm 0.06$, $z_e = 2 \pm 0.2$, $z_l = 4 \pm 0.2$, and $\sigma = 0 \pm 0.1$ [9]. Clearly, these exponents satisfy the scaling law (3.6). Excellent data collapse is obtained by plotting $\mathcal{A}(L,t)/L^{\alpha}$ versus t/L^{z_l}, shown in Fig. 3.3 for a range of system sizes. The same indices are observed for several vacancies, provided their number remains *constant* as the system size L is varied, corresponding to a vacancy exponent $\gamma = 0$.

We note briefly how the exponent σ comes into play [9]. First, for $\gamma = 0$, σ is required to accomplish good data collapse in dimensions greater than 2. Second, another natural case is $\gamma = d - 1$, corresponding to a situation where the defects are initially "frozen" at the interfaces, and their number scales with the interfacial area. Such a scenario could occur in surface catalysis or in welding. Since the data are restricted to $d = 2$, only the case $\gamma = 1$, i.e., $M \propto L$, has been examined. Here, the data collapse only if *(i)* curves corresponding to different system sizes are shifted by an M-dependent factor along the $\ln t$-axis, and *(ii)* the late crossover exponent takes

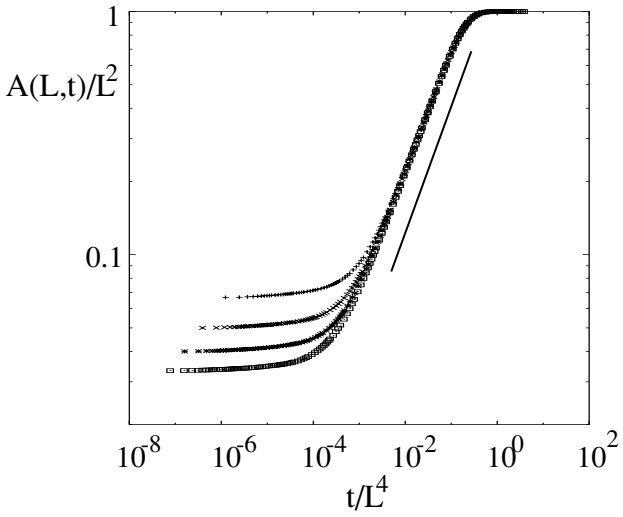

Figure 3.3: *The scaling plot of* $A(L,t)/L^2$ *vs* t/L^4 *for* $L = 30(+), 40(\times), 50(*)$, *and* $60(\sqcap)$ *with* $T = \infty$. *The straight reference line has slope* 0.5.

on the new value $z_l = 3 \pm 0.2$, while α and β remain unchanged. This behavior suggests that the exponent σ depends *non-trivially* on γ. For $\gamma = 1$, the data are consistent with $\sigma = 1/2$, so that the scaling form (3.5) still holds and the scaling law (3.6) is satisfied with the modified exponent z_l.

This concludes the discussion of our simulation results. We now turn to an analytic description of the disordering process.

3.2.2 Mean-Field Theory

As a first step, we summarize the exactly known results for the initial configuration and the final, fully disordered state. The analysis is easily performed in general dimension, for a hypercube of side length L with fully periodic boundary conditions. The initial value of the disorder parameter is given by the number of broken bonds across the two initial, flat interfaces between black and white particles: $\mathcal{A}(L, t = 0) = 2L^{d-1} + O(M)$. The saturation value, $\mathcal{A}_{sat}(L) = \frac{d}{2}L^{2d}/(L^d - 1)$ follows easily from the fact that the final steady state is completely random for the Brownian vacancy case with $T = \infty$. Thus, we can read off the *exact* result $\alpha = d$.

To proceed further, we derive a set of equations of motion, for the coarse-grained local hole and particle densities. Starting from the microscopic master equation, we can easily obtain evolution equations for the discrete densities, $\phi(\mathbf{r}, t)$ and $\psi(\mathbf{r}, t)$. Since there is no feedback from the particle background, the equation for $\phi(\mathbf{r}, t)$ is completely independent of $\psi(\mathbf{r}, t)$. In contrast, the motion of the particles is slaved to that of the vacancy, so that the equation for $\psi(\mathbf{r}, t)$ is inherently nonlinear and contains two-point functions of the form $\langle \sigma_{\mathbf{r}'} \delta_{\sigma_{\mathbf{r}},0} \rangle$. Here, a mean-field assumption is required, to truncate these averages. Finally, we take the continuum limit, by letting the lattice

constant vanish at fixed system size L. For simplicity, we use the same notation for discrete densities and their continuous counterparts. The position vector $\mathbf{r} \equiv (x_1,....,x_d)$ denotes a point in the hypercube $-L/2 \leq x_i \leq +L/2$, $i = 1, 2, ..., d$, with volume $V \equiv L^d$. We also retain the symbol t for time, since Monte Carlo time and its coarse-grained counterpart differ only by a scale factor. After some suitable rescalings, we obtain the desired mean-field equations [9]:

$$\begin{aligned} \partial_t \phi(\mathbf{r},t) &= \nabla^2 \phi(\mathbf{r},t) \\ \partial_t \psi(\mathbf{r},t) &= \nabla[\phi(\mathbf{r},t)\nabla\psi(\mathbf{r},t) - \psi(\mathbf{r},t)\nabla\phi(\mathbf{r},t)]. \end{aligned} \tag{3.7}$$

Here, ∇ is the d-dimensional gradient. The simple diffusion equation for ϕ reflects the Brownian random walk of the vacancies. The magnetization density ψ obeys a balance equation: the first term reflects a gain, provided a vacancy is initially present and a particle "diffuses" in from a neighboring site. The second term accounts for a loss, due to a particle jumping to a vacant nearest-neighbor site. Similar equations have been discussed in the context of biased diffusion of two species [31] and vacancy-mediated interdiffusion [16]. Note that both equations take the form of continuity equations, due to the conservation laws on the particle numbers. The two densities are normalized, according to $\int_V \phi(\mathbf{r},t) = M$, and the constraint $\int_V \psi(\mathbf{r},t) = 0$. Given fully periodic boundary conditions, these equations have to be supplemented with appropriate initial conditions. For our simulations, we choose $\phi(\mathbf{r},0) = \frac{M}{L^{d-1}}\delta(y)$ where $y \equiv x_d$, and $\psi(\mathbf{r},0) = 2\theta(y) - 1$. The final state is, of course, trivial: $\phi(\mathbf{r},\infty) \equiv \phi_o = M/V$, and $\psi(\mathbf{r},\infty) = 0$.

To solve for the hole and magnetization densities, we seek the separation of time scales, first observed in the Monte Carlo data, in the equations (3.7). The hole density, with a diffusion coefficient of $O(1)$, relaxes rapidly to the final value M/V. By contrast, the magnetization is essentially slaved to $\phi(\mathbf{r},t)$ and relaxes with a diffusion "coefficient" of $O(1/V)$. The hole density spreads diffusively and reaches the boundaries of the system after a time of $O(L^2)$, marking the end of the early regime. Thus, we identify the *early* crossover time $t_e \propto L^2$ and read off $z_e = 2$. For later times, the vacancies are uniformly distributed over the system, so that ϕ may be replaced by its stationary value, $\phi_o = \frac{M}{V}$. Inserting this into the equation for ψ results in a simple diffusion equation

$$\partial_t \psi = \phi_o \nabla^2 \psi \tag{3.8}$$

with a diffusion coefficient M/V. Its solution, subject to the initial and fully periodic boundary conditions, is easily found [9]:

$$\psi(\mathbf{r},t) = \frac{4}{\pi}\sum_{n=1}^{\infty} \frac{\sin[2\pi(2n-1)y/L]}{2n-1}\, e^{-\epsilon\, t(2n-1)^2}\ , \tag{3.9}$$

where $\epsilon \equiv 4\pi^2\phi_o/L^2$. Of course, $\psi(\mathbf{r},t)$ depends on y only, reflecting the homogeneity of initial and boundary conditions in the $d-1$ transverse directions. We also note that, while this form is exact, it converges rapidly only for late times, $\epsilon\, t \gg 1$, corresponding to the saturation regime. There, the profile is harmonic with a rapidly decaying amplitude: $\psi(\mathbf{r},t) \simeq \frac{4}{\pi} sin[2\pi y/L] e^{-\epsilon\, t}$. Below, we will present an equivalent form with good convergence in the opposite limit.

To describe the simulation results, an expression for the disorder parameter $\mathcal{A}$ is needed. Recalling its connection to the average Ising energy, Eqn. (3.3), we invoke the continuum limit of

the latter [32], $\langle \mathcal{H} \rangle = -dJ \int_V \psi(\mathbf{r},t)^2$, which is correct up to surface terms of $O(1/L^{d-1})$. Thus, we obtain [9]:

$$\mathcal{A}(L,t) = \frac{d}{2}\left[V - \int_V \psi(\mathbf{r},t)^2\right] \quad . \tag{3.10}$$

We note that this form is manifestly extensive. Moreover, since surface terms have been dropped, the initial value of $\mathcal{A}$ is now simply 0.

The time evolution of this quantity follows from (3.9):

$$\mathcal{A}(L,t) = \frac{d}{2} V \left[1 - S(2\epsilon t)\right] \ , \tag{3.11}$$

where $S(\zeta) \equiv \frac{8}{\pi^2} \sum_1^\infty e^{-\zeta(2n-1)^2}/(2n-1)^2$. Since $S(0) = 1$ and $S(\infty) = 0$, we verify that $\mathcal{A}$ does take on the correct initial and final values. It is also consistent with our postulated scaling form, Eqn. (3.5), provided we identify the scaling exponent α with d and the scaling variable t/t_l with ϵt. This suggests to define the late crossover time as $t_l \equiv 1/\epsilon$. Collecting the dependence on system size, we identify $t_l \propto L^2/\phi_o = L^{d+2-\gamma}$. Hence, we read off $z_l = d + 2 - \gamma$ for the scaling exponent which controls the late crossover time. Thus, $\epsilon t \gg 1$ marks the saturation regime where Eqn. (3.11) converges well, exhibiting a simple exponential approach to the saturation value: $\mathcal{A}(L,t) = \frac{d}{2} V \left[1 - \frac{8}{\pi^2} e^{-2\epsilon t} + O(e^{-4\epsilon t})\right]$.

In contrast, the intermediate regime (II) corresponds to $\epsilon t \ll 1$. To capture the time dependence here, we re-express the infinite sum via a Poisson resummation [33]. The key advantage of this procedure is to convert a sum with rapid convergence in one limit ($\epsilon t \gg 1$) into an equivalent sum with good convergence in the opposite ($\epsilon t \ll 1$) limit. Deferring technical details to an Appendix IA, we introduce $u_m \equiv \pi m/\sqrt{8\epsilon t}$ and arrive at [9]:

$$\mathcal{A}(L,t) \simeq \frac{2d}{\pi^{3/2}} V \sqrt{2\epsilon t} \left\{1 + 2\sum_{m=1}^{\infty} (-1)^m \left[e^{-u_m^2} - u_m \Gamma\left(\frac{1}{2}, u_m^2\right)\right]\right\} \tag{3.12}$$

where $\Gamma(\bullet,\bullet)$ denotes the incomplete Gamma function. In this form, the sum over m is suppressed for small ϵt. Thus, $\mathcal{A}(L,t) \propto V\sqrt{2\epsilon t} \propto L^d \sqrt{Mt/L^{2+d}}$, yielding the remaining indices, namely $\beta = \frac{1}{2}$ independent of dimension, and $\sigma = \frac{1}{2}(d + \gamma - 2)$. It is straightforward to check that these exponents satisfy the scaling relation (3.6). In two dimensions, our theory predicts $z_l = 4$ and $\sigma = 0$ for $\gamma = 0$, while $z_l = 3$ and $\sigma = \frac{1}{2}$ for $\gamma = 1$, in complete agreement with the Monte Carlo data.

Since the full magnetization profile contains more detailed information than the disorder parameter, one might also be interested in its form for early times, $\epsilon t \ll 1$. A similar Poisson resummation, of Eqn. (3.9), results in

$$\psi(\mathbf{r},t) = erf\left(\frac{\tilde{y}}{2\sqrt{\epsilon t}}\right) + \sum_{m=1}^{\infty} (-1)^m \left[erf\left(\frac{\tilde{y} + \pi m}{2\sqrt{\epsilon t}}\right) + erf\left(\frac{\tilde{y} - \pi m}{2\sqrt{\epsilon t}}\right)\right] \ ;, \tag{3.13}$$

where $\tilde{y} \equiv 2\pi y/L$. For $\epsilon t \ll 1$, this form still reflects the sharpness of the initial Θ-function which is only gradually "washed out".

This concludes our discussion of the mean-field theory, for the Brownian vacancy case. We note briefly that these results remain unchanged (up to a trivial amplitude) if periodic boundary conditions are replaced by reflecting ones. We should also reiterate that our focus here rests on the intermediate and late regimes. A full microscopic treatment of the early regime is beyond the scope of this thesis. For the benefit of the reader, however, a short summary is provided in the conclusions. Instead, we turn to the role of interactions.

3.3 The Effect of Interactions: $T_c < T < \infty$.

When the final temperature of the system is *finite*, $T < \infty$, the full Hamiltonian, Eqn. (3.1), comes into play when a vacancy attempts to move. In particular, the defects no longer perform a simple random walk, since the jump rates now carry information about the local environment, i.e., the distribution of black and white particles around the originating and receiving site. Thus, a feedback loop between vacancy and background is established, in stark contrast to the $T = \infty$ case. One should expect that this has significant consequences for profiles and disorder parameter, and that even dynamic scaling exponents might be modified. It is immediately obvious that we should distinguish final temperatures above criticality from those below. In the former case, the final steady-state configurations are still homogeneous, even if correlations become more noticeable. In the latter case, however, the equilibrium state itself is phase-separated, so that the only effect of the vacancies is to "soften" the initial interfaces. This aspect of vacancy-induced disordering should be particulary interesting in two dimensions, where Ising interfaces are known to be rough [34]. There, the vacancies must mediate both the development of an "intrinsic interfacial width" and the emergence of large-scale wanderings of the interface [35]. Certainly, we expect these two phenomena to take place on drastically different time scales, since they are associated with local *vs.* global disorder.

In this Section, we focus on final temperatures *above* criticality: $T_c < T < \infty$, and a single vacancy, $M = 1$. Starting with a set of typical evolution pictures, we investigate the dynamic scaling properties of the disorder parameter. Since the equations of motion now become highly nonlinear, we have not been able to solve them exactly, but an approximate solution, valid for high temperatures, can be found [51]. Thus, we offer only a few comments in conclusion.

Fig. 3.4 shows the evolution of a typical configuration, in a 60×60 system with a single vacancy at $T = 1.5T_c$. Note that the MC times, when the snapshots are taken, are the same as in Fig. 3.1. Again, we observe the gradual, yet eventually complete, destruction of the interfaces. In comparison with Fig. 3.1, however, two obvious differences emerge: First, the system takes longer to reach the final stationary state. Second, the final configuration shows clear evidence of a $finite$ correlation length. Both features are induced by the interactions. In particular, the disordering process is slowed down since the breaking of bonds is energetically costly. At a more quantitative level, this is documented by Fig. 3.5 which shows the disorder parameter, for a 60×60 system and several temperatures. One observes that the late crossover time shifts to later times as the temperature decreases. In contrast, the early crossover time appears to be less affected. Also, the saturation value of the disorder parameter decreases. However, being essentially the Ising energy, it remains extensive, with a T-dependent amplitude.

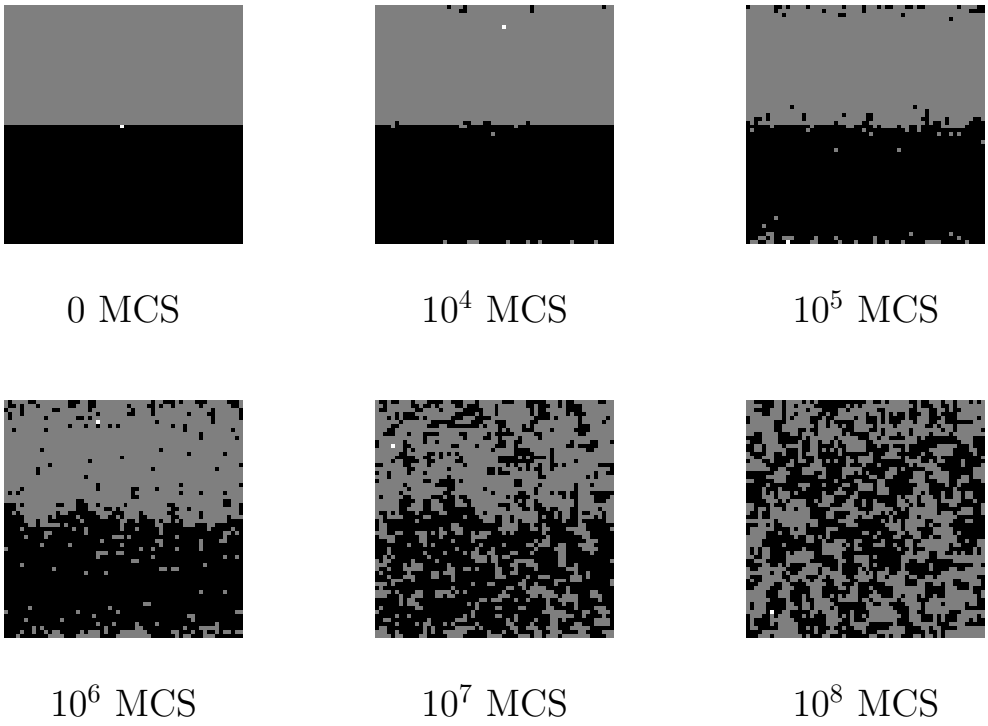

Figure 3.4: *Sequence of snapshots showing the disordering process of a* 60×60 *system with* $T = 1.5T_c$*. The black and gray squares represent the two types of particles(*$\sigma = \pm 1$*) and the white square denotes the vacancy(*$\sigma = 0$*). The configurations were recorded after* $0, 10^4, 10^5, 10^6, 10^7$ *and* 10^8 *MCS.*

It is natural to ask whether the scaling forms found in the previous section still hold. In Fig. 3.6, we present the scaling plots for the disorder parameter, i.e., we show $\mathcal{A}(L,t)/L^d$ plotted vs. t/L^4. Each graph corresponds to a different temperature: $T = 3.5T_c$ (Fig. 3.6a), $T = 1.5T_c$ (Fig. 3.6b), and $T = 1.1T_c$ (Fig. 3.6c). Focusing on Fig. 3.6a, it is quite evident that the data collapse just as well for $T = 3.5T_c$ as for $T = \infty$ (cf. Fig. 3.3). The three temporal regimes are well separated and easy to distinguish. In the intermediate regime, the disorder parameter follows the $t^{1/2}$ power law, over more than three decades. Thus, the data at this temperature still obey the scaling form (3.5), with the same set of exponents. However, for the next temperature, $T = 1.5T_c$ (Fig. 3.6b), the range of perfect data collapse begins to shrink: the curve for the smallest system size ($L = 30$) merges noticeably later than in Fig. 3.6a. Also, the power law no longer persists over such a wide region, and the exponent β becomes more difficult to determine. Still, the larger system sizes collapse rather well, so that there is still a well-defined scaling function even if its form appears to change. Finally, Fig. 3.6c shows the data for $T = 1.1T_c$: here, the imposed scaling form manifestly fails to match the data.

We conclude that, for temperatures not too close to the critical temperature T_c, the dynamic scaling form of the purely diffusive case, Eqn. (3.5), still holds. In two dimensions, we identify

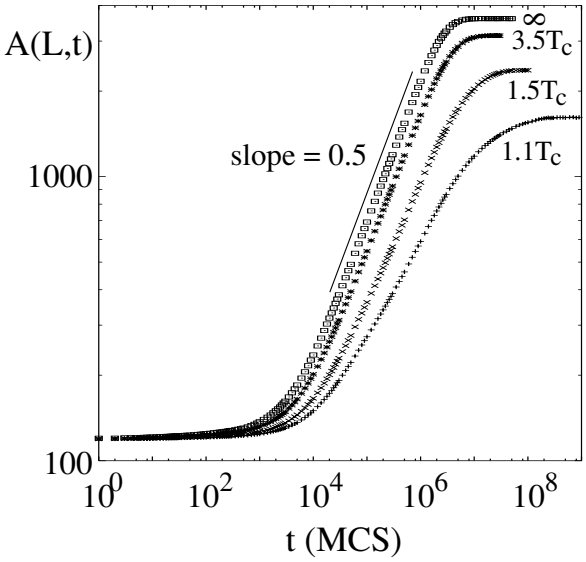

Figure 3.5: $A(L,t)$ *vs* t *for* $L = 60$ *with* $T = \infty$, $3.5T_c$, $1.5T_c$ *and* $1.1T_c$.

the saturation exponent $\alpha = 2$ and, for a single vacancy, the late crossover exponent $z_l = 4$. The scaling function itself, however, develops more curvature in the intermediate regime, so that it becomes more difficult to extract a pure power law, t^β. One might be tempted to fit the data to a pure power law, resulting in a *temperature-dependent* exponent β, noticeably smaller than 0.5. However, we believe that there is little physical support for such a drastic change in scaling properties, especially in the disordered phase of the Ising model. Instead, we conjecture that $\beta = 1/2$ is still valid but that T-dependent *corrections-to-scaling* begin to play a stronger role. In support, we checked that the data for $T = 1.5T_c$, in the earlier part of regime II, can be well fitted by a power law with an exponential correction, i.e., $\mathcal{A}(L,t)/L^2 \propto t^{1/2}\{1 + c_1(T)\exp[-c_2(T)t/L^4]\}$. This form is gleaned from Eqn. (3.12), by keeping the leading and first sub-leading term but allowing for two temperature-dependent fit parameters $c_1(T)$ and $c_2(T)$. Of course, we should anticipate significant changes in the scaling behavior upon entering the critical region. Since $1.1T_c$ is "at the doorstep" of the latter, some precursors such as an increased correlation length begin to make their influence felt.

In the following, we comment briefly on some analytic results. First, we can easily check that the saturation values, $\mathcal{A}_{sat}(L)$, are consistent with exact results for the two-dimensional Ising value. Table 1 shows this comparison for a 60×60 system with a single vacancy, at several temperatures. $\mathcal{A}_{sat}^{MC}$ is the *measured* saturation value of the disorder parameter. $\mathcal{A}_{sat}^{TH}$ is calculated on the basis of Eqn. (3.3), where $\langle\mathcal{H}\rangle$ is the *exact* bulk value for the average energy of the usual Ising model [28]. The effect of the vacancy has been neglected. The agreement is very good, within the statistical errors of our data. The discrepancies are of course largest for the last column, with T closest to T_c.

Table 3.1: *Comparison of exact and measured values of the saturated disorder parameter for several temperatures.*

T/T_c	∞	3.5	1.5	1.1
$\mathcal{A}_{sat}^{TH}$	3600.0	3134.6	2367.0	1602.9
$\mathcal{A}_{sat}^{MC}$	3598.6	3134.0	2368.9	1615.7

Finally, since $\langle \mathcal{H} \rangle$, and therefore $\mathcal{A}_{sat}(L)$, are extensive, we still have an *exact* value for the saturation exponent $\alpha = d$.

The time-dependence of the disorder parameter poses a much more difficult problem. It is of course possible to obtain the temperature-dependent generalization of Eqns. (3.7), by averaging the microscopic master equation, followed by a mean-field approximation and a naive continuum limit. For a dynamics slightly different from ours, this procedure was followed in [14]. However, these equations are no longer easily soluble: First, *both* of them are inherently nonlinear, due to interactions. Second, the equation for the local hole density, $\phi(\mathbf{r}, t)$, no longer decouples from the magnetization density $\psi(\mathbf{r}, t)$, since the background *feeds back* into the motion of the vacancy. Thus, it is not apparent how a clean time scale separation could emerge from these equations. As a consequence, we are reduced to numerical solutions or approximate techniques, such as a high temperature expansion. Results based on the latter provide support for our conjecture that $\beta = 1/2$ is still valid and that larger corrections-to-scaling are responsible for the curvature in the scaling function [51].

Another approach rests upon generalizing Eqns. (3.7) to the interacting case, and solving them in a high-temperature expansion. The results also support our conjecture that β remains $1/2$ outside the critical region [51].

To summarize this section briefly, our data indicate that, for temperatures not too close to the critical temperature T_c, the dynamic scaling form of the purely diffusive case still holds, even though corrections-to-scaling become more noticeable. In contrast, for T near T_c we observe a clear breakdown of these scaling forms.

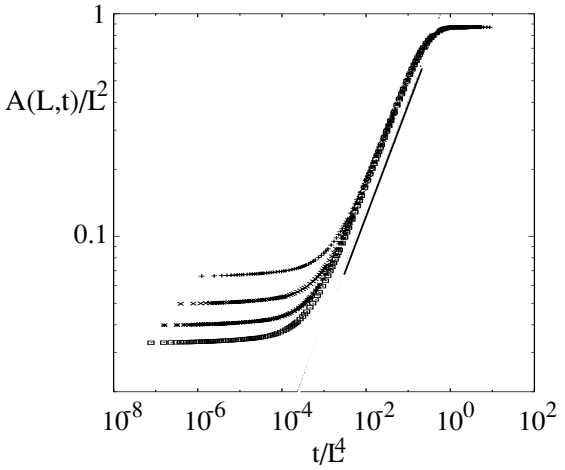

a)

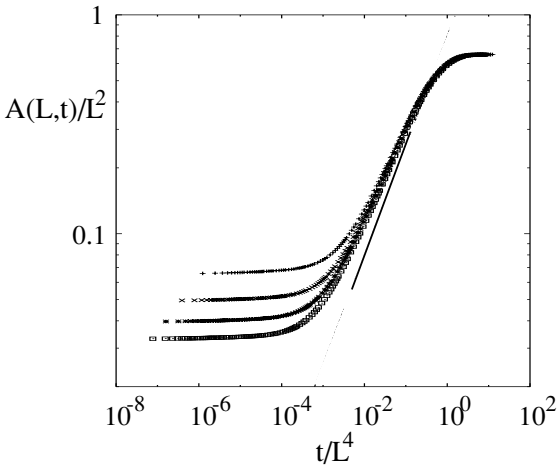

b)

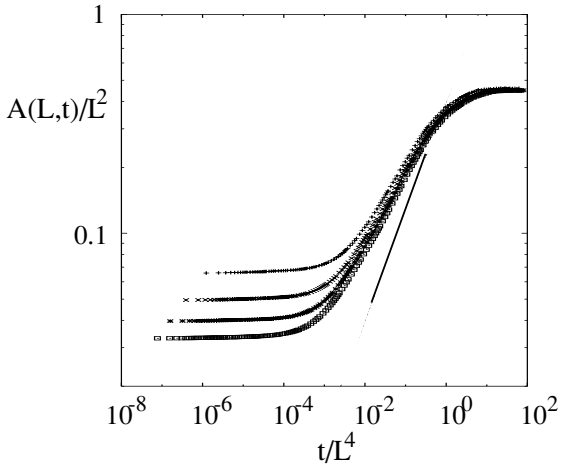

c)

Figure 3.6: *The scaling plot of* $A(L,t)/L^2$ *vs* t/L^4 *for* $L = 30(+), 40(\times), 50(*)$, *and* $60(\sqcap)$, *(a)* $T = 3.5T_c$, *(b)* $T = 1.5T_c$ *and (c)* $T = 1.1T_c$. *The straight reference lines have slope* 0.5.

Chapter 4

Universal aspects of vacancy-mediated disordering dynamics: the effect of external fields

4.1 The Model

In this chapter, we continue to investigate the lattice model introduced before. While the previous chapter focused on disordering at a *finite* temperature $T < \infty$, we now consider the effect of a *bias* E, aligned transverse to the initial interface, i.e., upwards along the (positive) y-axis. This is of course equivalent to the particles experiencing an external gravitational or electric field pointing along y. In order to expose the effects of the bias most succinctly, we set $J = 0$ in Eqn. (3.1), i.e., we do not include inter-particle interactions.

At each Monte Carlo time step (MCS), one of the four nearest neighbors of the vacancy is chosen at random. The exchange is performed using Metropolis [27] rates: $\min\left\{1, e^{Ea\delta y}\right\}$, modelling a *local* electrostatic or gravitational potential. Here, $\delta y = 0, \pm 1$ is the change in the y-coordinate of the vacancy, in units of the lattice constant a. Thus, moves *against* the field are exponentially suppressed while all others are accepted. No particle-particle exchanges are allowed. We note that a factor $1/T$ has been absorbed into the parameter E; i.e., we are considering the *high-temperature, high-field limit* of a more complex interacting system.

Next, we specify the boundary conditions. In combination with the bias, they determine whether any spatial inhomogeneities survive in the long-time limit, with potential consequences for scaling exponents or functions. In the unbiased case, the stationary state is completely uniform [9], and the choice of boundary conditions affects at most nonuniversal amplitudes. To test the effect of spatial inhomogeneities, we consider two scenarios, namely, reflecting (also referred to as "brick wall") boundary condition (BWBC) or periodic (PBC) boundary conditions for the top and bottom edges. The right and left boundaries, being aligned with the drive, are not expected to play a significant role; we choose them to be periodic in both cases. These two scenarios differ in two important respects. First, reflecting boundary conditions allow some spatial inhomogeneities

to persist, while periodic boundary conditions lead to homogeneous distributions. Second, we will see in the next section that, under BWBC, the system approaches an *equilibrium* state in which all transport currents have subsided. In contrast, periodic boundary conditions are incompatible with a global Hamiltonian, so that the steady state is a *non-equilibrium* one, carrying a net mass current.

The two control parameters for the Monte Carlo simulations will be the field strength, E, and the system size, L. To study the temporal evolution of the system, we measure the disorder parameter, namely, $\mathcal{A}(L, E; t)$ [9], as a function of time t. We will also investigate the local hole and magnetization densities, whose stationary forms are easily found from the known steady-state distributions, as we will presently see. Their time-dependent versions will again be computed within a mean-field approach, in analogy to chapter 3. We finally note that, for the analytic part of our work, it is straightforward to generalize our model to d dimensions: Denoting a lattice site by $\mathbf{r} \equiv (x_1, ..., x_{d-1}, x_d \equiv y)$, the field selects a *one-dimensional* subspace, with reflecting or periodic boundary conditions, along the y-direction. The $(d-1)$-dimensional transverse subspace retains periodic boundaries.

4.2 Exact results: the steady states

As emphasized in chapter 3, even if we cannot diagonalize the full master equation, Eqn. (3.2), we can often find its stationary solution, $P_o(\{\sigma_\mathbf{r}\}) \equiv \lim_{t\to\infty} P(\{\sigma_\mathbf{r}\}, t)$. This procedure is particularly simple for the case of brick wall (reflecting) boundary conditions. Here, we can immediately write down the internal energy (the "Hamiltonian") of the system, being the electrostatic energy of a single charge in a uniform electric field. Thus, $P_o(\{\sigma_\mathbf{r}\}) \propto \exp\left[\sum_\mathbf{r} Eay\delta_{\sigma_\mathbf{r},0}\right]$ is just the associated equilibrium Boltzmann factor. Since interparticle interactions are restricted to the excluded volume constraint, P_o is "color-blind", i.e., it gives equal weight to all configurations of *particles* at *fixed* vacancy position. Of course, any additional interactions could easily be incorporated into the Hamiltonian.

In contrast, the toroidal geometry of periodic boundary conditions, in combination with a uniform drive, prevents the existence of a global, *time-independent* potential. Therefore, the steady state is far from equilibrium. Yet fortunately, the stationary distribution is still exactly known [38] and even simpler: P_o is *completely* uniform, giving equal weight to *all* configurations of vacancy and particles. In this case, however, it is entirely unknown how to generalize this solution to more complex interparticle interactions.

Given the stationary distributions, the steady-state *densities*, defined via $\phi_o(\mathbf{r}) \equiv \lim_{t\to\infty} \phi(\mathbf{r}, t)$ and $\psi_o(\mathbf{r}) \equiv \lim_{t\to\infty} \psi(\mathbf{r}, t)$, are easily computed. For reflecting boundary conditions, ϕ_o is spatially *inhomogeneous*, following the usual exponential profile. Since the steady state is color-blind, the magnetization density is uniform. For simplicity, we place the coordinate origin into the center of the system. Thus,

$$\phi_o(\mathbf{r}) = C\exp(Eay) \quad and \quad \psi_o(\mathbf{r}) = 0\ , \tag{4.1}$$

where the normalization $C = \sinh(Ea/2)/[L^{d-1}\sinh(Ea(L+1)/2)]$ ensures that the system contains only one vacancy. The second equation just reflects the fact that there are equal numbers

of positive and negative particles [37]. It is noteworthy, and may not be entirely trivial at first sight, that the inhomogeneities in ϕ leave no trace at all in the magnetization distribution.

The corresponding results for periodic boundary conditions are even simpler:

$$\phi_o(\mathbf{r}) = \frac{1}{L^d} \quad and \quad \psi_o(\mathbf{r}) = 0 \tag{4.2}$$

Here, $\phi_o(\mathbf{r})$ is also uniform, reflecting a single vacancy in a system of L^d sites.

Finally, the saturation value for the number of broken bonds is readily found, since the particle configurations in the steady state are completely random. Since each of the four types of particle-particle bonds is equally likely, to leading order in $1/L$, we obtain

$$\mathcal{A}_{sat}(L,E) \equiv \lim_{t\to\infty} \mathcal{A}(L,E;t) = \frac{d}{2} L^d \left[1 + O(L^{-1})\right] \ .$$

The corrections include surface terms which distinguish the boundary conditions: for BWBC, we find $O(L^{-1}) = -2^{d+1}/(dL)$ while the leading correction for PBC is only $1/L^d$. The vacancy plays an even smaller role since it affects only $2d$ bonds: this contribution is neglected here.

Having established the key features of the steady state, we now turn to simulation results.

4.3 Separation of time scales

Our aim in this section is to motivate the key ingredient which will be required for most of our mean-field results, namely, that the vacancy equilibrates on a much faster time scale than the particles. Thus, the presence of a bias does not destroy the time scale separation of early, intermediate, and saturation regime. Since this observation will be based on Monte Carlo data, we first summarize the parameters of our numerical work.

We have performed detailed simulations of our model, using two-dimensional square lattices with L ranging from 20 to 60. The lattice constant a is set to 1. Both types of boundary conditions, reflecting and periodic, are implemented. For reflecting boundary conditions, the external field varies between 0 and 1.0. Larger values of E or L equilibrate too slowly for our computational resources. For periodic boundary conditions, equilibration takes place much faster, and therefore, E varies between 0 and 10.0. Our data are averaged over $10^2 - 10^5$ realizations, depending on the desired accuracy. The length of the runs varies with system size, up to a maximum of 10^8 MCS.

To obtain a visual impression of the disordering process, Fig. 4.1 shows the evolution of a typical configuration, in a 40×40 lattice with $E = 0.05$ and brickwall boundary conditions. One clearly observes how the initial interface, perfectly smooth at $t = 0$, becomes more diffuse as time progresses, and eventually vanishes completely. As in chapter 3, we invoke the number of broken bonds, $\mathcal{A}(L,E;t)$, as a suitable quantitative measure for the growing disorder. It is shown in Fig. 4.2 for the same set of system parameters. Similar to the unbiased case [9], it clearly exhibits three regimes, drawn schematically in the inset: an *early* regime (I), an *intermediate* regime (II), and a *late* or *saturation* regime (III) in which the system has reached steady state. As the system size increases, the intermediate regime spans a widening time range, showing that the three regimes are temporally well separated. In practice, this is already the case for $L \geq 20$.

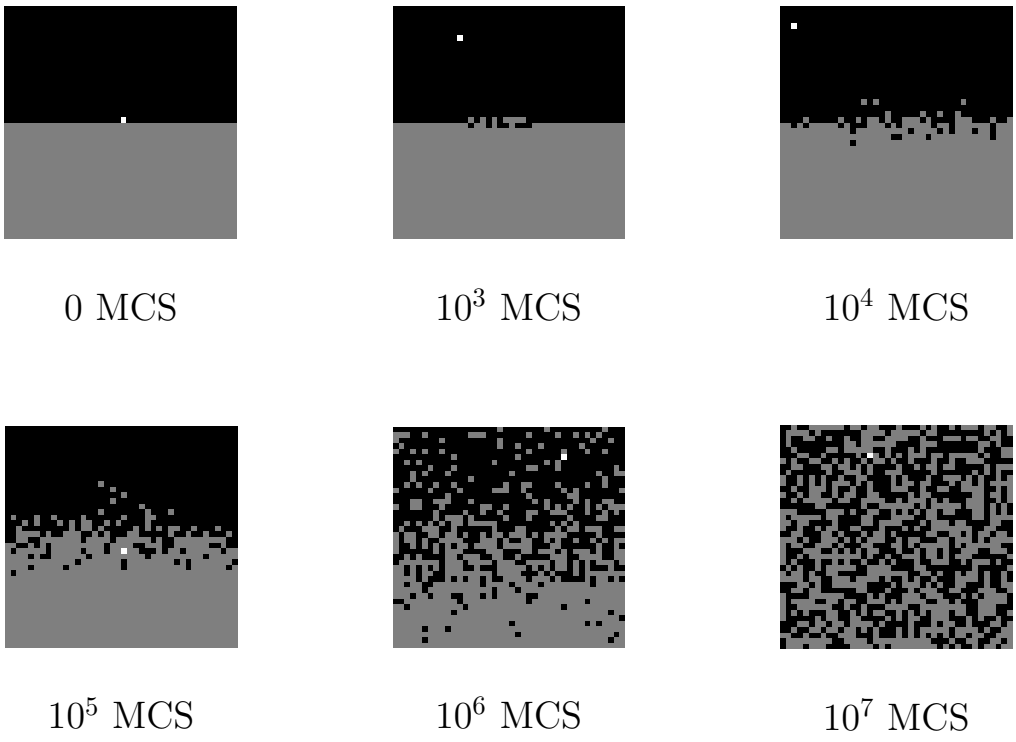

Figure 4.1: *Sequence of snapshots showing the disordering process of* 40×40 *system with* $E = 0.05$ *and BWBC. The black and gray squares represent the two types of particles*($\sigma = \pm 1$) *and the white square denotes the vacancy*($\sigma = 0$). *The configurations were recorded after* $0, 10^3, 10^4, 10^5, 10^6$ *and* 10^7 *MCS.*

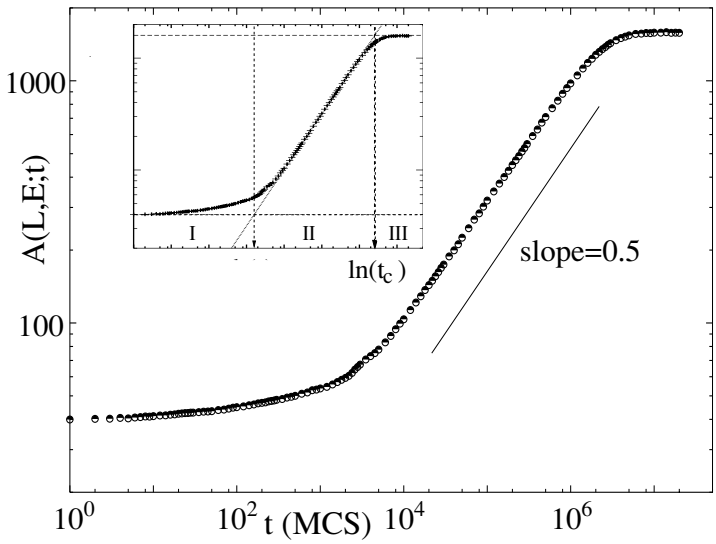

Figure 4.2: *Plot of $A(L, E; t)$ vs t, for $L = 40$, $E = 0.05$ and BWBC. The inset shows the emergence of an* early *regime (I), an* intermediate, *or* scaling, *regime (II), and a* late *or* saturation *regime (III). See text for additional details.*

This separation of time scales is also observed for larger values of the bias. Physically, the three regimes are characterized as in the previous chapter.

Our goal in the following is to test for dynamic scaling. Since our data involve the three variables L, E and t, as well as two types of boundary conditions, the appropriate scaling forms may not be a priori obvious. We shall therefore first consider an analytic approach, before turning to a detailed comparison with the data.

4.4 Mean-field theory

4.4.1 The equations of motion.

Since an exact solution of the full master equation is not available, we seek a simpler formulation of the dynamics. For our purposes, a set of equations of motion for the two conserved densities, ϕ and ψ, provides a suitable starting point. We immediately focus on the d-dimensional case. Following the same procedure as in chapter 3, we derive a set of equations for the average local densities, Eqns. (3.4), directly from the master equation. Again, a mean-field approximation is required, to factorize higher-order correlations which are induced by the excluded volume constraint. Finally, we take the continuum limit, by letting the lattice constant a vanish at fixed *physical* system size L and field E. The microscopic time scale is identified with $a^2/2d$. Thus, the resulting densities are functions of a *continuous* d-dimensional coordinate $\mathbf{r} \equiv (x_1, \ldots, x_{d-1}, x_d \equiv y)$ and

time t. The spatial origin is chosen at the center of the system so that $-L/2 \leq x_i \leq L/2$ for $i = 1, 2, ...d$. Letting $\hat{\mathbf{y}}$ denote the unit vector along the direction of E, we finally obtain the basic equations of motion:

$$\partial_t \phi(\mathbf{r}, t) = \nabla[\nabla\phi(\mathbf{r}, t) - E\hat{\mathbf{y}}\phi(\mathbf{r}, t)] \tag{4.3}$$

$$\partial_t \psi(\mathbf{r}, t) = \nabla[\phi(\mathbf{r}, t)\nabla\psi(\mathbf{r}, t) - \psi(\mathbf{r}, t)\nabla\phi(\mathbf{r}, t) + E\hat{\mathbf{y}}\phi(\mathbf{r}, t)\psi(\mathbf{r}, t)] \tag{4.4}$$

Clearly, both equations take the form of continuity equations, reflecting the conservation laws. The right-hand sides are the (negative) gradients of the associated hole and magnetization currents. In the field-free limit $E = 0$, these are just the results of Ref. [9], Eqn. (3.7). Of course, the bias induces additional terms which reflect systematic Ohmic currents: Since particles can only move when the vacancy is present, the extra *magnetization* current, $-E\hat{y}\phi\psi$, is proportional to ϕ. In contrast, the *hole* current $E\hat{y}\phi$ is independent of the local particle background, as one should have expected. We also note here that E has dimensions of inverse length. This suggests that the *dimensionless* combination LE will emerge as a convenient scaling variable.

Eqns. (4.3) and (4.4) have to be supplemented with the constraints on the total hole and particle [37] numbers:

$$\int_V \phi(\mathbf{r}, t) = 1 \quad \text{and} \quad \int_V \psi(\mathbf{r}, t) = 0 \ . \tag{4.5}$$

Here, $V = L^d$ is the volume of the system. Next, we consider the boundary conditions. In the PBC case, the solutions of Eqns. (4.3) and (4.4) must be fully periodic functions of $\mathbf{r}$, with period L. For reflecting boundary conditions, the periodicity of the solutions is restricted to the transverse subspace. *Along* E, we demand instead that the hole and magnetization *currents* vanish on the boundary $y = \pm L/2$.

Finally, we specify the initial conditions. The vacancy starts at the origin

$$\phi(\mathbf{r}, 0) = \delta(\mathbf{r}) \tag{4.6}$$

and the particles are perfectly phase-separated:

$$\psi(\mathbf{r}, 0) = 2\theta(y) - 1 \tag{4.7}$$

This completes the discussion of the equations of motion and their constraints. We now focus on their solution.

4.4.2 Solutions

As a starting point, we first establish the steady-state solutions of Eqns. (4.3) and (4.4). When turning to the full time dependence, progress is only possible if we simplify the equations of motion by invoking the separation of time scales. We shall mostly focus on *brick wall* boundary conditions, since this situation is physically more complex, as we shall shortly see. At the end, we briefly summarize our results for the fully periodic case. Anticipating inhomogeneities along the y-direction only, due to the bias, we seek *steady-state* solutions of the form $\phi(\mathbf{r}, t) = \phi_o(y)$ and $\psi(\mathbf{r}, t) = \psi_o(y)$. Eqn. (4.3) can now be integrated once, and the reflecting boundary conditions

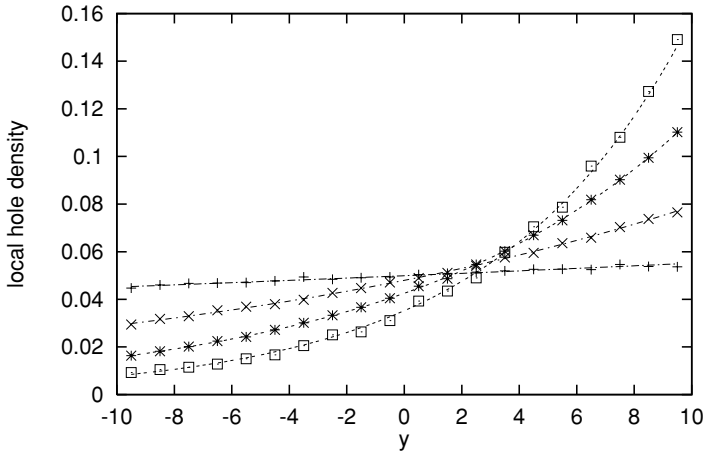

Figure 4.3: *Simulation data for the steady state hole profile with* $L = 20$ *and* $E = 0.01(+), 0.05(\times), 0.10(*)$ *and* $0.15(\sqcap)$*, BWBC. The dashed lines denote the mean-field profiles, Eqn. (4.8) and (4.9), at the same parameter values.*

force the integration constant, i.e., the hole current, to zero. We can immediately integrate again, whence

$$\phi_o(y) = C \exp(Ey) \ . \tag{4.8}$$

The constant C follows from the normalization condition, (4.5):

$$C = \frac{EL}{2L^d \sinh(EL/2)} \ . \tag{4.9}$$

Not surprisingly, this expression is just the continuum ($a \to 0$) limit of the exact result, Eqn. (4.1). One should note the emergence of the conjectured scaling variable LE. In Fig. 4.3, we compare the mean-field profiles for $L = 20$ and a range of E's with the corresponding Monte Carlo data. The agreement is clearly excellent. Finally, a similar integration of Eqn. (4.4), using (4.8), yields $\psi_o(y) = 0$, also consistent with the exact form.

Unfortunately, the solution of the time-dependent equations is not so simple. The full solution $\phi(\mathbf{r}, t)$ of Eqn. (4.3) must be found and inserted into Eqn. (4.4). The latter poses a formidable problem: even though it is a linear, second order partial differential equation of parabolic type, its coefficients are rather complicated functions of space and time. Fortunately, a complete solution is possible if we restrict our attention to the *intermediate and late* regimes. Here, the vacancy density has already reached steady state, so that only the purely exponential $\phi_o(y)$ enters into Eqn. (4.4). Of course, the reduced equation should be supplemented with the initial condition (4.7). Symmetry considerations as well as the data suggest that the magnetization density is uniform transverse to E, so that we seek a solution of the form $\psi(\mathbf{r}, t) = \psi(y, t)$. Letting ∂ denote the partial derivative with respect to y, we arrive at a much simpler version of Eqn. (4.4),

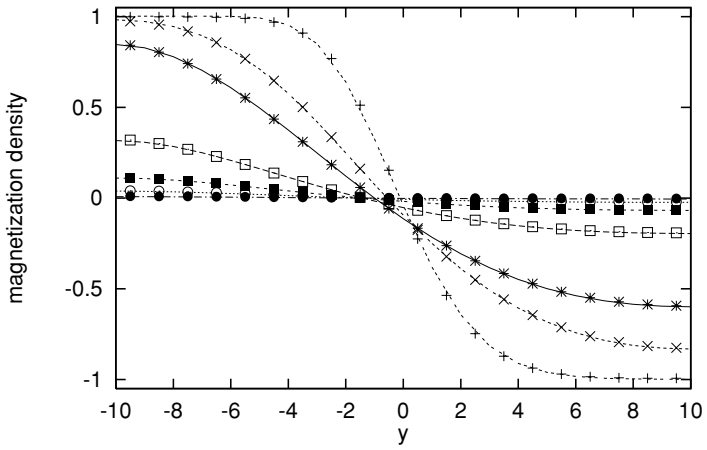

Figure 4.4: *Simulation data for charge density profile with $L = 20$, $E = 0.1$ and BWBC after $10^4(+), 5 \times 10^4(\times), 10^5(*), 3 \times 10^5(\sqcap), 5 \times 10^5(\star), 7 \times 10^5(\circ)$, and $10^6(\bullet)$ MCS. The dashed lines show the corresponding mean-field profiles based on Eqn. (4.12). See text for details.*

describing the magnetization density at intermediate and late times:

$$\partial_t \psi(y,t) = \partial[\phi_o(y)\partial\psi(y,t)] \; . \tag{4.10}$$

It is subject to the initial condition (4.7) and the brick wall boundary condition

$$\partial\psi(\pm\frac{L}{2},t) = 0 \tag{4.11}$$

which ensures that the magnetization current through the ends of the system vanishes.

This differential equation can be reduced to an eigenvalue problem with a complete and orthonormal set of eigenfunctions $\{U_n(y)\}$ which are linear combinations of Bessel functions. The eigenvalues κ_n are real, discrete and strictly positive. Deferring all mathematical details to the Appendix IB, we only quote the form of the solution, expressed as an eigenfunction expansion:

$$\psi(y,t) = \sum_{n=1}^{\infty} A_n U_n(y) \exp(-\kappa_n t) \tag{4.12}$$

The expansion coefficients A_n are chosen so as to match the initial condition (4.7).

Combined with the explicit expressions for its constituents (cf. the Appendix IC), Eqn. (4.12) is exact within our mean-field approach. It agrees remarkably well with Monte Carlo data, as demonstrated by Fig. 4.4. There, we compare the sum of the first 1000 terms in Eqn. (4.12), for several values of t, with simulation results. A single fit parameter is required, which converts t into the number of MCS. One sees clearly how the initially phase-segregated system disorders with time.

Having established the structure of the densities, we turn to the disorder parameter. Rewriting Eqn. (3.10) slightly, we obtain [9]:

$$\mathcal{A}(L,E;t) = \frac{d}{2}L^d\left[1 - \frac{1}{L}\int_{-L/2}^{+L/2} dy\,\psi^2(y,t)\right] + O(L^{d-1})\ . \tag{4.13}$$

We emphasize that the boundary conditions only affect surface terms. These will be neglected in the following, leading only to small errors since $L \geq 20$ in the data. To the same accuracy, the initial condition for $\mathcal{A}$ is just $\mathcal{A}(L,E;0) = 0$. Using Eqn. (4.12) and carrying out the integral, we find the time evolution of the disorder parameter, for *brick wall* boundary conditions:

$$\mathcal{A}_R(L,E;t) = \frac{d}{2}L^d\left[1 - \frac{1}{EL}\sum_{n=1}^{\infty} A_n^2\exp(-2\kappa_n t)\right]\ . \tag{4.14}$$

Here, we have introduced a subscript, R ("reflecting"), to distinguish this expression from its counterpart for periodic boundary conditions, labelled P ("periodic") which we will presently discuss.

We conclude by focusing briefly on the case of *fully periodic* boundary conditions. The steady-state solutions of Eqns. (4.3) and (4.4), consistent with the constraints (4.5), are $\phi_o(\mathbf{r}) = 1/L^d$ and $\psi_o(\mathbf{r}) = 0$. To obtain the time-dependent excess density $\psi(\mathbf{r},t)$, we invoke the separation of time scales again. Noting that the vacancy density has equilibrated at the beginning of the intermediate regime, we insert its steady-state form, ϕ_o, into Eqn. (4.4), whence

$$\partial_t\psi(\mathbf{r},t) = \nabla[\phi_o(\nabla + E\hat{\mathbf{y}})\psi(\mathbf{r},t)]$$

This simplified form holds in the intermediate and late regimes. A Galilei-transformation $\mathbf{r} \equiv \mathbf{r}' + E\phi_o\hat{\mathbf{y}}t$ recasts it as an ordinary diffusion equation, with diffusion coefficient ϕ_o:

$$\partial_t\psi(\mathbf{r}',t) = \phi_o\nabla^2\psi(\mathbf{r}',t) \tag{4.15}$$

Quite remarkably, we observe that all effects of the field disappear in a suitably chosen *co-moving* frame. Thus, the solution of Eqn. (4.15) and the accompanying disorder parameter can be read off immediately from Eqn. (3.12) [9]. In the original frame, the whole profile $\psi(\mathbf{r},t)$ *drifts* with velocity $-EL^{-d}\hat{\mathbf{y}}$. Of course, no such drift is observed in $\mathcal{A}_P(L,E;t)$, by virtue of the spatial integration in Eqn. (4.13):

$$\mathcal{A}_P(L,E;t) = \frac{d}{2}L^d\left[1 - \frac{8}{\pi^2}\sum_{n=1,3,\ldots}^{\infty}\frac{\exp(-2\kappa_n t)}{n^2}\right] \tag{4.16}$$

where $\kappa_n \equiv (2\pi n)^2/L^{d+2}$.

This completes the discussion of our mean-field equations and their solutions. We now turn to the underlying scaling behavior and compare it to Monte Carlo data.

4.5 Dynamic scaling: Analytic predictions and numerical tests

In this section, we extract the scaling forms for the number of broken bonds, $\mathcal{A}(L, E; t)$. We begin with Eqn. (4.14) for *brick wall* boundary conditions. In the Appendix ID, it is shown that both the coefficients A_n and the eigenvalues κ_n exhibit characteristic scaling forms: A_n is a function of the new scaling variable LE alone, while the eigenvalues obey

$$\kappa_n = L^{-(d+2)} g_n(LE)$$

where g_n is a known function (cf. Appendix ID). Therefore, the scaling form of $\mathcal{A}_R(L, E; t)$ is apparent, namely,

$$\mathcal{A}_R(L, E; t) = L^d \mathcal{F}_R\left(LE, t/t_c\right) \ . \tag{4.17}$$

where $\mathcal{F}_R$ is an appropriate scaling function. The temporal scale factor t_c is itself still a function of LE and can be chosen in different ways. Here, we focus on the crossover from the intermediate to the saturation regime and define t_c as a measure for the *late crossover time*,

$$t_c(L, E) \equiv \kappa_1^{-1} = L^{d+2} \tau_c(LE) \tag{4.18}$$

The limits of the scaling function $\tau_c \equiv g_1^{-1}$ are discussed in the Appendix ID: It approaches its field-free limit for *vanishing* LE and increases exponentially with LE in the *opposite* limit, reflecting the increasing confinement of the vacancy. We already note one of our key results here, namely the emergence of a *new* scaling variable, LE. Its physical origin is clear: it determines how easily the vacancy can escape from the top ($y = L/2$) edge of the system, where the field tends to localize it, in order to travel to the center of the system where most of the disordering is taking place.

It is interesting to contrast the behavior of the disorder parameter, and hence the scaling function $\mathcal{F}_R$ for "late" and "early" times, $t/t_c \gg 1$ and $t/t_c \ll 1$ (but already within the intermediate regime) respectively. For late times, the disorder parameter has saturated so that $\lim_{y\to\infty} \mathcal{F}_R(x, y) = d/2$ independent of $x \equiv LE$. The short-time limit requires some care since Eqn. (4.14) does not converge well there. However, using a Poisson resummation (see Appendix ID for details), we can recast it in an alternate form that converges rapidly for small $\zeta \propto t/t_c$:

$$\mathcal{A}_R(L, E; t) \simeq \frac{d}{2} L^d \frac{8}{\sqrt{\pi}} \sqrt{t/t_s} \left\{1 + O\left[\exp(-\pi^2/\zeta^2)\right]\right\} \tag{4.19}$$

Thus, we conclude that the disorder parameter increases as a power law, t^β, for short times, with an exponent $\beta = 1/2$. The *short-time* scale factor exhibits a similar scaling form as the late crossover time,

$$t_s(L, E) = L^{d+2} \tau_s(LE) \ . \tag{4.20}$$

but we emphasize that its scaling function τ_s *differs* from τ_c in its dependence on LE. This feature finds its origin in the short-time limit of the scaling function, $\lim_{y\to 0} \mathcal{F}_R(x, y) = \mathcal{G}_R(x) y^{1/2}$, expressed by Eqn. (4.19): The presence of the second argument, $x = LE$, leads to the non-trivial prefactor $\mathcal{G}_R(x)$ which translates between the two scaling functions τ_s and τ_c.

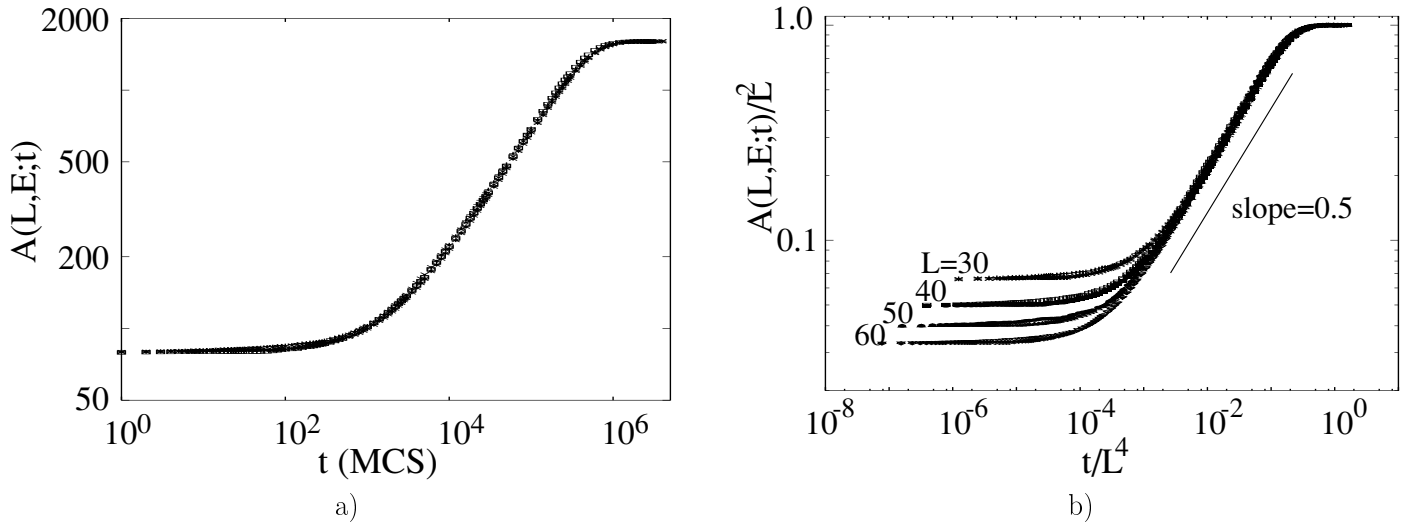

Figure 4.5: *Plot of the total number of broken bonds with PBC. (a) Plot of* $A(L,E;t)$ *vs* t *of* 40×40 *with* $E = 0.00(+), 0.10(\times), 1.00(*)$ *and* $10.0(\sqcap)$. *(b) Scaling plot of* $A(L,E;t)/L^2$ *vs* t/L^4 *for* $L = 30-60$ *with* $E = 0.00, 1.00$ *and* 10.0.

Before turning to a comparison with the data, we first contrast Eqns. (4.17-4.20) with the corresponding results for periodic boundary conditions:

$$\mathcal{A}_P(L,E;t) = L^d \mathcal{F}_P\left(tL^{-(d+2)}\right) \equiv L^d \mathcal{F}_P(t/t_c)\ . \tag{4.21}$$

All dependence on E *disappears* here: The scaling function $\mathcal{F}_P$ has been discussed in chapter 3 [9], and the late crossover time t_c is just L^{d+2}. A Poisson resummation yields the short-time behavior $\mathcal{A}_P \propto \frac{d}{2} L^d \sqrt{t/t_c}\,\{1 + O\left[\exp(-\pi^2/\zeta^2)\right]\}$, for $\zeta \propto t/t_c \ll 1$. Thus, we also find a power law increase here, $\mathcal{A}_P \propto t^\beta$, with the *same* exponent $\beta = 1/2$.

These predictions are tested in Figs. 4.5 and 4.6, for periodic and reflecting boundary conditions, respectively.

In Fig. 4.5a, we show the disorder parameter $\mathcal{A}_P$, for *one* system size but *several* values of E. Some slight deviations are observable at short times, before the vacancy density equilibrates. In the intermediate and late regimes, however, it is quite striking yet entirely consistent with our expectations that all data points fall onto the same curve, without any scaling being required. In Fig. 4.5b, we show a scaling plot for *several* L *and* E. Excellent data collapse is observed in the intermediate and late regimes, where our scaling predictions are expected to hold. Again, we emphasize that the scaled axes depend only on L, but not on E.

Fig. 4.6 shows the disorder parameter $\mathcal{A}_R$ for reflecting boundary conditions. Several values of E are plotted, for $L = 40$. As anticipated, the mixing process proceeds more slowly for larger values of E, since these tend to confine the vacancy more strongly to the upper edge ($y = +L/2$) of the system. The corresponding scaling plot is shown in Fig. 4.6b: Here, several values of L and E are chosen such that $LE = 2.0$ remains *constant*. The data collapse in the intermediate and late regimes lends full support to our prediction, Eqn. (4.17).

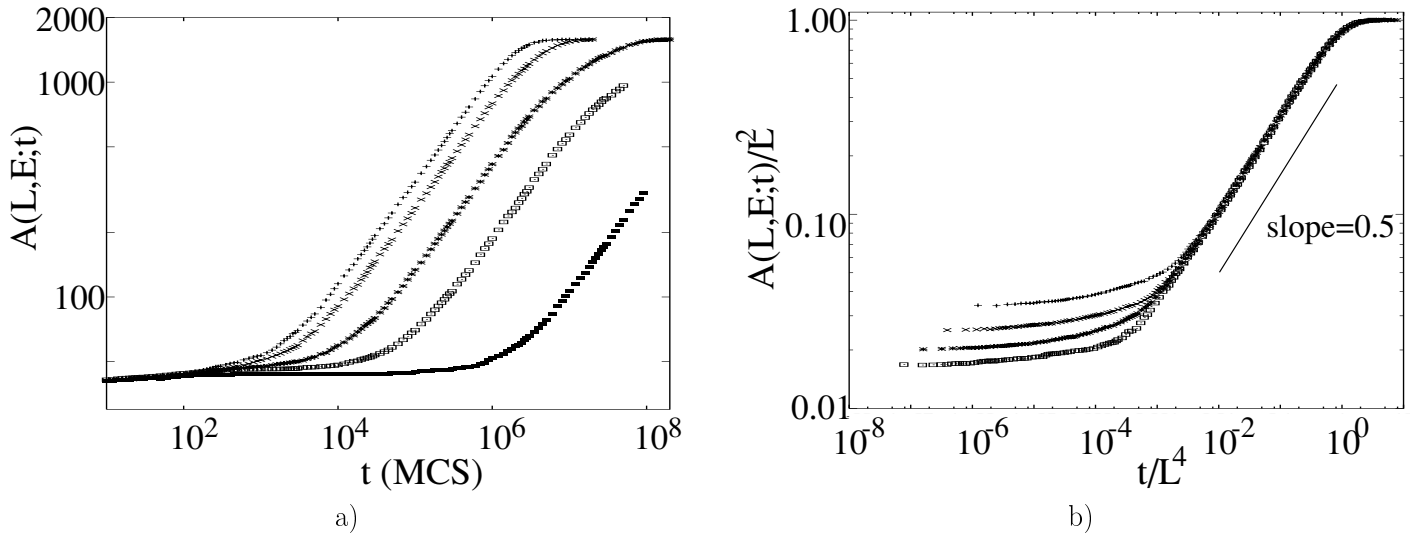

Figure 4.6: *Plot of the total number of broken bonds with BWBC. (a) Plot of* $A(L,E;t)$ *vs* t *of* 40×40 *with* $E = 0.00(+), 0.10(\times), 0.20(*), 0.30(\ )$ *and* $0.50(\diamondsuit)$. *(b) The scaling plot of* $A(L,E;t)/L^2$ *vs* t/L^4 *for L=*$30(+), 40(\times), 50(*)$ *and* $60(\sqcap)$ *with* $LE = 2.0$.

Focusing on the intermediate regime ($O(L^2) \leq t \ll t_c$), Figs. 4.5b and 3.6b show very clearly that the disorder parameter increases as a *power law* there, $\mathcal{A}(L,E;t) \propto t^\beta$. Since this behavior persists over at least three decades, we can extract a reliable numerical estimate for the exponent, resulting in $\beta = 0.5 \pm 0.01$ for both reflecting and for periodic boundary conditions, in agreement with our prediction.

Our results so far can be summarized more succinctly. Defining a set of characteristic exponents and scaling functions, the scaling of the disorder parameter, for both types of boundary conditions, can by written as

$$\mathcal{A}(L,E;t) \sim L^\alpha \mathcal{F}\left(LE, t/t_c\right) \qquad with \qquad t_c(L,E) \sim L^z \tau(LE)\ . \tag{4.22}$$

Remarkably, we find that the *exponents* α and z are *universal*, i.e., independent of boundary conditions and drive. Our results, $\alpha = d$ which is exact and $z = d + 2$ which follows from our mean-field theory, are completely consistent with the Monte Carlo data and agree with the corresponding exponents for the unbiased case [9]. The short-time behavior can be written as

$$\mathcal{A}(L,E;t) \sim L^\sigma (t/\tau_s)^\beta\ , \tag{4.23}$$

with a "growth" exponent $\beta = 1/2$ which is also manifestly universal. The additional exponent σ is related to the others via the consistency condition $\mathcal{A}(L,E;t_c) \sim \mathcal{A}(L,E;t \to \infty)$, whence $\sigma = d - z\beta = (d-2)/2$. This scaling law is obviously satisfied by our results.

In contrast to the exponents, the scaling *functions* $\mathcal{F}$ and τ are profoundly affected by the bias and the boundary conditions. For PBC, we just recover the results of the unbiased case, whereas a nontrivial dependence on a new scaling variable, LE, emerges in the brick wall case.

So far, we have restricted our attention to systems containing only a single vacancy. However, in real systems, one should expect that the number of vacancies, M, scales with system size [9], with a *vacancy number exponent* $0 \leq \gamma \leq d$, defined via $M \sim L^{\gamma}$. Thus, $\gamma = 1$ describes a situation where the vacancies ("defects") prefer the interfacial region before the upquench occurs. Our previous results correspond to the case $\gamma = 0$ but are easily extended. We simply need to modify the normalization condition for the hole density profile, Eqn (4.5), so that the constant C, given in Eqn (4.9), becomes $C = EL/[2L^{d-\gamma}\sinh(EL/2)]$. As a consequence, the late crossover time, Eqn (4.18), now scales as $t_c(L,E) = L^{d+2-\gamma}\tau_c(LE)$, so that $z = d+2-\gamma$ and $\sigma = (d+\gamma-2)/2$. Of course, these exponents are again universal.

Chapter 5

Summary, discussion and conclusion

In this part, we analyzed the vacancy-driven disordering process of an initially phase segregated binary system, seeking dynamic scaling behavior and associated universal features. Our starting point was a base-line study [9] focusing on a dilute Ising model with a very small concentration of vacancies. Their number scales with the linear system size L as L^γ, where the vacancy exponent γ is a parameter. Following a temperature upquench from $T = 0$ to $T = \infty$, each vacancy performs a simple Brownian random walk which scrambles the background spins. To quantify the evolution of the system from the perfectly phase-segregated initial state to the completely disordered final state we monitor the number of broken bonds, $\mathcal{A}(L, t)$, as a function of time t. This disorder parameter allows us to identify three well-separated temporal regimes, distinguished by the distribution of the particles and the vacancies through the system. Our key result is that the intermediate and late stages of this process exhibit dynamic scaling. A set of exponents $\{z_e, z_l, \alpha, \sigma; \beta\}$ can be defined, characterizing, respectively, the system size dependence of two crossover times, the final saturation value of the disorder parameter, and its amplitude in the intermediate regime. The temporal growth of $\mathcal{A}$ during the latter regime is captured by the exponent β. A set of equations of motion for the vacancy and magnetization densities can be solved in a mean-field approximation, so that all exponents can be computed analytically, in excellent agreement with the data. In particular, one finds that the typical time scale $t_l \sim L^{z_l}$, which controls the crossover between increasing disorder and saturation, is set by $z_l = 2 + d - \gamma$, and thus depends explicitly on both the space and vacancy dimensionalities, d and γ. Measurements of z_l can therefore provide information about the vacancy distribution in a sample. In the most familiar case, standard vacancy diffusion in solids, the number of vacancies is extensive ($\gamma = d$), so that the well-known result $z_l = 2$ is reproduced [11]. In contrast, in two dimensions we find $z_l = 4$ for a single vacancy ($\gamma = 0$) and $z_l = 3$ if the defects are generated at the initial interface.

Our work extends the findings of the base-line study in two directions. First, we consider upquenches to *finite* temperatures $T > T_c$. This is a non-trivial modification since the hopping rates of the vacancy now depend on the spin configuration in its vicinity: this introduces a *feedback* mechanism which was absent for Brownian vacancies. Since the final temperature remains above the coexistence line of the Ising model, the steady state is still disordered; however, some

correlations persist which result in a lowering of the saturation value of $\mathcal{A}$, compared to its $T = \infty$ value. Performing Monte Carlo simulations for a range of temperatures T, we seek to establish whether the scaling exponents and scaling functions of the Brownian vacancy case remain valid. For *finite* temperature $T \geq 1.5T_c$, we observe that these scaling forms still hold. Even though interparticle interactions now play a role, correlations in the system are still short-ranged, so that the vacancy still performs a random walk if viewed on a length scale which exceeds the correlation length, $\xi(T)$. As T approaches T_c, however, $\xi(T)$ reaches $O(L)$ so that the simple random walk scenario must break down. In our simulations, significant deviations from the high-temperature scaling form appear already for $T = 1.1T_c$, where $\xi(T) \simeq 6$, in units of the lattice spacing [28].

All the investigations above are focused on up-quenches to the disordered state. A natural extension of this project is to set the final temperature below criticality. Needless to say, new questions and interesting phenomena can be expected. In particular, the final equilibrium state is still phase separated, so that all the interfacial properties come into play. With a single vacancy in a finite system, there may be a further separation of time scales. We expect that, soon after the early stage, the "intrinsic" density profile of the interface will be built. At this point, the interfacial width, w, is most likely controlled by ξ. On the other hand, at sufficiently long times, the capillary waves will surely make their presence felt. In the $d = 2$ case, the interface is always rough, so that we can always expect the latter crossover to occur. How, and if, $w(\xi, L; t)$ scales will be of great interest. Besides dynamics and timescales, we could study the equilibrium probability profile of the *vacancy*, i.e., where the vacancy spends most of its time. In case more than one vacancy is present, this profile should map into a density profile for the vacancies. In either case, we expect the vacancies to be trapped, to a greater or lesser extent, at the interface. Now, if more and more vacancies are added to system, the interface profile should be altered, since a preponderance of vacancies may significantly modify the interfacial energy. For $d = 3$ Ising models, there are further interesting phenomena, associated with roughening transitions. Given that interfacial energies should depend on vacancy concentrations, how the locations (if not the nature) of such transitions are affected is a natural question. Finally, it would be interesting to study the dynamic content of these systems, such as scaling properties, when the up-quench is set at the roughening temperature.

Finally, we should add a few remarks on the early regime. As pointed out above, for an infinite system with a single vacancy, this is the *only* regime. First, notice that only the phenomenon of interfacial destruction is relevant, since bulk disordering would take infinitely long times. Next, considering the effective range of a Brownian walker, it is clear that the size of the disordered region grows at most with $t^{1/2}$. In more detail, we see that there are two distinct types of disorder. Loosely, we will label them "transverse" and "longitudinal." The first type is associated with a monolayer-like disorder from the initially sharp interface, spreading from where the vacancy began its journey. In particular, each time the vacancy crosses the plane at a new location, a particle is moved into the "wrong" phase. Thus, we may expect transverse disorder to spread like $t^{1/2}$. The second type is a measure of the width of the interfacial profile. For this to occur, the vacancy must "carry" e.g. a black particle deeper and deeper into the sea of white ones. Thus, the return probability of the walker plays a crucial role. Only in $d = 2$ is this probability both relevant and non-trivial. Applying the well-known results of random walks [3], it is found that "longitudinal" disorder grows as $(\ln t)^{1/2}$[24].

The second extension of the base-line study maintains infinite final temperature, but includes the effect of a bias, acting like an electric or gravitational field on the sample. Two types of boundary conditions, reflecting ("brick wall") and periodic, were studied. Starting from a perfectly phase-segregated initial configuration, the vacancy mediates atom exchanges, leading to fully disordered *exactly known* final states. For brickwall boundary conditions, the final state is an *equilibrium* one, characterized by a Boltzmann distribution and an exponential hole density profile. In contrast, the steady state established by periodic boundary conditions is a *non-equilibrium* one, with homogeneous configurational distribution and profiles. Using Monte Carlo simulations, we have monitored the time evolution of the system by measuring local profiles and the disorder parameter. For both types of boundary conditions,the familiar three temporal regimes emerge again: the early one, where the vacancy has not reached the boundaries of the system, the intermediate one in which the vacancy has already equilibrated, but the particle distributions are still inhomogeneous, and the late (saturation) regime where the system has reached steady state. To predict scaling exponents and scaling functions, we developed a theoretical description in terms of a set of mean-field equations of motion for the local densities. Invoking the separation of time scales, the mean-field equations can be solved exactly in the intermediate and late time regimes, providing us with explicit expressions for the observables of interest. We find that the disorder parameter exhibits dynamic scaling and observe excellent agreement of Monte Carlo data and mean-field predictions. Once again, it is natural to explore to what extent the scaling exponents and scaling functions for Brownian vacancies survive. Remarkably, we recover the same set of *universal scaling exponents* as in the unbiased case, independent of bias and boundary conditions. For example, in all cases the number of broken bonds increases as $t^{1/2}$, before saturating at a value of $O(L^d)$. In contrast, the scaling *functions* for the disorder parameter exhibit a *lesser* degree of universality: While they remain independent of the bias in the case of periodic boundary conditions, an additional scaling variable, LE, must be taken into account for reflecting boundary conditions. This variable also controls the shape of the excess density (magnetization) profile.

We conclude by noting the different symmetries which characterize the BWBC and the PBC case, in the *presence* of the bias. Periodic boundary conditions are compatible with translational invariance, but violate the detailed balance condition: the driving force is not compensated by a chemical potential gradient. In contrast, detailed balance holds for reflecting boundary conditions, but translational invariance is broken. It is quite remarkable that the scaling exponents remain unaffected by such profound differences in symmetry. Moreover, as we saw in the first part of our studies, the same scaling exponents also describe upquenches to finite temperatures above T_c, where interparticle interactions come into play. This considerable degree of universality is the key result of our work.

Even though our model is very simple, it forms the basis for the description of a large variety of related systems. Moreover, it is truly gratifying that considerable analytic progress is possible for a problem that is both *nonlinear* and *time-dependent*.

Part II

The System without Conservation of Total Magnetization

Chapter 6

Introduction and Outline

In this part we shall focus on systems violating the conservation of total magnetization.[1] Again, we consider one or several Brownian agent (BA) which disorder a binary system. If we represent the binary system in Ising language by up- or down-spins, the key dynamic process here is the flipping ("switching") of a local spin when it encounters the BA. In chapter 7 we shall study the simplest possible model, where the switching probability is independent of the value of the local spin. We first define the model carefully (section 7.1), using discrete space and time, within the master equation formulation of stochastic processes. We shall derive some general statistical properties of the process, but we shall not enter into any explicit calculations. This is deferred to sections 7.2 in which we introduce a very simple continuum theory for the process, which is motivated by viewing the process as a stochastic cellular automaton. Using the complementary descriptions of quantum mechanics (*i.e.* the Schrödinger equation and the Feynman path integral), we shall demonstrate its equivalence to the master equation formulation of section 7.1. We then examine the case of one spatial dimension in section 7.3. The model is tractable, and a great deal of information may be derived concerning the mean density of disordered elements, their spatial correlations, and finally their entire distribution function. In section 7.4, we present results from extensive numerical simulations of the discrete process. In all cases, we find good agreement between the simulation results and the predictions of the continuum theory.

In order to make contact with a wider range of processes it is necessary to consider a more general model. This is the aim of the work in chapter 8. We shall extend our original investigation in three directions. First, we shall present a careful analysis of two spatial dimensions. We concentrate on calculating $\bar{\rho}$. Given that two is the critical dimension of the process, we need to introduce some form of regularization, and the results are modulated by logarithmic corrections. Therefore great care is needed to compare different theoretical predictions and numerical results. We shall present (briefly) four alternative methods of calculation, and show that they all predict the same asymptotic behavior, and agree with the numerical simulations once the strong corrections to scaling are included. Using these results, we are also able to approximately reconstruct the probability distribution for the density of disorder.

Second, we shall consider a system containing more than one BA, thereby inducing "compe-

[1] The work in this part has been done in collaboration with T.J. Newman

tition" as each BA interferes with the disorder created by the others. We derive an exact integral expression (for asymptotically large times) for the disordering efficacy $\sigma_N(d)$ (*i.e.* the global amount of disorder due to N agents as compared to one agent) for arbitrary N. The main result here is that the disordering efficacy is massively reduced for dimensions less than two, whereas in precisely two dimensions, each BA eventually becomes independent (in that the disorder it creates is not reordered by other BA's). We shall present calculations based on the continuum model to make these statements quantitative.

Third, we shall consider two kinds of generalized couplings between the BA and the binary medium: asymmetric and quenched random switching probabilities. In the former case, the spin flips $0 \to 1$ and $1 \to 0$ occur with different probabilities, while in the latter, these probabilities acquire different values at each lattice site, represented as quenched random variables. We shall argue that these generalized couplings may be modeled within the continuum limit by simple generalizations of our original model, based on the idea that relative to the non-zero "background disorder" the dynamics of the system are the same as the symmetric case. In this case we argue that $\bar{\rho}$ picks up logarithmic corrections in time, while the global amount of disorder remains unaffected. We shall also discuss the quenched average of the distribution function of disorder density, and show that it is very sensitive to the distribution of the couplings. In all cases, we shall support our results by numerical simulations of the underlying lattice model.

We end this part with a summary, discussion and conclusions to both chapters.

Chapter 7

Binary data corruption due to a Brownian agent I

7.1 Discrete formulation of the model

We consider binary data bits on a d-dimensional hypercubic lattice. For convenience we shall represent each bit by an Ising spin $\sigma_{\mathbf{r}}$, where the index $\mathbf{r}$ represents a discrete lattice vector. The spin takes the value $+1(-1)$ for a data bit which is uncorrupted (corrupted). Thus, the initial configuration is a lattice of spins, all of which take the value $+1$. For later reference, we note that it is of course easy to translate the lattice spins back into corrupted or uncorrupted data bits, via $\sigma_{\mathbf{r}}$ by $(1-2n_{\mathbf{r}})$, where $n_{\mathbf{r}}$ denotes the presence (with value unity) or absence (with value zero) of a corrupted bit. Using spin language allows us to use such familiar concepts as 'magnetization density', or 'global magnetization'. Similarly, we shall often refer to the average magnetization density m, which is related to the average density of corrupted bits $\bar{\rho}$ via $m = 1-2\bar{\rho}$. We denote the position of the BA by the lattice vector $\mathbf{R}$. At each time step, the BA has a probability p to make a jump to one of its $(2d)$ nearest neighbors. For the sake of generality, we will not insist that the BA always flips a spin (*i.e.* changes a data bit) as it moves. Thus, on a given jump, we allow the BA to flip the spin at the site it is leaving with a probability q. We illustrate the process in Fig 7.1, for the case $d = 2$ and $q = 1$.

In this section we shall describe the process via a master equation. Namely, we shall define the dynamics through the evolution of the distribution $P(\mathbf{R}, \{\sigma_{\mathbf{r}}\}, t)$, which is the probability that at time t the BA is at position $\mathbf{R}$, and the spins have configuration $\{\sigma_{\mathbf{r}}\}$. Given the above rules, the master equation takes the form

$$\begin{aligned} P(\mathbf{R}, \{\sigma_{\mathbf{r}}\}, t+\delta t) = (1-p)P(\mathbf{R}, \{\sigma_{\mathbf{r}}\}, t) &+ \frac{p(1-q)}{2d}\sum_{\mathbf{l}} P(\mathbf{R}+\mathbf{l}, \{\sigma_{\mathbf{r}}\}, t) \\ &+ \frac{pq}{2d}\sum_{\mathbf{l}} P(\mathbf{R}+\mathbf{l}, \cdots, -\sigma_{\mathbf{R}+\mathbf{l}}, \cdots, t) \ , \end{aligned} \tag{7.1}$$

where $\{\mathbf{l}\}$ represent the $2d$ orthogonal lattice vectors (which have magnitude l).

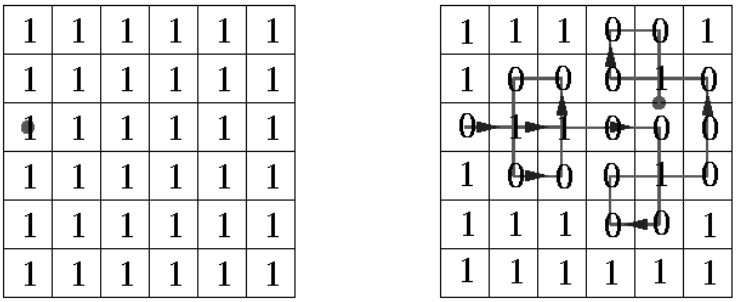

Figure 7.1: *Illustration of the data corruption process for $d = 2$. The initial uncorrupted state is shown on the left, with the BA represented by the filled circle. On the right we show a typical walk of ~ 20 steps. The BA flips a spin with each visit, so those spins visited an even number of times are restored to their original value.*

The natural quantities to extract from the distribution P are marginal averages. The simplest is the mean value of the spin at position $\mathbf{r}_1$ at time t, given the BA is at position $\mathbf{R}$. This is defined via

$$\Theta(\mathbf{r}_1, \mathbf{R}, t) \equiv \mathrm{Tr}_\sigma \ \sigma_{\mathbf{r}_1} \ P(\mathbf{R}, \{\sigma_{\mathbf{r}}\}, t) \ . \tag{7.2}$$

Higher order marginal averages may be defined accordingly. Performing the spin trace over the master equation with a weight of $\sigma_{\mathbf{r}}$ yields

$$\begin{aligned} \Theta(\mathbf{r}, \mathbf{R}, t + \delta t) - \Theta(\mathbf{r}, \mathbf{R}, t) &= \frac{p}{2d} \sum_{\mathbf{l}} [\Theta(\mathbf{r}, \mathbf{R} + \mathbf{l}, t) - \Theta(\mathbf{r}, \mathbf{R}, t)] \\ &- \frac{pq}{d} \ \Theta(\mathbf{r}, \mathbf{r}, t) \sum_{\mathbf{l}} \delta_{\mathbf{r}, \mathbf{R}+\mathbf{l}} \ . \end{aligned} \tag{7.3}$$

The above equation has a physically appealing form. The rate of change of Θ has two contributions. The first is lattice diffusion, as given by the first sum on the r.h.s. The second contribution vanishes unless the spin in question is in the immediate vicinity of the BA, in which case it acts as a sink.

At this point in the discussion it is worthwhile to consider the continuum limit. Namely we take the time scale δt and the lattice scale l to zero, and define a diffusion constant $D \equiv l^2 p/\delta t$. We also introduce a coupling $\lambda \propto pqld/\delta t$. Then replacing the Kronecker δ-function in Eqn. (7.3) by a Dirac δ-function we find

$$\partial_t \Theta(\mathbf{r}, \mathbf{R}, t) = \frac{D}{2} \nabla^2_{\mathbf{R}} \Theta(\mathbf{r}, \mathbf{R}, t) - \lambda \ \Theta(\mathbf{r}, \mathbf{r}, t) \delta^d(\mathbf{r} - \mathbf{R}) \ . \tag{7.4}$$

It is important to note that this continuum equation is not strictly derived from Eqn. (7.3), as we have not proved that the continuum limit exists. In fact, we shall find that for $d \geq 2$, the lattice scale l is crucial, and consequently we must soften the Dirac δ-function to a function $\Delta_l(\mathbf{r})$ which is sharply peaked (over a linear scale l) with unit integral over $\mathcal{R}^d$. One actually expects

this to be the case, as Eqn. (7.4) is the imaginary-time Schrödinger equation for a particle under the influence of a repulsive δ-function potential. [Note the independent spatial variable in this quantum system is $\mathbf{R}$, with the variable $\mathbf{r}$ simply labelling the position of the potential.] It is well known [44] that the repulsive δ-function potential is 'invisible' to the particle for $d \geq 2$, and one usually cures this by smearing the potential just as described above. The quantum mechanics analogy will prove useful in the next section when we construct an alternative continuum model.

Before leaving this section we shall indicate the derivation of a non-trivial statistical relation hidden inside Eqn. (7.3). First, we must define the initial condition. As mentioned before, given that up-spins denote uncorrupted data, the initial value of each spin is $+1$. There is a slight subtlety of definition regarding the value of the spin at the site where the BA is initially planted. (This position shall be taken to be the origin, without any loss of generality.) We shall take this spin to be initially -1 so that immediately after the BA has moved away the spin at the origin has value $+1$. Thus we have

$$P(\mathbf{R}, \{\sigma_{\mathbf{r}}\}, 0) = \delta_{\mathbf{R},\mathbf{0}} \delta_{\sigma_{\mathbf{0}},-1} \prod_{\mathbf{r}\neq\mathbf{0}} \delta_{\sigma_{\mathbf{r}},1} \ , \tag{7.5}$$

and consequently,

$$\Theta(\mathbf{r}, \mathbf{R}, 0) = \delta_{\mathbf{R},\mathbf{0}}(1 - 2\delta_{\mathbf{r},\mathbf{0}}) \ . \tag{7.6}$$

We may obtain the following two averages from $\Theta(\mathbf{r}, \mathbf{R}, t)$. The first is the average value of the spin at the origin. This is simply given by $m_{\mathbf{0}}(t) = \sum_{\mathbf{R}} \Theta(\mathbf{0}, \mathbf{R}, t)$. The second average is the quantity $\sum_{\mathbf{R}} \Theta(\mathbf{R}, \mathbf{R}, t)$, which corresponds to averaging the value of the spin at the site where the BA happens to be at time t. One can prove that

$$\sum_{\mathbf{R}} \Theta(\mathbf{0}, \mathbf{R}, t) = \sum_{\mathbf{R}} \Theta(\mathbf{R}, \mathbf{R}, t) \ , \tag{7.7}$$

for all t. We arrive at the above result by essentially solving the partial difference equation (7.3) using discrete Fourier and Laplace transforms. The details can be found in Appendix IIA.

This result is useful for proving a more physically relevant relation. Let us denote the average global magnetization by

$$M(t) = \sum_{\mathbf{R}} \sum_{\mathbf{r}} [\Theta(\mathbf{r}, \mathbf{R}, 0) - \Theta(\mathbf{r}, \mathbf{R}, t)] \ , \tag{7.8}$$

where we have defined it relative to the (infinite) initial magnetization. This quantity essentially measures the average of the total number of corrupted bits (up to a factor of 2). Summing Eqn. (7.3) over $\mathbf{r}$ and $\mathbf{R}$ gives

$$M(t + \delta t) - M(t) = 2pq \sum_{\mathbf{r}} \Theta(\mathbf{r}, \mathbf{r}, t) \ . \tag{7.9}$$

Then using (7.7) we can rewrite the above relation in the form

$$M(t + \delta t) - M(t) = 2pq \sum_{\mathbf{R}} \Theta(\mathbf{0}, \mathbf{R}, t) = 2pq \ m_{\mathbf{0}}(t) \ . \tag{7.10}$$

In other words, the rate of change of the mean global magnetization is proportional to the mean magnetization density at the origin. This is a non-trivial relation between a global and a local quantity.

In principle, one can obtain exact results for many interesting quantities (like the mean magnetization density, or correlation functions) by directly solving for the marginal averages, as illustrated in Appendix IIA. However, we prefer to obtain results from a continuum theory; partly because the calculations are a little easier, but more importantly because we can access more sophisticated properties of the system, such as the probability distribution of the coarse-grained magnetization density.

7.2 Continuum theory

In this section we shall motivate a particularly simple continuum description of the data corruption process, and show its equivalence to the discrete theory of the previous section.

There is an alternative method of characterizing the evolution of the system, other than using the evolution of the probability distribution $P(\mathbf{R}, \{\sigma_{\mathbf{r}}\}, t)$ via the master equation. This method consists of writing the local rules for the process in the spirit of a stochastic cellular automaton (SCA) [45]. Let us focus on the case that at each time step the BA makes a random jump to one of its nearest neighbors, and that the spin at the site which it leaves behind, definitely flips. This corresponds to setting $p = q = 1$. The local rules for such a process are easily written down. Let us denote the time-dependent position of the BA by $\mathbf{R}(t)$, a randomly chosen unit lattice vector by $\mathbf{l}(t)$, and the time-dependent value of the spin at site $\mathbf{r}$ by $\sigma_{\mathbf{r}}(t)$. Then we have

$$\mathbf{R}(t + \delta t) = \mathbf{R}(t) + \mathbf{l}(t) \tag{7.11}$$

$$\sigma_{\mathbf{r}}(t + \delta t) = \sigma_{\mathbf{r}}(t)(1 - 2\delta_{\mathbf{r},\mathbf{R}(t)}) \tag{7.12}$$

We are interested in a continuum limit of these two rules. The first is nothing more than a random walk. We take the lattice vector $\mathbf{R}(t)$ to be a continuum vector (*i.e.* each of the d components is a real number), and we replace the random unit lattice vector $\mathbf{l}(t)$ by a continuum vector $\xi(t)$, each component of which is a uncorrelated Gaussian random variable with zero mean (*i.e.* $\xi_i(t)$ is a white noise process). The correlator of ξ is given by

$$\langle \xi_i(t)\xi_j(t') \rangle = D'\delta_{i,j}\delta(t - t') \ , \tag{7.13}$$

where here and henceforth, angled brackets indicate an average over the noise (or equivalently the paths of the BA). Then, on taking $\delta t \to 0$, Eqn. (7.11) assumes the form

$$\frac{d\mathbf{R}}{dt} = \xi(t) \ , \tag{7.14}$$

which is the familiar equation for a continuum random walker where D' is the diffusion constant [43]. The second SCA rule is more complicated to generalize to the continuum. As a first step let us define a coarse-grained magnetization density $\phi(\mathbf{r}, t)$ in the following way. We imagine defining a large region around the lattice site $\mathbf{r}$ and summing all the spins in that region. Their

sum (suitably normalized) constitutes $\phi(\mathbf{r},t)$, with the label $\mathbf{r}$ denoting a point in the $\mathcal{R}^d$ continuum. An entirely analogous procedure is used in motivating the Landau-Wilson free energy functional from the Ising model of ferromagnetism [46]. The difficulty in our case is that we cannot derive a closed equation for ϕ from the discrete rule (7.12). We therefore make the following approximation. Splitting the r.h.s. of (7.12) into two pieces, we see that the first may be taken over to the l.h.s. which may then be taken to be a time derivative in the limit of $\delta t \to 0$. The second piece resembles a decay term centered at $\mathbf{r} = \mathbf{R}$. So, we postulate that the coarse-grained magnetization density satisfies

$$\partial_t \phi(\mathbf{r},t) = -\lambda' \phi(\mathbf{r},t) \delta^d(\mathbf{r} - \mathbf{R}(t)) \ , \tag{7.15}$$

where λ' is a phenomenological parameter which describes how strongly the magnetization density is coupled to the BA. We stress that the field $\phi(\mathbf{r},t)$ is a function of the continuous space and time variables $\mathbf{r}$ and t, and a *functional* of the path $\mathbf{R}(t)$ of the BA.

Now, the above heuristic derivation of the continuum theory was based on a SCA for the case in which the BA always moves ($p = 1$), and for which the spin located at the previous BA position is always flipped ($q = 1$). In general p and q are both less than unity. Intuitively we expect a very simple renormalization of our phenomenological parameters as p and q are changed. The diffusion constant D' should be proportional to p, and the strength of the spin-BA coupling λ' should be proportional to both p and, more importantly, q. Thus we see a very close correspondence between D' and λ' in the current continuum theory, and the parameters D and λ which were introduced in the continuum limit (7.4) of the discrete equation (7.3). In fact they are identical, as will emerge in the following discussion.

One of the positive features of the continuum theory as described by (7.15) is that one may immediately integrate the equation to find the magnetization density as an explicit functional of the path of the BA. As an initial condition we take $\phi(\mathbf{r},0) = 1$ for all $\mathbf{r}$. The subtlety encountered in the discrete theory concerning the initial value of the spin at the origin disappears here since the coarse grained function ϕ is not sensitive to the value of one inverted spin. Straightforward integration of (7.15) yields

$$\phi(\mathbf{r},t) = \exp\left[-\lambda' \int_0^t dt' \ \delta^d(\mathbf{r} - \mathbf{R}(t')) \right] \ . \tag{7.16}$$

It is important to note at this stage that the magnetization density ϕ is clearly positive for all $\mathbf{r}$ and t. Therefore within our continuum formulation, we have ignored paths of the BA which create large patches containing a majority of down spins (*i.e.* corrupted bits). Such patches will occur, but their frequency of occurrence is certainly very small since the system starts in a completely uncorrupted state. For instance, the probability for the BA to create a purely negative domain of N spins is of the order e^{-N}. Therefore, so long as we coarse-grain the original spin model over a sufficiently large scale, we can be confident that the most important configurations have been retained in the continuum theory. Ultimately, one must justify such an approximation *a posteriori* by comparison with either results from the discrete theory, or from numerical simulations. As we shall see, both of these support the current continuum model and the approximations contained therein.

We shall now connect the continuum theory as given by (7.16), and the continuum limit (7.4) of the discrete theory, as given by (7.3). The mean magnetization density in the discrete theory is given by

$$m_{\mathbf{r}}(t) = \sum_{\mathbf{R}} \Theta(\mathbf{r}, \mathbf{R}, t) \mathrm{CL} \longrightarrow \int d^d R \; \Theta(\mathbf{r}, \mathbf{R}, t) \tag{7.17}$$

where in the continuum limit, we have replaced the sum over BA positions by an integral, and the field Θ satisfies the imaginary-time Schrödinger equation as given in (7.4). In the alternative continuum theory, we can find the mean magnetization density by averaging the coarse-grained density $\phi(\mathbf{r}, t)$ over all paths $\mathbf{R}(t)$. Each path is weighted by a Gaussian factor

$$\mathcal{N} \exp\left\{ -\frac{1}{2D'} \int_0^t dt' \; \xi(t')^2 \right\} = \mathcal{N} \exp\left\{ -\frac{1}{2D'} \int_0^t dt' \; \left(\frac{d\mathbf{R}}{dt'} \right)^2 \right\} \; , \tag{7.18}$$

where $\mathcal{N}$ is a normalization factor. Therefore we can write the average of ϕ as a functional integral

$$\begin{aligned} m(\mathbf{r}, t) &= \langle \phi(\mathbf{r}, t) \rangle \\ &= \mathcal{N} \int \mathcal{D}\mathbf{R}(t') \; \exp\left\{ -\frac{1}{2D'} \int_0^t dt' \; \left(\frac{d\mathbf{R}}{dt'} \right)^2 \right\} \; \phi(\mathbf{r}, t) \; , \\ &= \mathcal{N} \int \mathcal{D}\mathbf{R}(t') \; \exp\left\{ -\int_0^t dt' \; \left[\frac{1}{2D'} \left(\frac{d\mathbf{R}}{dt'} \right)^2 + \lambda' \delta^d(\mathbf{r} - \mathbf{R}(t')) \right] \right\} \; , \\ &= \mathcal{N} \int d^d R_f \int^{\mathbf{R}_f} \mathcal{D}\mathbf{R}(t') \; \exp\left\{ -\int_0^t dt' \; \left[\frac{1}{2D'} \left(\frac{d\mathbf{R}}{dt'} \right)^2 + \lambda' \delta^d(\mathbf{r} - \mathbf{R}(t')) \right] \right\} \; , \end{aligned} \tag{7.19}$$

where we have used (7.16) in going from the first line to the second, and we have introduced the final position of the BA (*i.e.* $\mathbf{R}$(t)) as a free integration variable $\mathbf{R}_f$ in rewriting the second line as the third. The reason for this cosmetic change is to make explicit the fact that $\langle \phi(\mathbf{r}, t) \rangle$ can be expressed as a spatial integral over the final BA position, where the integrand is itself a path integral over BA trajectories. This path integral is nothing more than a re-expression of the solution of an imaginary time Schrödinger equation (using the well-known Feynman path integral formulation of quantum mechanics [47]) for a particle in a repulsive δ-function potential. We can now see the connection: Eqn. (7.19) is an exact restatement of Eqns. (7.4) and (7.17), with the identification $D' = D$ and $\lambda' = \lambda$. [So, henceforth we shall drop the primes in the material parameters.] To summarize, by utilizing the complementary formulations of quantum mechanics via the Schrödinger equation and the Feynman path integral, we have shown that the continuum limit of the master equation is identical to the continuum theory constructed at the beginning of this section.

Two final points are in order. First, as noted in the previous section, the δ-function potential must be replaced by a smeared function $\Delta_l(\mathbf{r})$ for $d \geq 2$; thus in our continuum theory encapsulated in Eqn. (7.15), we shall make a similar replacement when studying two or higher dimensions. Second, we have established a connection between the master equation and Eqn. (7.15) only at

the level of the first moment. It is straightforward to extend each formulation to higher order correlation functions, and indeed one finds an exact correspondence. For instance, we can define the marginal spin-spin correlation function within the discrete theory

$$\Theta(\mathbf{r}_1, \mathbf{r}_2, \mathbf{R}, t) \equiv \mathrm{Tr}_\sigma \ \sigma_{\mathbf{r}_1}\sigma_{\mathbf{r}_2} \ P(\mathbf{R}, \{\sigma_{\mathbf{r}}\}, t) \ . \tag{7.20}$$

Using the master equation one can show that in the continuum limit this function satisfies the Schrödinger equation for a particle under the influence of two repulsive δ-function potentials located at $\mathbf{r}_1$ and $\mathbf{r}_2$. Similarly, we can construct the coarse-grained two-point correlation function from Eqn. (7.16) by evaluating $\langle\phi(\mathbf{r}_1, t)\phi(\mathbf{r}_2, t)\rangle$. It is easy to see that this quantity is given by an integral over the analogous path-integral for two repulsive δ-function potentials.

Having completed our formulation of a simple continuum theory, and shown its equivalence to the continuum limit of the master equation, we shall proceed to the next section in which we present a comprehensive solution of the model in one dimension.

7.3 Results in one dimension

In this section we restrict ourselves to one dimension. This does not necessarily mean a single chain of sites. Rather, we shall exclusively study the continuum theory of the last section, and in this case, for large enough times, $d = 1$ refers to any system which has an infinite longitudinal dimension, and finite transverse dimensions (for instance an infinitely long strip). This is the case, since as time proceeds, the correlation length will eventually become greater than the transverse size of the system, thereby only allowing the longitudinal fluctuations to continue growing, as is the case in a strictly one-dimensional system.

The continuum model described in the previous section can be viewed as a 'non-conserved' cousin of the continuum theory of vacancy mediated diffusion (a process which in the spin language conserves magnetization) introduced recently [9, 8]. An exact analysis of the latter theory was possible using infinite order perturbation theory in the spin-BA coupling λ. We shall use the same technique here, as it leads rather directly to a full solution. Alternatively, one may solve the Schrödinger equation for the marginal averages. However, there are some important quantities (like the distribution of the magnetization density) which cannot be easily recovered from the latter approach.

Our starting point is the integrated solution of the continuum formulation as given in Eqn. (7.16). First, we shall derive an expression for the magnetization density $m(x, t)$. Performing a direct average of Eqn. (7.16) and expanding in powers of λ ($= \lambda'$), we have

$$m(x, t) = \langle\phi(x, t)\rangle = \sum_{n=0}^{\infty} (-\lambda)^n \chi_n(x, t) \ , \tag{7.21}$$

where $\chi_0(x, t) = 1$, and for $n > 0$

$$\chi_n(x, t) = \frac{1}{n!} \left\langle \left[\int_0^t d\tau \ \delta(x - R(\tau)) \right]^n \right\rangle \ . \tag{7.22}$$

We refer the reader to Appendix IIB in which the above average is explicitly calculated. The result is

$$\chi_n(x,t) = \int_0^t d\tau_1 \int_0^{\tau_1} d\tau_2 \cdots \int_0^{\tau_{n-1}} d\tau_n \; g(0,\tau_1-\tau_2)\cdots g(0,\tau_{n-1}-\tau_n) g(x,\tau_n) \; , \tag{7.23}$$

where $g(x,t) = (2\pi Dt)^{-1/2}\exp(-x^2/2Dt)$ is the probability density of the BA.

The structure of Eqn. (7.23) is that of an n-fold convolution, so we may utilize a Laplace transform to good effect. We have (for $n>0$)

$$\hat{\chi}_n(x,s) \equiv \int_0^\infty dt \; e^{-st} \; \chi_n(x,t) = \frac{1}{s} \; \hat{g}(0,s)^{n-1}\hat{g}(x,s) \; . \tag{7.24}$$

Performing the sum over these functions as dictated by Eqn. (7.21) we find

$$\hat{m}(x,s) = \frac{1}{s}\left[1 - \frac{\lambda \hat{g}(x,s)}{1+\lambda\hat{g}(0,s)}\right] \; . \tag{7.25}$$

We note in passing that a similar result is easily derived for any $d \in (0,2)$. The case of $d \geq 2$ is more complicated as the function $g(0,t)$ is no longer integrable.

This expression for the Laplace transform of m is exact. This will prove to be important when we come to evaluate the distribution function of $\mathcal{P}(m)$. The inverse of the Laplace transform is given by

$$m(x,t) = \mathrm{erf}\left[\frac{|x|}{(2Dt)^{1/2}}\right] + \exp\left(\frac{\lambda|x|}{D} + \frac{\lambda^2 t}{2D}\right) \; \mathrm{erfc}\left[\lambda\left(\frac{t}{2D}\right)^{1/2} + \frac{|x|}{(2Dt)^{1/2}}\right] \; , \tag{7.26}$$

where $\mathrm{erf}(z)$ and $\mathrm{erfc}(z)$ are error functions [48]. Considering the long time behavior of the above expression, we have for $x=0$

$$m(0,t) = \left(\frac{2D}{\pi\lambda^2 t}\right)^{1/2}\left[1 + O\left(\frac{D}{\lambda^2 t}\right)\right] \; . \tag{7.27}$$

One can also retrieve the spatial behavior with little effort. For small x we have

$$m(x,t) = m(0,t) + \left(\frac{2x^2}{\pi Dt}\right)^{1/2} + \cdots \quad , \; x \ll (Dt)^{1/2} \; . \tag{7.28}$$

The large x behavior has two regimes:

$$m(x,t) = 1 - \left(\frac{2Dt}{\pi x^2}\right)^{1/2}\exp\left(\frac{-x^2}{2Dt}\right) + \cdots \quad , (Dt)^{1/2} \ll x \ll \lambda t \tag{7.29}$$

$$m(x,t) = 1 - \left(\frac{\lambda t}{|x|}\right)\left(\frac{2Dt}{\pi x^2}\right)^{1/2}\exp\left(\frac{-x^2}{2Dt}\right) + \cdots \quad , x \gg \lambda t \; . \tag{7.30}$$

It is interesting to note that apart from the natural diffusion scale $(Dt)^{1/2}$, there is a larger 'ballistic' scale λt in the system, beyond which the disordering efficacy of the BA is much reduced, since it makes so few visits to these distant sites. There is no simple (i.e. single length) scaling form for $m(x,t)$.

Next we consider the continuum analogues of Eqns. (7.7)-(7.10). We define the average global magnetization (relative to its initial value) as

$$M(t) = \int_{-\infty}^{\infty} dx \ [\langle\phi(x,0)\rangle - \langle\phi(x,t)\rangle] \ , \tag{7.31}$$

which may be compared to the discrete version in Eqn. (7.8). Integrating and averaging the continuum model (7.15) yields

$$\frac{dM(t)}{dt} = \lambda\langle\phi(R(t),t)\rangle \ , \tag{7.32}$$

which is to be compared with Eqn. (7.9). This last equation indicates that we may explicitly find an expression for $\langle\phi(R(t),t)\rangle$ by calculating the time derivative of the spatial integral of $m(x,t) = \langle\phi(x,t)\rangle$. This may be done at the level of the perturbation series (7.21), from which one may show that the following relation holds exactly, for all times:

$$m(0,t) = \langle\phi(R(t),t)\rangle \ , \tag{7.33}$$

which is the continuum analogue of Eqn. (7.7). Finally, combining Eqns. (7.32) and (7.33) we have

$$\frac{dM(t)}{dt} = \lambda m(0,t) \ . \tag{7.34}$$

Thus, the non-trivial relation between the rate of change of the global magnetization, and the mean of the magnetization density at the origin, is seen to be exact within the continuum model (which complements the exact relation (7.10) found in the discrete framework). Similar results are easily obtained for all $d \in (0,2)$. Directly from Eqns. (7.27) and (7.34) we note that $M(t) \sim \sqrt{Dt}$; thus, the average number of corrupted bits in $d = 1$ increases as the square root of time, and surprisingly independent of the coupling λ.

We now turn to spatial correlations in the system. These are most easily probed via the two-point correlation function

$$\begin{aligned} C(x,t) &= \langle\phi(x,t)\phi(0,t)\rangle \\ &= \left\langle \exp\left(-\lambda \int_0^t dt' \ [\delta(x - R(t')) + \delta(R(t'))]\right)\right\rangle \ , \end{aligned} \tag{7.35}$$

where we have used the solution (7.16) in the second line. This average can be calculated using infinite order perturbation theory in λ, just as was used to evaluate $m(x,t)$. We write

$$C(x,t) = \sum_{n=0}^{\infty} (-\lambda)^n c_n(x,t) \ , \tag{7.36}$$

with $c_0 = 1$. For $n > 0$, a given term c_n can be explicitly evaluated by making integral representations of the n δ-functions, and performing the average over the paths $R(t)$ (as described in Appendix IIB). Thus one has

$$c_n(x,t) = \int_0^t d\tau_1 \int_0^{\tau_1} d\tau_2 \cdots \int_0^{\tau_{n-1}} d\tau_n \int \frac{dk_1}{2\pi}\,(1+e^{-ik_1x}) \cdots \int \frac{dk_n}{2\pi}\,(1+e^{-ik_nx}) \times \exp\left[-\frac{D}{2}\sum_{m=1}^{n}\left(\sum_{l=1}^{m} k_l^2\right)(\tau_m - \tau_{m+1})\right] , \tag{7.37}$$

with the notation $\tau_{n+1} \equiv 0$. This $2n$-fold integral can be reduced using Laplace transform in time, such that the integrals over $\{k_i\}$ may be performed, as described in Appendix IIC. The result is

$$\hat{c}_n(x,s) = \frac{1}{s(2sD)^{n/2}}\left(1+\exp\left[-\left(\frac{2s}{D}\right)^{1/2}|x|\right]\right)^n . \tag{7.38}$$

Summing over these functions with a weight of $(-\lambda)^n$ and inverting the Laplace transform using a Bromwich integral [49], we have

$$C(x,t) = \int_\gamma \frac{ds}{2\pi i}\,\frac{\exp(s\tilde{t})}{s^{1/2}[1+s^{1/2}+\exp(-s^{1/2}|\tilde{x}|)]} , \tag{7.39}$$

where, as usual, the contour γ is parallel to the imaginary axis, and to the right of any singularities. We have rescaled space and time as $\tilde{x} = x\lambda/D$ and $\tilde{t} = t\lambda^2/2D$.

This integral may be evaluated for large $\tilde{t}$ in the following way. We re-express the integral as an expansion in powers of $\exp(-s^{1/2}|\tilde{x}|)$ (which is *not* the same as our original expansion in powers of λ). So we have

$$C(x,t) = \sum_{n=0}^{\infty}(-1)^n I_n(\tilde{x},\tilde{t}) , \tag{7.40}$$

with

$$\begin{aligned} I_n &= \int_\gamma \frac{ds}{2\pi i}\,\frac{e^{s\tilde{t}-ns^{1/2}|\tilde{x}|}}{s^{1/2}(1+s^{1/2})^{n+1}} \\ &= \frac{1}{2\pi}\int_0^\infty du\,\frac{e^{-u\tilde{t}}}{u^{1/2}}\left[\frac{e^{-inu^{1/2}|\tilde{x}|}}{(1+iu^{1/2})^n}+\frac{e^{inu^{1/2}|\tilde{x}|}}{(1-iu^{1/2})^n}\right] , \end{aligned} \tag{7.41}$$

where the second line is the explicit form of the integral after integrating around the only singularity – a branch point located at $s = 0$. The integral over u may be simplified for $\tilde{t} \gg 1$ to give

$$\begin{aligned} I_n &\simeq \frac{1}{\pi\tilde{t}^{1/2}}\int_0^\infty du\,\frac{e^{-u}}{u^{1/2}}\cos\left(\frac{nu^{1/2}|\tilde{x}|}{\tilde{t}^{1/2}}\right) \\ &= \frac{1}{(\pi\tilde{t})^{1/2}}\exp\left(-\frac{n^2\tilde{x}^2}{4\tilde{t}}\right) . \end{aligned} \tag{7.42}$$

In these rescaled units, we have from Eqn. (7.27) $m(0,\tilde{t}) \simeq (\pi\tilde{t})^{-1/2}$ (for large $\tilde{t}$). Thus, we may resum the functions $\{I_n\}$ to find

$$\begin{aligned}\frac{C(x,t)}{m(0,t)} &\simeq \sum_{n=0}^{\infty}(-1)^n \exp\left(-\frac{n^2\tilde{x}^2}{4\tilde{t}}\right) \\ &= \frac{1}{2}\left[1+\theta_4\left(0,\exp(-x^2/2Dt)\right)\right] \ , \end{aligned} \tag{7.43}$$

where $\theta_4(z,q)$ is a Jacobi theta function (with norm q) [48]. Note, we have written the last line in unscaled variables, and we see that the ratio of the correlation function to $m(0,t)$ does not depend on λ for large times. The behavior of $C(x,t)$ in the limits of large and small x are as follows. For large x, the fields at the origin and at x will be uncorrelated, so that $C(x,t) \simeq m(0,t)m(x,t) \simeq m(0,t)$, the latter result following since $m(x,t) \simeq 1$ for $x \gg \sqrt{t}$. At the other extreme, as $x \to 0$, $C(x,t) \to \langle\phi(0,t)^2\rangle$. Referring to the exact solution of the continuum model, Eqn. (7.16), one can see that the second moment of the magnetization density is actually given exactly by $m(0,t;2\lambda)$ (where the last (optional) argument indicates the parametric dependence on the spin-BA coupling). So for long times we take the expression for $m(0,t;\lambda)$ given in Eqn. (7.27) and replace λ by 2λ. Therefore $\langle\phi(0,t)^2\rangle \simeq m(0,t;\lambda)/2$ for $\tilde{t} \gg 1$. Thus, the limits of the function $C(x,t)/m(0,t)$ are $1/2$ (for small x) and unity (for large x), which is naturally consistent with the analytic form given above in terms of the Jacobi theta function. In section 7.4 we shall compare this expression with results from a numerical simulation of the discrete model described earlier.

To complete our study of the properties of this system in one dimension, we shall consider the complete probability distribution $\mathcal{P}(\phi,x,t)$ of the magnetization density. We shall be able to calculate this exactly, since i) we can see from (7.16) that the n^{th} moment of the density is related to the mean density with a replacement $\lambda \to n\lambda$; and ii) we have an *exact* expression for the mean density (albeit in the Laplace transform variable s). The first point is a fortuitous property of our continuum model which we should certainly exploit. The second property is less obvious. One might imagine that, given we know all density moments via the first, even the asymptotic form for the mean density would be sufficient to calculate the probability distribution (for large times). This is not the case as we shall see – the complete analytic structure of $m(x,t;\lambda)$ is required in order to reconstruct the distribution $\mathcal{P}$.

We define $\mathcal{P}$ via

$$\mathcal{P}(\phi,x,t) = \langle\delta(\phi-\phi_R(x,t))\rangle \ , \tag{7.44}$$

where $\phi_R(x,t)$ is the stochastic field solution given in Eqn. (7.16). We can re-express the δ-function using a frequency integral, and expand in powers of the field as follows:

$$\begin{aligned}\mathcal{P}(\phi,x,t) &= \int_{-\infty}^{\infty}\frac{d\omega}{2\pi}\ e^{-i\omega\phi}\ \langle\exp\left[i\omega\phi_R(x,t)\right]\rangle \\ &= \int_{-\infty}^{\infty}\frac{d\omega}{2\pi}\ e^{-i\omega\phi}\ \sum_{n=0}^{\infty}\frac{(i\omega)^n}{n!}\langle\phi_R(x,t)^n\rangle\end{aligned}$$

$$= \int_{-\infty}^{\infty} \frac{d\omega}{2\pi}\, e^{-i\omega\phi} \sum_{n=0}^{\infty} \frac{(i\omega)^n}{n!} m(x,t;n\lambda)\ , \tag{7.45}$$

the last line following from the property i) alluded to above.

So the Laplace transform (over time) of $\mathcal{P}$ is given in terms of the Laplace transform of $m(x,t;n\lambda)$. From Eqn. (7.25) we have

$$\begin{aligned} \hat{m}(x,s;n\lambda) &= \frac{1}{s}\left[1 - \frac{n\lambda\hat{g}(x,s)}{1+n\lambda\hat{g}(o,s)}\right] \\ &= \frac{\hat{g}(0,s)-\hat{g}(x,s)}{s\hat{g}(0,s)} + \frac{\hat{g}(x,s)}{s\hat{g}(0,s)(1+n\lambda\hat{g}(0,s))}\ , \end{aligned} \tag{7.46}$$

where the second line follows from some algebraic manipulations. The first term is easily handled as it is independent of n. Thus the sum over n for this term (as is required in Eqn. (7.45)) yields a factor of $\exp(i\omega)$ which finally yields a factor of $\delta(1-\phi)$ when integrated over ω. The second term is more interesting. Details of how to perform the sum over n and the frequency integral may be found in Appendix IID. The final result for $\hat{\mathcal{P}}(\phi,x,s)$ reads

$$\hat{\mathcal{P}}(\phi,x,s) = \frac{\hat{g}(0,s)-\hat{g}(x,s)}{s\hat{g}(0,s)}\delta(1-\phi) + \frac{\hat{g}(x,s)}{\hat{g}(0,s)^2}\frac{1}{s\lambda\phi}\exp\left[-\frac{1}{\lambda\hat{g}(0,s)}\log\left(\frac{1}{\phi}\right)\right]\ . \tag{7.47}$$

This form for the Laplace transform of the probability distribution may be easily generalized for any $d \in (0,2)$. Finally we must invert the Laplace transform. To this end we note that

$$\hat{g}(x,s) = \frac{1}{(2Ds)^{1/2}}\ \exp\left[-\left(\frac{2s}{D}\right)^{1/2}|x|\right]\ . \tag{7.48}$$

Inserting (7.48) into (7.47) and inverting the transform we have our final result

$$\mathcal{P}(\phi,x,t) = \delta(1-\phi)\ \mathrm{erf}\left[\frac{|x|}{(2Dt)^{1/2}}\right] + \frac{1}{(\pi t)^{1/2}}\ \frac{1}{\tilde{\lambda}\phi}\exp\left\{-\left[\frac{|x|}{(2Dt)^{1/2}} - \frac{\log(\phi)}{2\tilde{\lambda}t^{1/2}}\right]^2\right\}\ , \tag{7.49}$$

where $\mathrm{erf}(z)$ is the error function [48], and we have defined $\tilde{\lambda} = \lambda/(2D)^{1/2}$. This is illustrated in Fig. 7.2 for $x=1$ (and $D=1$, $\tilde{\lambda}=\sqrt{2}$), and three different times corresponding to $x^2 \gg 2Dt$, $x^2 \sim 2Dt$ and $x^2 \ll 2Dt$.

In particular, the probability distribution for the magnetization density at the origin takes the form

$$\mathcal{P}(\phi,0,t) = \frac{1}{(\pi t)^{1/2}}\ \frac{1}{\tilde{\lambda}\phi}\exp\left[-\frac{(\log(\phi))^2}{4\tilde{\lambda}^2 t}\right]\ , \tag{7.50}$$

which is a pure log-normal distribution. This result is very revealing, as it shows that the fluctuations in this system are extreme. For instance, we have already seen that the *mean* value of the density (at the origin) decays as $m(0,t) \sim 1/\sqrt{t}$. However, if one asks how the *typical* (or most likely) value decays, one can see from (7.50) that $\langle\phi(0,t)\rangle_{\mathrm{typ}} \sim \exp(-2\tilde{\lambda}^2 t)$. Thus, as time

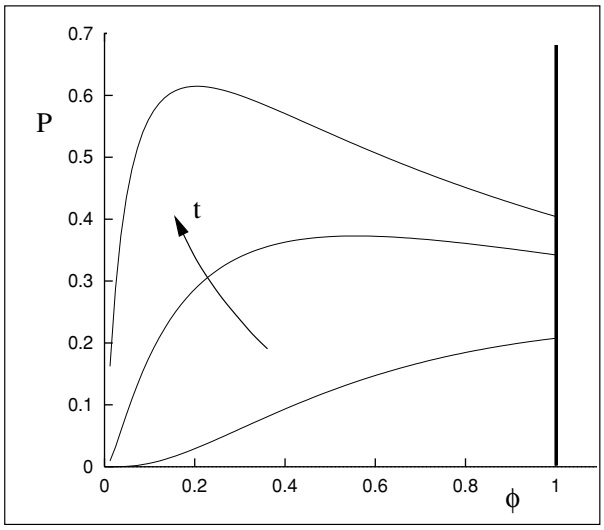

Figure 7.2: $\mathcal{P}(\phi, x, t)$ *versus* ϕ*, as given in Eqn. (7.49), with* $x = 1, \tilde{\lambda} = \sqrt{2}$*, for three different times,* $t = 0.5,\ 1.0,\ 1.5$*. The thick vertical line represents the* δ*-function at* $\phi = 1$*.*

proceeds, the typical value of ϕ decays to zero exponentially fast, while the mean decays slowly as $1/\sqrt{t}$. This is possible because the log-normal distribution has a long tail, extending out to the extreme value of $\phi = 1$. In fact the end point of the distribution (*i.e.* $\mathcal{P}(1, 0, t)$) also decays as $1/\sqrt{t}$ which is consistent with the known persistence properties of a random walker in $d = 1$ (namely, the probability of a walker *never* having returned to the origin after time t decays as $1/\sqrt{t}$). In Fig. 7.3 we illustrate $\mathcal{P}(\phi, 0, t)$ for three different times. As a final remark, we note that if we erroneously use the asymptotic form (7.27) for $m(0, t; n\lambda)$ to build the distribution function, we find that $\partial_\phi \mathcal{P}(\phi, 0, t)$ is equal to $\partial_\phi \delta(\phi) - \delta(1 - \phi)/\lambda\sqrt{t}$; thus emphasizing the fact that we need the entire analytic form of $m(0, t; n\lambda)$ to successfully construct the distribution $\mathcal{P}$. This ends the section on the analytic properties of the continuum model in $d = 1$.

7.4 Numerical simulation

We have performed extensive numerical simulations of the discrete model, as defined in section 7.1, in order to test the results obtained in the last two sections from the continuum theory. In all of the simulations for which we present results, we have set the hopping rate p of the BA, along with the flipping probability q, to unity. We have experimented with decreasing the flipping probability, and have found that its only effect is to renormalize the effective spin-BA coupling λ, such that $\lambda \propto q$, as expected.

Most of our results are obtained from a one-dimensional chain of sites. The chain length is unimportant, so long as one ensures that the BA has never touched the edges in any of its realizations up to the latest time at which data is extracted. Generally we average over between

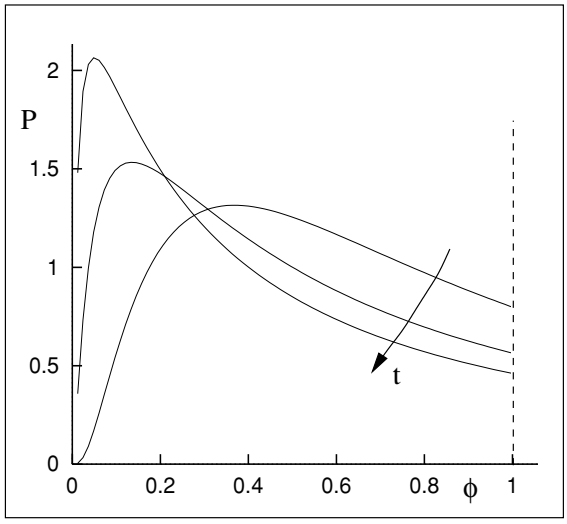

Figure 7.3: *$\mathcal{P}(\phi, 0, t)$ versus ϕ, as given in Eq.(7.50), for three different times.*

10^6 and 10^8 realizations (or runs) depending on the desired quality of the data. Such simulations required a few days on a DEC Alpha 233 MHz workstation. In a given run, at each time step the BA is moved left or right with equal probability and the spin it leaves behind is flipped. Each run starts with the same initial configuration; namely all spins up, except the spin at the origin (which is the starting site of the BA) which is pointed down. (This means that all spins are up after one time step, since the BA has moved away from the origin and flipped the down spin.) In Fig. 7.4 we show the measured mean magnetization density at the origin, along with the quantity $\sum_R \Theta(R, R, t)$ (cf. Eqn. (7.2)). They are seen to be identical thus confirming relations Eqn. (7.7) and its continuum counterpart (7.33). The solid line is the asymptotic prediction (7.27) from the continuum theory. It is seen to be in good agreement with the data, as the line has a slope of (-1/2). From the fit of this log-log plot we can read off the effective value of λ, since from (7.27) the prefactor of $1/\sqrt{t}$ is given by $(2/\pi\lambda^2)^{1/2}$. (The diffusion constant for the lattice random walk is unity.) We have fitted the data to $c/\sqrt{t}$ with $c = 0.40(1)$, which yields $\lambda = 1.99(1)$. In Fig. 7.5 we plot the small $x/\sqrt{t}$ dependence of $m(x, t)$ on a log-log scale. The data is well fitted by the prediction given in Eqn. (7.28). In Fig. 7.6 we plot $1 - m(x, t)$ versus $x/\sqrt{t}$. Note that good data collapse is found for intermediate values of $x/\sqrt{t}$. We have been unable to numerically probe the ballistic scale λt. (Note, the theoretical curves shown in the last two figures are plotted with no free parameters.)

In Fig. 7.7 we plot the discrete time derivative of the total number of down spins $N(t)$ (which is $M(t)/2$), along with $m(0, t)$. The two curves are indistinguishable within the numerical noise, thus confirming the global/local relation (7.10). This also provides secondary confirmation of the continuum form of this relation Eqn. (7.34) with $\lambda \simeq 2$. In Fig. 7.8 we plot the ratio of the measured two point correlation function (divided by $m(0, t)$) versus $x/\sqrt{t}$. Note that it varies from 1/2 (at small x) to unity (at large x) as expected. The data from two different times is

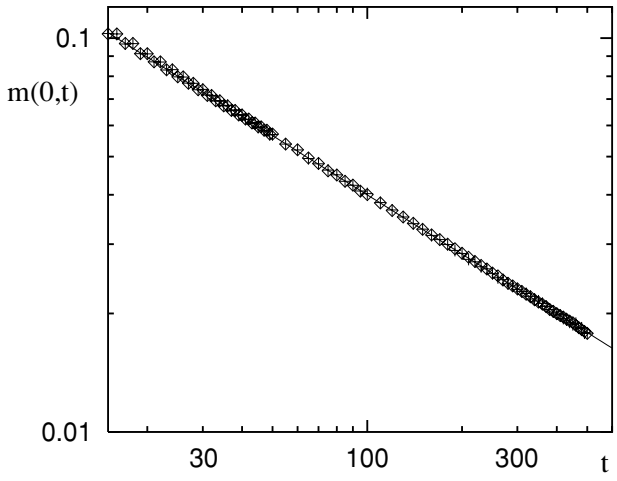

Figure 7.4: *Log-log plot of* $m_0(t)$ $(\diamondsuit)$*and*$\sum_R \Theta(R,R,t)$ $(+)$ *versus time from* $d = 1$ *numerical simulation. The solid line is the asymptotic theoretical prediction (7.27).*

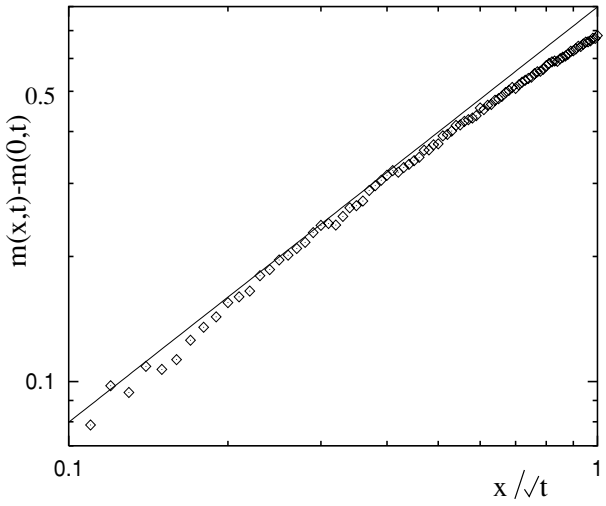

Figure 7.5: *Log-log plot of* $m_x(t) - m_0(t)$ *versus* $x/\sqrt{t}$ *for a time of* 10^3 *in* $d = 1$*. The solid line is the theoretical prediction (7.28).*

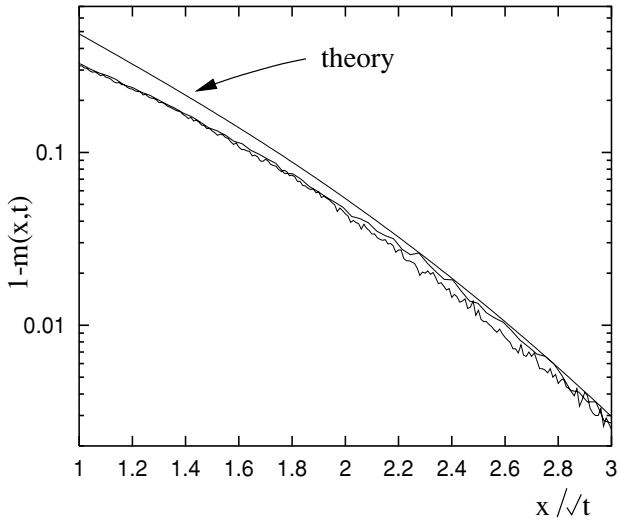

Figure 7.6: *Log-log plot of* $1 - m_0(t)$ *versus* $x/\sqrt{t}$ *for times* 10^3 *and* 10^4 *in* $d = 1$. *Also shown is the theoretical prediction (7.29) for the intermediate regime.*

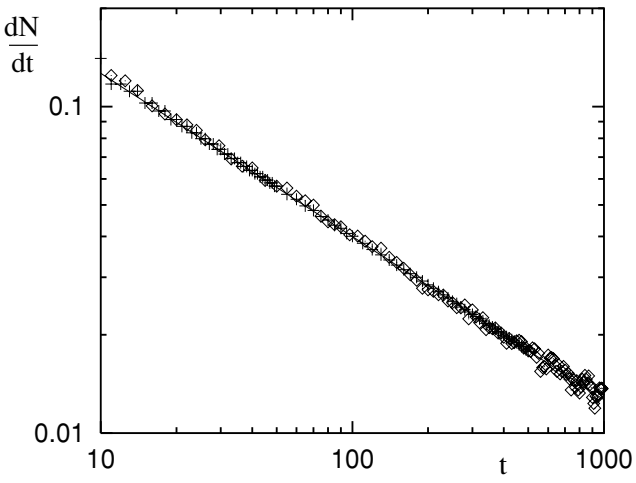

Figure 7.7: *Log-log plot of the time derivative of the total number of minus spins* ($\diamondsuit$) *and of* $m_0(t)$ *(+) versus time in* $d = 1$. *The solid line is the theoretical prediction (7.27).*

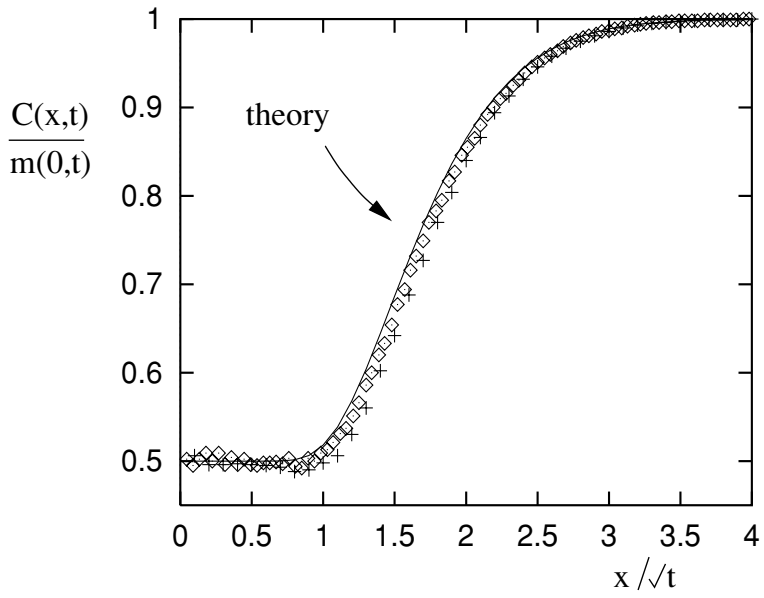

Figure 7.8: *The ratio $C_x(t)/m_0(t)$ plotted against $x/\sqrt{t}$ for times of* 100 *(+) and* 500($\diamondsuit$) *in $d = 1$. The solid line is the theoretical prediction (7.43).*

shown, and one sees excellent agreement with the theoretical prediction (7.43), which is plotted with *no* free parameters. This agreement provides very strong evidence for the validity of our whole continuum approach.

Finally we mention our attempt to measure the probability distribution of the coarse grained magnetization density at the origin (in $d = 1$), which was found from the continuum theory to be a log-normal distribution. Clearly it does not make sense to measure moments of the spin at the origin, since the odd (even) moments are equal to $m_0(t)$ (unity). Therefore, we define a coarse grained magnetization over a patch of spins. If the patch is taken too small, the coarse-graining will be ineffective, whilst if the patch is taken too large, the BA will take a long time to leave the patch, and the asymptotic behavior will be numerically inaccessible. So we have compromised and have used a patch containing 21 spins. We have binned the patch magnetization from 10^8 independent runs and generated the histograms shown in Fig. 7.9 Note, that because the patch size is modest, the histograms have non-zero weight in the negative ϕ region, in contrast to the strict continuum limit. However, we do see that for ϕ near unity, the histograms have a robust tail, which is the signature that extreme fluctuations are important.

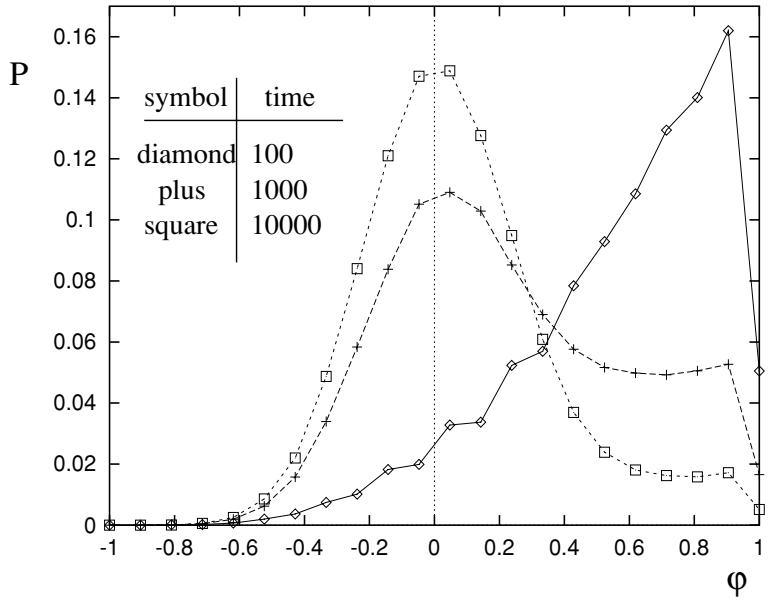

Figure 7.9: *Probability distribution of patch (21 spins) magnetization for times of* 10^2, 10^3, *and* 10^4 *in* $d = 1$. *Note the robust tail for values of patch magnetization near unity.*

Chapter 8

Binary data corruption due to a Brownian agent II

8.1 Analytic results in two dimensional systems

In this section we shall present a careful analysis of the case of two dimensions. The simple random walk is recurrent for dimensions $d \leq 2$, whereas for $d > 2$ the walker has a probability less than unity for ever returning to its starting point [3]. This basic fact from the theory of random walks has an immediate implication for our data corruption problem. The non-recurrent nature of random walks for $d > 2$ implies that the BA will continually corrupt new regions of the system, and rarely revisit sites which it has previously corrupted. Thus the relative density of disorder (or average magnetization density) at the origin $m(\mathbf{0}, t)$ will decay to a non-zero (and non-universal) value, and the total amount of disorder (or average global magnetization) $M(t)$ will increase linearly in time, with a non-universal prefactor. For practical applications, in which one wishes to limit the disordering capabilities of the BA, the first requirement is to restrict the geometry of the system to a dimension $d \leq 2$. So $d = 2$ is the critical dimension of the problem, and because of this we can expect logarithmic corrections to modulate the leading order results, and also to cause long cross-over times, thus making numerical results more difficult to interpret.

In this section we shall derive the form of $m(\mathbf{0}, t)$ very carefully. The reasons for this are threefold: first, so that we can have confidence in the leading order result, and also get some idea of the sub-leading corrections; second, to provide insight into the relation between the discrete and continuum approaches in two dimensions (which is important given that the latter must be regularized for $d = 2$); and third, to allow us to construct the form of the probability distribution of the magnetization density (for which we need as much information about $m(\mathbf{0}, t)$ as possible).

We shall use four different methods (which will each be described with brevity) to derive the form of $m(\mathbf{0}, t)$. Each has its strong and weak points as we shall see. The methods to be used are i) calculation from the exact lattice formulation for the marginal average (7.3), ii) solution of the diffusion equation (7.4) using a smeared sink function, iii) calculation with infinite-order perturbation theory of the continuum theory (7.16) using a crude temporal cut-off (as described

in chapter 7), and finally iv) analytic continuation from the exact result (7.25) valid for $d < 2$.

8.1.1 Lattice calculation

Referring to the equation of motion (7.3) for the marginal average we set $d = 2$, and for convenience we set the hopping probability $p = 1$, giving

$$\Theta(\mathbf{r}, \mathbf{R}, t + \delta t) = \frac{1}{4} \sum_{\mathbf{l}} \Theta(\mathbf{r}, \mathbf{R} + \mathbf{l}, t) - \frac{q}{2}\ \Theta(\mathbf{r}, \mathbf{r}, t) \sum_{\mathbf{l}} \delta_{\mathbf{r}, \mathbf{R}+\mathbf{l}}\ . \tag{8.1}$$

As an initial condition we take the BA to be located at the origin, and all spins to be $+1$, except the spin at the origin which is taken to be -1. This convention is useful for $q = 1$ so that all spins have value $+1$ after one time step. However if $q \ll 1$ it is more convenient to take the spin at the origin to be initially $+1$ as the chance of it flipping after one time step is small. We stress that these different choices for the initial value of the spin at the origin have no effect on the asymptotic properties of the system, and only serve to smoothen the magnetization density in the immediate vicinity of the origin. Thus $\Theta(\mathbf{r}, \mathbf{R}, 0) = \delta_{\mathbf{R},\mathbf{0}}(1 - 2\delta_{\mathbf{r},\mathbf{0}})$. The solution of (8.1) may be attained by discrete Fourier and Laplace transform. Defining the former via

$$\tilde{\Theta}(\mathbf{r}, \mathbf{k}, t) = \sum_{\mathbf{R}} \Theta(\mathbf{r}, \mathbf{R}, t) e^{i\mathbf{k}\cdot\mathbf{R}} \tag{8.2}$$

and the latter via

$$\hat{\Theta}(\mathbf{r}, \mathbf{R}, z) = \sum_{n=0}^{\infty} \Theta(\mathbf{r}, \mathbf{R}, n\delta t)\ z^n\ , \tag{8.3}$$

it is fairly straightforward to diagonalize Eqn. (8.1) to the form

$$\tilde{\Theta}(\mathbf{r}, \mathbf{k}, z) = \frac{(1 - 2\delta_{\mathbf{r},\mathbf{0}}) - 2qzf(\mathbf{k})e^{i\mathbf{k}\cdot\mathbf{r}}\ \hat{\Theta}(\mathbf{r}, \mathbf{r}, z)}{1 - zf(\mathbf{k})}\ , \tag{8.4}$$

where $f(\mathbf{k}) = [\cos\ k_1 l + \cos\ k_2 l]/2$. One may now solve the above equation self-consistently for $\hat{\Theta}(\mathbf{r}, \mathbf{r}, z)$ by inverting the discrete Fourier transform. One has

$$\hat{\Theta}(\mathbf{r}, \mathbf{r}, z) = \frac{(1 - 2\delta_{\mathbf{r},\mathbf{0}}) \int d\mathbf{k}\ e^{-i\mathbf{k}\cdot\mathbf{r}} D(\mathbf{k}, z)}{1 + 2qz \int d\mathbf{k}\ f(\mathbf{k}) D(\mathbf{k}, z)}\ , \tag{8.5}$$

where $D(\mathbf{k}) = [1 - zf(\mathbf{k})]^{-1}$ and the momentum integrals are over the two-dimensional Brillouin zone. The average magnetization density at the origin is given by summing $\Theta(\mathbf{0}, \mathbf{R}, t)$ over $\mathbf{R}$, which is equivalent to the zero Fourier mode $\tilde{\Theta}(\mathbf{0}, \mathbf{0}, t)$. Thus, substituting (8.5) into (8.4) we have after some rearrangement

$$\sum_{\mathbf{R}} \hat{\Theta}(\mathbf{0}, \mathbf{R}, z) = \frac{-1}{(1 - z)} \left[\frac{1 + q'(1 - z) \int d\mathbf{k}\ D(\mathbf{k}, z)}{1 + q' \int d\mathbf{k}\ D(\mathbf{k}, z)}\right]\ , \tag{8.6}$$

where $q' \equiv 2q/(1 - 2q)$. We note that the function $\int d\mathbf{k}\ D(\mathbf{k}, z)$ is very well known in the theory of random walks [3], and is the discrete Laplace transform of the probability of a random walker

to return to its starting point after n steps. Finally we must inverse Laplace transform the above equation. For large n we can extract the asymptotic form of the average magnetization by invoking the Tauberian theorem [3]. In this case we need the form of the Laplace transform as $z \to 1$. Using [3]

$$\int d\mathbf{k}\ D(\mathbf{k}, z) \sim \frac{1}{\pi} \log\left(\frac{8}{1-z}\right)\ [1 + O(1-z)]\ , \tag{8.7}$$

we have from the Tauberian theorem the asymptotic result

$$\sum_{\mathbf{R}} \Theta(\mathbf{0}, \mathbf{R}, n\delta t) = \frac{-1}{(q'/\pi)\log n + C(q)}\ . \tag{8.8}$$

The constant $C(q)$ is not accessible from the Tauberian theorem, although it could in principle be calculated from a careful inverse Laplace transform of Eqn. (8.6).

In our simulations we generally take the switching probability q to be unity which implies $q' = -2$ and thus

$$\sum_{\mathbf{R}} \Theta(\mathbf{0}, \mathbf{R}, n\delta t) = \frac{1}{(2/\pi)\log n - C(1)}\ . \tag{8.9}$$

In section 8.4 we shall make a direct comparison of this result with numerical simulations in two dimensions. It is also interesting to note from Eqn. (8.6) that setting the switching probability $q = 1/2$ gives $\sum_{\mathbf{R}} \Theta(\mathbf{0}, \mathbf{R}, n\delta t) = -\delta_{n,0}$. In other words, the average value of the spin at the origin remains at zero after one jump of the agent. This "maximal uncertainty" for $q = 1/2$ only holds at the origin, and spins at other lattice sites will have a positive mean for all times. As a final note, if $q \ll 1$ it is more convenient to choose the initial value of the spin at the origin to be $+1$ in which case we find from the foregoing analysis

$$\sum_{\mathbf{R}} \Theta(\mathbf{0}, \mathbf{R}, n\delta t) = \frac{1}{(2q/\pi)\log n + C(q)}\ . \tag{8.10}$$

8.1.2 Diffusion equation with smeared sink function

We now wish to solve for the coarse-grained magnetization density $m(\mathbf{0}, t)$ within some continuum limit. In this subsection we accomplish this by solving the diffusion equation (7.4) with a smeared sink function. This calculation is the closest in spirit to the lattice calculation since (7.4) is the direct continuum analog of the discrete equation (7.3) solved in the previous subsection. Setting $\mathbf{r} = 0$, Eqn. (7.4) takes the form

$$\partial_t \Theta(\mathbf{0}, \mathbf{R}, t) = \frac{D}{2} \nabla^2_{\mathbf{R}} \Theta(\mathbf{0}, \mathbf{R}, t) - \lambda\ \Theta(\mathbf{0}, \mathbf{R}, t) \Delta_l(\mathbf{R})\ . \tag{8.11}$$

The simplest finite range form to take for the sink function Δ_l is a radial function which is zero outside a radius l, and (through normalization) equal to $(1/\pi l^2)$ within this radius. It is also convenient to smear the initial condition of Θ in a similar way:

$$\Theta(\mathbf{0}, \mathbf{R}, 0) = \begin{cases} 1/\pi l^2\ , & |\mathbf{R}| < l \\ 0\ , & |\mathbf{R}| > l\ . \end{cases} \tag{8.12}$$

Given the radial symmetry of both the sink function and the initial condition, $\Theta(\mathbf{0}, \mathbf{R}, t)$ is a function only of the radial coordinate R and t. Thus we define $\Theta_1(R,t)$ and $\Theta_2(R,t)$ to describe the original function respectively inside and outside the radius l. On Laplace transforming these functions in time, it is straightforward to show using boundary value techniques that

$$\begin{aligned} \hat{\Theta}_1(R,s) &= \frac{1}{\pi l^2 (s+\lambda')} + A(s) I_0\left(\sqrt{s+\lambda'}\ R'\right) \\ \hat{\Theta}_2(R,s) &= B(s) K_0\left(\sqrt{s}\ R'\right) \ , \end{aligned} \tag{8.13}$$

where we have introduced the scaled quantities $R' = R(2/D)^{1/2}$ and $\lambda' = \lambda/\pi l^2$, and where $I_0(z)$ and $K_0(z)$ are modified Bessel functions [48].

The functions $A(s)$ and $B(s)$ can be determined by demanding continuity of Θ and its radial derivative at the boundary $R = l$. Their forms are complicated and we shall not write them explicitly here. The average magnetization density $m(\mathbf{0}, t)$ is obtained by integrating $\Theta(\mathbf{0}, \mathbf{R}, t)$ over $\mathbf{R}$. Using the properties of integrals of modified Bessel functions [48] we have the closed form expression

$$\hat{m}(\mathbf{0}, s) = \frac{1}{s+\lambda'} + \frac{2\lambda' \zeta(s)}{l' s^{1/2} (s+\lambda')^{3/2}} \ , \tag{8.14}$$

where

$$\zeta(s) = \frac{K_1(\sqrt{s}\ l')\ I_1(\sqrt{s+\lambda'}\ l')}{\sqrt{s} K_1(\sqrt{s}\ l') I_0(\sqrt{s+\lambda'}\ l') + \sqrt{s+\lambda'}\ K_0(\sqrt{s}\ l') I_1(\sqrt{s+\lambda'}\ l')} \ , \tag{8.15}$$

and $l' = l(2/D)^{1/2}$. We may now take the lateral size l of the sink function to zero, and retain the leading terms in the above expression. Using the properties of Bessel functions at small argument [48] we finally arrive at

$$\hat{m}(\mathbf{0}, s) = \frac{1}{s} \left[\frac{1}{w(\tilde{\lambda}) - \tilde{\lambda} \log(s l'^2)} \right] \ , \tag{8.16}$$

where $\tilde{\lambda} = \lambda/2\pi D$ and $w(x) = \sqrt{x} I_0(2\sqrt{x})/I_1(2\sqrt{x})$ which approaches unity for small x. It is important to mention that this expression is not valid for Re $(s) > 1/l'$, and thus the apparent pole is an artifact of the limit $l \to 0$. Examination of the complete form (8.14) indicates there is no pole for Re $(s) > 0$, as expected on physical grounds. We refer the reader to Appendix IIE in which this Laplace transform is inverted. For large t the result takes the form

$$m(\mathbf{0}, t) = \frac{1}{w(\tilde{\lambda}) + \tilde{\lambda} \log(t/\tau)} \ , \tag{8.17}$$

where $\tau = l'^2 e^{-\gamma}$ and $\gamma = 0.57721...$ is Euler's constant.

Thus we have arrived at our result, and indeed the leading order behavior has the same functional form as Eqn. (8.10) derived in the previous subsection. A closer comparison of the leading terms indicates that $\lambda \propto q$ for $q \ll 1$ as expected on physical grounds. In the present continuum calculation, we have also extracted an explicit form for the sub-leading term (*i.e.* $w(\tilde{\lambda})$) which is non-universal and depends on the precise form of the smeared sink function.

8.1.3 Infinite order perturbation theory

In chapter 7 we concentrated on analyzing the continuum solution Eqn. (7.16) using infinite order perturbation theory in λ, using a Dirac delta function in place of the sink function Δ_l. For $d < 2$ each term may be averaged, and the series may then be resummed exactly after Laplace transform. No divergences appear, and one arrives at the exact result (7.25). Exactly in two dimensions a similar procedure may be used, but now each term in the perturbation expansion diverges after averaging over the noise. A controlled analysis requires one to work with a particular sink function, but as noted in chapter 7, resummation of the perturbation series is much more difficult .

The continuum theory requires some regularization for $d \geq 2$. This can be most easily (and physically) accomplished by smearing the δ-function interaction between the BA and the spins. Thus, our continuum model takes the form

$$\partial_t \phi(\mathbf{r}, t) = -\lambda \phi(\mathbf{r}, t) \Delta_l(\mathbf{r} - \mathbf{R}(t)) \ , \tag{8.18}$$

where $\Delta_l(\mathbf{r})$ is a normalized function which is sharply peaked over a region of linear dimension l around the point $\mathbf{r}$. [A good choice would be $\Delta_l \sim l^{-d} \exp(-r^2/l^2)$.]

In this section we shall analyze some basic properties of Eqn. (8.18) for general Δ_l. Then we will use a somewhat more crude approach to estimate the mean magnetization density (at the origin) as a function of time in $d = 2$.

Although we have generalized our continuum theory somewhat, we can still make substantial headway by first integrating the equation of motion, and then using infinite order perturbation theory. The first step yields

$$\phi(\mathbf{r}, t) = \exp\left[-\lambda \int_0^t dt' \ \Delta_l(\mathbf{r} - \mathbf{R}(t')) \right] \ , \tag{8.19}$$

whilst the second consists of expanding this equation in powers of λ and averaging term by term:

$$m(\mathbf{r}, t) = \langle \phi(\mathbf{r}, t) \rangle = \sum_{n=0}^{\infty} (-\lambda)^n \chi_n(\mathbf{r}, t) \ , \tag{8.20}$$

where $\chi_0(\mathbf{r}, t) = 1$, and for $n > 0$

$$\chi_n(\mathbf{r}, t) = \frac{1}{n!} \left\langle \left[\int_0^t d\tau \ \Delta_l(\mathbf{r} - \mathbf{R}(\tau)) \right]^n \right\rangle \ . \tag{8.21}$$

By making a Fourier representation of the interaction function Δ_l, performing the average over paths (see Appendix B), and finally Laplace transforming in time, we arrive at

$$\hat{\chi}_n(\mathbf{r}, s) = \frac{1}{s} \left\{ \prod_{m=1}^{n} \int \frac{d^d k_m}{(2\pi)^d} \ \frac{\tilde{\Delta}_l(\mathbf{k}_m - \mathbf{k}_{m-1})}{(s + k_m^2)} \right\} \ \exp[i \mathbf{k}_n \cdot \mathbf{r}] \ , \tag{8.22}$$

with the convention $\mathbf{k}_0 \equiv 0$.

We shall be concerned with two quantities. The first is a smeared mean magnetization density near the origin, and the second is the global magnetization. These are given by

$$m_{\rm s}(\mathbf{0},t) \equiv \int d^d r\ \Delta_l(\mathbf{r}) m(\mathbf{r},t) \tag{8.23}$$

and

$$M(t) = \int d^d r\ [\langle\phi(\mathbf{r},0)\rangle - \langle\phi(\mathbf{r},t)\rangle] \tag{8.24}$$

respectively. We shall prove that

$$\frac{dM(t)}{dt} = \lambda m_{\rm s}(\mathbf{0},t)\ , \tag{8.25}$$

which is the smeared analogue of the global versus (strictly) local relation (7.34) we proved for $d < 2$. Comparing Eqs.(8.20) and (8.23) we see that

$$m_{\rm s}(\mathbf{0},t) = \sum_{n=0}^{\infty} (-\lambda)^n \eta_n(t)\ , \tag{8.26}$$

where in Laplace transform space

$$\hat{\eta}_n(s) = \int d^d r\ \Delta_l(\mathbf{r})\hat{\chi}_n(s) = \frac{1}{s}\left\{\prod_{m=1}^{n} \int \frac{d^d k_m}{(2\pi)^d}\ \frac{\tilde{\Delta}_l(\mathbf{k}_m - \mathbf{k}_{m-1})}{(s+k_m^2)}\right\}\ \tilde{\Delta}_l(\mathbf{k}_n)\ . \tag{8.27}$$

Similarly we have

$$\frac{dM(t)}{dt} = -\sum_{n=0}^{\infty} (-\lambda)^n \zeta_n(t)\ , \tag{8.28}$$

with

$$\zeta_n(t) = \frac{d}{dt}\int d^d r\ \chi_n(\mathbf{r},t)\ . \tag{8.29}$$

For $n > 0$, $\chi_n(\mathbf{r},0) = 0$, so that

$$\tilde{\zeta}_n(s) = s\int d^d r\ \tilde{\chi}_n(\mathbf{r},s)\ . \tag{8.30}$$

Using Eq.(8.22) we may evaluate the above integral to give

$$\tilde{\zeta}_n(s) = \left\{\prod_{m=1}^{n} \int \frac{d^d k_m}{(2\pi)^d}\ \frac{\tilde{\Delta}_l(\mathbf{k}_m - \mathbf{k}_{m-1})}{(s+k_m^2)}\right\}\ \delta^d(\mathbf{k}_n)\ . \tag{8.31}$$

Performing the integral over $\mathbf{k}_n$ immediately yields

$$\hat{\zeta}_n(s) = \tilde{\eta}_{n-1}(s)\ . \tag{8.32}$$

Thus comparing Eqs.(8.26), (8.28) and (8.32) we see the validity of relation Eq.(8.25).

As a corollary, by integrating the averaged equation of motion (8.18) over space, we have

$$\frac{dM(t)}{dt} = \lambda \int d^d r \, \left\langle \Delta_l(\mathbf{r} - \mathbf{R}(t))\phi(\mathbf{r}, t) \right\rangle \, , \tag{8.33}$$

When compared with Eq.(8.25), the above relation gives us

$$m_s(t) = \int d^d r \, \Delta_l(\mathbf{r}) \langle \phi(\mathbf{r}, t) \rangle = \int d^d r \, \langle \Delta_l(\mathbf{r} - \mathbf{R}(t))\phi(\mathbf{r}, t) \rangle \, , \tag{8.34}$$

which is the smeared version of the local relation (7.33) proven in section III. We note that, although we have been concerned with a sharply peaked interaction function, the relations (8.25) and (8.34) hold for *any* function $\Delta(\mathbf{r})$.

This ends the more rigorous part of the present section. In the remainder we shall just mention some explicit results for the mean local magnetization density (at the origin), which are obtained with a cruder regularization.

The difficulty with making headway using the smoothing function, is that the n-fold integrals over the Δ_l's are intractable (unless one can find a particularly 'friendly' form for Δ_l.) As an alternative approach, we return to the sharp Dirac δ-function as used in section IV. We remarked that the n-fold convolution integrals were divergent due to the non-integrability of $g(\mathbf{0}, t)$ for $d \geq 2$. To evade this difficulty we can simply impose a cut-off into the integration limits. This is closely connected to introducing a microscopic time scale into the temporal correlations of the BA. Such an regularization procedure was used in Ref. [54], and the results so obtained were shown to be equivalent to previously known exact results[7]. So we shall use the same procedure here, but with due caution.

First, we consider $d = 2$. In a precisely analogous way to the calculation in section IV, we expand the field solution (7.16) in powers of λ and average term by term. Thus, we have (cf. Eqs. (7.21) - (7.23))

$$m(\mathbf{0}, t) = \langle \phi(\mathbf{0}, t) \rangle = \sum_{n=0}^{\infty} (-\lambda)^n \chi_n(\mathbf{0}, t) \, , \tag{8.35}$$

where $\chi_0(\mathbf{0}, t) = 1$, and for $n > 0$

$$\chi_n(\mathbf{0}, t) = \int_{t_0}^{t-t_0} d\tau_1 \int_{t_0}^{\tau_1 - t_0} d\tau_2 \cdots \int_{t_0}^{\tau_{n-1} - t_0} d\tau_n \; g(\mathbf{0}, \tau_1 - \tau_2) \cdots g(\mathbf{0}, \tau_{n-1} - \tau_n) g(\mathbf{0}, \tau_n) \, , \tag{8.36}$$

In this case, the probability distribution of the BA at the origin has the form $g(\mathbf{0}, t) = (2\pi D t)^{-1}$. Note we have inserted the microscopic time regulator t_0 in the limits of the time integrals. Our strategy is to evaluate the time integrals one by one, keeping only the most singular term at each step. We shall use the general result (for $t \gg t_0$)

$$\int_{t_0}^{t-t_0} d\tau \; \frac{[\log(\tau/t_0)]^m}{(t-\tau)\tau} \sim \frac{(m+2)}{(m+1)} \; \frac{[\log(t/t_0)]^{m+1}}{t} \, . \tag{8.37}$$

Therefore we have the dominant contribution

$$\chi_n(\mathbf{0},t) \sim \frac{[\log(t/t_0)]^n}{(2\pi D)^n} \ . \tag{8.38}$$

Inserting this result into Eq. (8.35) and summing over n we have the asymptotic form

$$m(\mathbf{0},t) \sim \left[1 + \frac{\lambda}{2\pi D}\log\left(\frac{t}{t_0}\right)\right]^{-1} \ . \tag{8.39}$$

Thus the magnetization at the origin does decay to zero for large times, but logarithmically slowly. From the relation (8.25) we see that the mean global magnetization increases as $M(t) \sim t/\log(t)$.

The same kind of analysis can be repeated for $d > 2$, and one finds that $m(\mathbf{0},t)$ saturates to a constant for large times, which implies that $M(t) \sim t$ for large times. These results are easily understood from the recurrent properties of the BA (*i.e.* a random walker returns to its starting point with probability one, only for $d \leq 2$). It would be more interesting to derive the distribution of the magnetization density for $d \geq 2$, but this requires the more careful regularization method involving the smoothing function $\Delta_l(\mathbf{r})$ and thus lies beyond the scope of the present work. We also refer the reader to Ref. [8] where the same regularization scheme was used in calculations on vacancy-mediated diffusion, and produced scaling results in accord with exact lattice calculations [7].

Using the time cut-off regularization scheme allows one to extract the dominant contribution from each term in the perturbation expansion, and to resum the series. The result is

$$m(\mathbf{0},t) = \frac{1}{1+\tilde{\lambda}\log(t/t_0)} \ . \tag{8.40}$$

It is interesting to compare this result with Eqn. (8.17) obtained in the previous subsection. They are seen to agree (for small λ, in which case $w(\tilde{\lambda}) \approx 1$) if we make the identification $t_0 = \tau \ (= 2l^2e^{-\gamma}/D)$. This indeed supports the role of t_0 as a microscopic correlation time of the noise, since it is seen to correspond to the time taken for the diffusion process to correlate a microscopic region of size $\sim l^2$.

8.1.4 Analytic continuation

As a fourth method of extracting the form of $m(\mathbf{0},t)$ for $d = 2$ we briefly mention analytic continuation from $d < 2$. As discussed in the previous section, no regularization is required in the perturbation expansion method for $d < 2$, and one retrieves the exact result

$$\hat{m}(\mathbf{0},s) = \frac{1}{s}\left[\frac{1}{1+\lambda\hat{g}(\mathbf{0},s)}\right] \ , \tag{8.41}$$

where

$$\hat{g}(\mathbf{0},s) = \frac{\Gamma(1-d/2)}{(2\pi D)^{d/2}s^{1-d/2}} \ , \tag{8.42}$$

and $\Gamma(z)$ is the gamma function [48]. Using the result $\Gamma(z) \sim 1/z$ for $z \to 0$ we have for $\epsilon \equiv 2 - d \to 0$

$$\hat{m}(\mathbf{0}, s) = \frac{1}{s}\left[\frac{1}{1 - \tilde{\lambda}\log(s/s_0)}\right] , \tag{8.43}$$

where $s_0 = e^{-2/\epsilon}$.

On comparing this result with Eqn. (8.16) obtained in section 8.1.2, we see that they are equivalent (for small λ, in which case $w(\tilde{\lambda}) \approx 1$) if we make the identification $1/\epsilon = \log(1/l')$. This relation has only a formal meaning, as there is no physical sense in continuing dimensionality. However, it is instructive to learn that the leading order result may be retrieved intact from analytic continuation. Indeed, we shall use this tool in section 8.2 to study competing agents in two dimensions.

8.1.5 Calculation of the probability distribution

To complete this section, we shall briefly discuss the probability distribution of the magnetization density at the origin. As mentioned before, the continuum theory (7.16) has the property $\langle \phi(\mathbf{0}, t; \lambda)^n \rangle = \langle \phi(\mathbf{0}, t; n\lambda) \rangle$. Thus, knowledge of the λ dependence of the first moment allows one to reconstruct all the moments of the magnetization density, and thus the probability density $\mathcal{P}(\phi, \mathbf{0}, t)$ for this quantity. The method for retrieving $\mathcal{P}$ from the moments is given in detail in chapter 7 for the case of $d = 1$. A similar calculation suffices for $d = 2$, so long as one has an "accurate" form for the mean magnetization density. In the present section we have attacked this problem from four different directions and have arrived at agreement for the asymptotically dominant term for $m(\mathbf{0}, t)$. However, as noted in chapter 7, it is necessary to have more information than this in order to construct $\mathcal{P}$ correctly. If one tries to calculate $\mathcal{P}$ using $m(\mathbf{0}, t; \lambda) \sim 1/\tilde{\lambda}\log t$ one obtains a distribution $\mathcal{P} \sim m(\mathbf{0}, t)/\phi$ which is singular at $\phi = 0$. The sub-leading correction to $m(\mathbf{0}, t; \lambda)$ is crucial to determine the distribution correctly. Our results from the previous four subsections are in agreement with regard to the time dependence, but differ in the way in which λ appears in the sub-leading term. We prefer Eqn. (8.17) in that an explicit form $w(\tilde{\lambda})$ appears. However, we have been unable so far to reconstruct $\mathcal{P}$ using this form due to the complicated nature of w. For small λ, $w(\tilde{\lambda}) \approx 1$, and Eqn. (8.17) then coincides with the less controlled results (8.40) and (8.43) of subsections 8.1.3 and 8.1.4 respectively. The reconstruction of $\mathcal{P}$ is possible from these forms and one finds

$$\mathcal{P}(\phi, \mathbf{0}, t) = \beta(t)\phi^{\beta(t)-1} , \tag{8.44}$$

with $\beta(t) = 1/\tilde{\lambda}\log(t/t_0)$. As $t \to \infty$ this distribution approaches the form $m(\mathbf{0}, t)/\phi$, but is not singular for finite times. In section 8.4 we shall describe our attempts to measure $\mathcal{P}$ for two dimensional systems. Our numerical results are in surprisingly good agreement with Eqn. (8.44) above.

8.2 Competing agents

In this section we shall analyze the effects of many BA's within the system. We shall assume the BA's to be non-interacting, in the sense that they are unaware of each other's immediate presence. The non-trivial statistics reside in the fact that the disordering effects of the BA's statistically interact via the overlap of the BA histories. As we have already seen, a single BA interferes with the previous disorder it has created, such that the amount of disorder does not simply increase linearly in time. This effect is more severe when more than one BA is present, as each BA can disturb the disorder that another BA has previously created.

We measure the strength of this interference via a quantity called the "disordering efficacy" of the agents, defined as

$$\sigma_N(d) \equiv \lim_{t\to\infty} \frac{M^{(N)}(t)}{M^{(1)}(t)} \ , \tag{8.45}$$

where $M^N(t)$ is the average global disorder created by N agents. If the BA's were truly independent (in terms of the disorder they create) then we would expect $\sigma_N = N$. As we shall see, for $d < 2$ the value of σ_N is strongly reduced below this value. However, for $d = 2$ this value is recovered, but only in the deep asymptotic regime ($t \gg e^N$).

The extension to many BA's is easily modeled within the continuum theory. We introduce N random walkers, each of which is described by a position vector $\mathbf{R}_\alpha(t)$, $\alpha = 1, 2, \cdots, N$. Since the BA's are independent we have

$$\frac{d\mathbf{R}_\alpha}{dt} = \xi_\alpha(t) \ , \tag{8.46}$$

where $\xi_\alpha(t)$ are independent Gaussian white noise sources with zero mean. The equation of motion for the coarse-grained magnetization density $\phi^{(N)}$ takes the form

$$\partial_t \phi^{(N)}(\mathbf{r}, t) = -\lambda \phi^{(N)}(\mathbf{r}, t) \sum_{\alpha=1}^{N} \Delta_l(\mathbf{r} - \mathbf{R}_\alpha(t)) \ , \tag{8.47}$$

with solution

$$\phi^{(N)}(\mathbf{r}, t) = \prod_{\alpha=1}^{N} \exp\left[-\lambda \int_0^t dt' \ \Delta_l(\mathbf{r} - \mathbf{R}_\alpha(t'))\right] \ . \tag{8.48}$$

On averaging over the paths of the N agents, we have the particularly simple result

$$m^{(N)}(\mathbf{r}, t) \equiv \langle \phi^{(N)}(\mathbf{r}, t) \rangle = m^{(1)}(\mathbf{r}, t)^N \ . \tag{8.49}$$

Thus the average global magnetization is given by

$$M^{(N)}(\mathbf{r}, t) \equiv \int d^d r \ \left[m^{(N)}(\mathbf{r}, 0) - m^{(N)}(\mathbf{r}, t)\right] = \int d^d r \ \left[1 - m^{(1)}(\mathbf{r}, t)^N\right] \ . \tag{8.50}$$

Scaling the spatial coordinate by the diffusion length scale $(2Dt)^{d/2}$, we have from Eqns. (8.45) and (8.50)

$$\sigma_N(d) = \lim_{t\to\infty} \frac{\int d^d r \ \left[1 - m^{(1)}(\mathbf{r}/(2Dt)^{1/2}, t)^N\right]}{\int d^d r \ [1 - m^{(1)}(\mathbf{r}/(2Dt)^{1/2}, t)]} \ . \tag{8.51}$$

To proceed with the calculation it is convenient to first perform the large-t limit. We concentrate on $d < 2$, and therefore replace $\Delta_l(\mathbf{r})$ by the Dirac delta-function. From Eqns. (7.25) and $g(x,t) = (2\pi Dt)^{-1/2}\exp(-x^2/2Dt)$ (the probability density of the BA). it is a fairly straightforward matter to show that

$$m(r) \equiv \lim_{t\to\infty} m^{(1)}(\mathbf{r}/(2Dt)^{1/2}, t) = \frac{2}{\Gamma(1-d/2)} \int_0^r du \ u^{1-d} \ e^{-u^2} \ . \tag{8.52}$$

We may use this result to explicitly evaluate the denominator of Eqn. (8.51) giving us

$$\sigma_N(d) = d \ \Gamma(1-d/2) \int_0^\infty dr \ r^{d-1} \ (1 - m(r)^N) \ . \tag{8.53}$$

We refer the reader to Appendix IIF where it is demonstrated that the above expression may be recast in the more useful form

$$\sigma_N(d) = \frac{2N(N-1)}{\Gamma(1-d/2)} \int_0^\infty dr \ r^{1-d} \ e^{-2r^2} \ m(r)^{N-2} \ , \tag{8.54}$$

for $N > 1$. We note that the result for two agents follows immediately from this expression, and we have $\sigma_2 = 2^{d/2}$. This result is striking. For the case of $d = 1$, we see that two agents create only $\sqrt{2}$ as much disorder as one agent. Also, assuming we may continue this result to exactly two dimensions, we find that $\sigma_2(2) = 2$ – *i.e.* two agents create disorder independently. In the remainder of this section we shall use Eqn. (8.54) for two purposes. First, we shall concentrate on $d = 1$ and evaluate the exact values of $\sigma_3(1)$ and $\sigma_4(1)$, which may be used to compare with numerical simulations. Second, we shall evaluate the integral for large N for arbitrary $d \in [0, 2]$ using a saddle point method. This calculation will make clear the tremendous difference in the large-N behavior of $\sigma_N(d)$ for $d < 2$ and $d = 2$. We end the section with a simple scaling argument which helps us to understand these analytic results.

For $d = 1$ the expression (8.52) is simply $m(x) = \mathrm{erf}(x)$, where $\mathrm{erf}(z)$ is the error function [48]. Thus we have from Eqn. (8.54)

$$\sigma_N(1) = \frac{2N(N-1)}{\pi^{1/2}} \int_0^\infty dx \ e^{-2x^2} \ \mathrm{erf}(x)^{N-2} \ . \tag{8.55}$$

We are able to evaluate these integrals for $N = 3$ and $N = 4$. The details may be found in Appendix IIG. The results are

$$\sigma_2(1) = \sqrt{2} \ , \qquad \sigma_3(1) = \frac{6\sqrt{2}}{\pi} \ \sin^{-1}\left(\frac{1}{\sqrt{3}}\right) \ , \qquad \sigma_4(1) = \frac{12\sqrt{2}}{\pi} \ \sin^{-1}\left(\frac{1}{3}\right) \ . \quad (8.56)$$

The numerical values of these expressions are presented in Table I along with the results from our computer simulations (the details of which may be found in section 8.4). Excellent agreement is found.

N	$\sigma_N(1)_{\rm theory}$	$\sigma_N(1)_{\rm simul}$
2	$1.414\cdots$	1.42(1)
3	$1.662\cdots$	1.66(1)
4	$1.835\cdots$	1.84(2)

Table 1: *The predicted values of $\sigma_N(1)$ for $N = 2, 3$ and 4, from Eqn. (8.56), compared with our numerical simulations.*

We now return to the case of arbitrary $d \in [0, 2]$ and consider the limit of large N. For the sake of generality, we study the integral

$$Q_N(\beta, d) = \int_0^\infty dr \ r^{1-d} \ e^{-\beta r^2} \ m(r)^N \ , \quad (8.57)$$

with $m(r)$ as given above in Eqn. (8.52). We can recover the disordering efficacy via

$$\sigma_N(d) = \frac{2N(N-1)}{\Gamma(1-d/2)} Q_{N-2}(2, d) \ . \quad (8.58)$$

We wish to implement a saddle point calculation, so we rewrite (8.57) as

$$Q_N(\beta, d) = \int_0^\infty dr \ r^{1-d} \ e^{-F_N(r)} \ , \quad (8.59)$$

where

$$F_N(r; \beta, d) = \beta r^2 - N \log(m(r)) \ . \quad (8.60)$$

The saddle point is defined via $dF_N/dr|_{r=r_0} = 0$, which yields for r_0 the transcendental equation

$$\beta r_0^d = \frac{N e^{-r_0^2}}{m(r_0)\Gamma(1-d/2)} \ . \quad (8.61)$$

For $N \gg 1$, it is easy to see that $r_0 \sim (\log N)^{1/2} \gg 1$, so that $F(r_0) \gg 1$ and the saddle point method is self-consistently justified. There are two stages to the calculation. First

we must evaluate $F(r_0)$ to the desired precision. Second, we must Taylor expand $F(r)$ about the saddle point to account for fluctuations. It turns out that we need to evaluate the leading *and* sub-leading terms in order to have a useful comparison to the numerical data. Thus the calculation is somewhat involved. For the first stage we iteratively solve Eqn. (8.61) to obtain

$$r_0^2 = \log\left[\frac{N}{\beta\Gamma(d/2)(\log N)^{d/2}}\right] + \frac{d^2}{4}\frac{\log(\log N)}{\log N} + O\left(\frac{1}{\log N}\right) \ . \tag{8.62}$$

Substituting this result into Eqn. (8.60), we have after some manipulations

$$\exp[-F_N(r_0)] = \left[\frac{\beta\Gamma(1-d/2)(\log N)^{d/2}}{eN}\right]^\beta \ \left[1 - \frac{\beta d^2}{4}\frac{\log(\log N)}{\log N} + O\left(\frac{1}{\log N}\right)\right] \ . \tag{8.63}$$

The second stage proceeds as follows. We Taylor expand the function F_N about its value at the saddle point:

$$F_N(r) = F_N(r_0) + \sum_{n=2}^{\infty} \frac{(r-r_0)^n}{n!}\frac{d^n F(r)}{dr^n}\bigg|_{r=r_0} \ . \tag{8.64}$$

When using the saddle point method, it is usually only necessary to consider the second derivative in the above expansion (the so-called Gaussian fluctuations). In the present case, it turns out that *all* terms in the expansion contribute equally to the fluctuations. It is relatively straightforward to show by repeated differentiation of $F_N(r)$ that

$$\frac{d^n F(r)}{dr^n}\bigg|_{r=r_0} = \beta(-2r_0)^n \ \left[1 + O\left(\frac{1}{r_0^2}\right)\right] \ . \tag{8.65}$$

Setting $r = r_0 + \hat{r}$ we have from Eqns. (8.64) and (8.65)

$$F_N(r) = F_N(r_0) + \beta\sum_{n=2}^{\infty} \frac{(-2r_0\hat{r})^n}{n!} \ \left[1 + O\left(\frac{1}{r_0^2}\right)\right] \ . \tag{8.66}$$

We now substitute this expansion into Eqn. (8.59). Scaling $\hat{r}$ by $2r_0$ and explicitly performing the sum over n we have

$$Q_N(\beta, d) = \frac{\exp[-F_N(r_0)]}{2r_0^d} \int_{-2r_0^2}^{\infty} d\hat{r} \ \exp\left[-\beta\left(e^{-\hat{r}} + \hat{r} - 1\right)\right] \ \left[1 + O\left(\frac{1}{r_0^2}\right)\right] \ . \tag{8.67}$$

Performing the integral and neglecting exponentially small terms we have

$$Q_N(\beta, d) = \left(\frac{e}{\beta}\right)^\beta \Gamma(\beta) \ \frac{\exp[-F_N(r_0)]}{2r_0^d} \ \left[1 + O\left(\frac{1}{r_0^2}\right)\right] \ . \tag{8.68}$$

Finally, we substitute into this expression the form (8.62) for r_0, and the result (8.63) for $F_N(r_0)$ to yield

$$Q_N(\beta,d) = \frac{\Gamma(\beta)\Gamma(1-d/2)^\beta}{2} \; \frac{(\log N)^{(\beta-1)d/2}}{N^\beta} \; \left[1 - \frac{(\beta-1)d^2}{4}\frac{\log(\log N)}{\log N} + O\left(\frac{1}{\log N}\right)\right] . \tag{8.69}$$

Combining Eqns. (8.58) and (8.69) then gives us the final large-N result

$$\sigma_N(d) = \Gamma(1-d/2) \; (\log N)^{d/2} \; \left[1 - \frac{d^2}{4}\frac{\log(\log N)}{\log N} + O\left(\frac{1}{\log N}\right)\right] . \tag{8.70}$$

In particular, for $d = 1$ the disordering efficacy increases as $(\log N)^{1/2}$ with strong logarithmic corrections. We also note that for real-valued $d < 2$, the disordering efficacy increases as $(\log N)^{d/2}$. In other words, the BA's overlap very strongly in their disordering for all $d < 2$.

The main reason for calculating $\sigma_N(d)$ for real-valued $d < 2$ was to attempt to analytically continue the result to $d = 2$ which is otherwise difficult to calculate due to the presence of an explicit regulator. However, if we simply set $d = 2$ in our expression for $\sigma_N(d)$ above, we find that the apparent behavior $\sigma_N(2) \sim \log N$ is multiplied by the infinite constant. This gives us the hint that the large-N behavior for $d = 2$ is stronger than $\log N$, but offers no more information than that. We can, however, trace the failure of the saddle point calculation for $d = 2$ back to the saddle point equation (8.61) for r_0. For large-N and $d < 2$ we have the leading result $r_0 \sim [\log \epsilon N]^{1/2}$, where $\epsilon = 2 - d$ (and we have obtained this result from (8.61) by taking the small ϵ and large r limit of $m(r)$). Thus for fixed $\epsilon > 0$ we may always take N large enough to create a saddle-point at a large value of r_0, in which case the result (8.70) is valid. However for fixed N (no matter how large), taking $\epsilon \to 0$ squeezes the saddle point back into the origin, in which case the saddle point method is of no use.

Therefore we cannot use Eqn. (8.70) to analytically continue to $d = 2$. However, a simpler method may be used to extract the result. We refer the reader to the original expressions for $\sigma_N(d)$ and $m(r)$ as given in Eqns. (8.54) and (8.52) respectively. Taking $\epsilon \ll 1$ and $N \gg 1$ these equations take the form

$$\sigma_N(d) = \epsilon N^2 \int_0^\infty dr \; r^{\epsilon-1} \; e^{-2r^2} \; m(r)^N \; , \tag{8.71}$$

and

$$m(r) = \epsilon \int_0^r du \; u^{\epsilon-1} \; e^{-u^2} \; . \tag{8.72}$$

On studying Eqn. (8.71) we see that as $\epsilon \to 0$ the integral is dominated by small r. Thus we require the small-r form for $m(r)$ which is easily extracted from (8.72) to be $m(r) \simeq r^\epsilon$.

We now break the integral in (8.71) into two pieces. The first piece encompasses the range $r \in (0,1)$ so that we can neglect the Gaussian factor and substitute the small r form of $m(r)$ to find the leading order result

$$\sigma_N^I(d) = \epsilon N^2 \int_0^1 dr\ r^{N\epsilon-1} = N\ . \tag{8.73}$$

The second piece encompasses the range $r \in (1,\infty)$ and for large enough N will have the asymptotic form $\sigma_N^{II}(d) \sim (\log N)/\epsilon$. To summarize, the contribution $\sigma_N^I(d)$ dominates for $N \ll 1/\epsilon$, and the contribution $\sigma_N^{II}(d)$ dominates for $N \gg 1/\epsilon$. Thus for $d = 2$ we have the result $\sigma_N(2) = N$ for all N. This is consistent with the analytic continuation to $d = 2$ of the exact result $\sigma_2(d) = 2^{d/2}$ found earlier.

These results may be understood in the following way. Consider N agents in a system of d dimensions. Since each agent performs a random walk, the amount of available space in which we can expect to find the agents has a volume $\sim t^{d/2}$. Also, we know from our previous results that the amount of disorder created by a single agent increases as $t^{d/2}$ for $d < 2$, but as $t/\log t$ for $d = 2$. Thus for $d < 2$ the available space for N agents and the amount of disorder created by a single agent both scale as $t^{d/2}$ which means that there is certain to be interference between the agents, which will become severe for large N as we have seen. However for $d = 2$ the amount of available space for N agents scales logarithmically faster with t than does the amount of disorder created by a single agent. Thus for times large enough such that $N \ll \log t$ we expect the disorder created by the agents to become statistically independent and thus $\sigma_N(2) = N$. Note that the "independence time" grows exponentially with the number of agents, making numerical observation difficult for even moderate values of N. Similar arguments have been made in the context of "the number of distinct sites visited by N random walkers" [52]. In section 8.4 we shall present results for $N = 2, 3$ and 4 in two dimensions. The disordering efficacy is seen to slowly approach its expected value.

8.3 Generalized couplings

In all of our work so far we have taken the coupling between the BA and the spins to be symmetric and spatially homogeneous. At least one of these properties is likely to be absent in a practical application of our model. Asymmetry in the switching probability is likely in data corruption since the states of a bit are not physically encoded in a symmetric way. Also in chemical kinetic applications, the reaction rates between two chemical species are unlikely to be symmetric. Spatial homogeneity of the couplings is also an idealized situation. Generally there will be quenched random fluctuations in the switching rates of different sites, and it is important to quantify the effect of this randomness on the results obtained so far. In the next two subsections we shall consider these generalizations in turn.

8.3.1 Asymmetric rates

Now we consider the lattice model with the additional property that the probability of flipping a spin depends on the value of the spin. If the BA leaves a site with spin $+1$ we flip that spin with probability q^+, whereas if the BA leaves a site with spin -1 we flip that spin with probability q^-. At a microscopic level the model is now considerably more complicated as the transition rates for flipping depend explicitly on the values of the spins. We shall not construct the master equation for this case. Rather, we shall try to construct an analog of the continuum model (7.15) using a simple physical idea.

The main effect of the asymmetric couplings is to favor one type of spin over the other. For the sake of argument let us take $q^+ < q^-$. In this case the probability that a site with spin $+1$ is flipped by the BA is less than that for a site with spin -1, so that after some time there will be considerably more sites *in the active zone* with spin $+1$ than sites with spin -1. By "active zone" we mean the region which has been thoroughly explored by the BA after an elapsed time t. This region will have a linear size which grows as $\sqrt{Dt}$. We may immediately obtain a rough estimate of the average global magnetization from this picture. Let us make the crude approximation that outside this region the magnetization density relative to its initial value of unity is zero, and that inside this region the relative density is $1 - m_{\rm eq}$. The quantity $m_{\rm eq}$ is the equilibrium value of the average spin value which has the form

$$m_{\rm eq} = \frac{q^- - q^+}{q^- + q^+} \ . \tag{8.74}$$

We may therefore estimate that the average total magnetization with asymmetric rates is related to that with symmetric rates via

$$M_A(t) = (1 - m_{\rm eq}) M_S(t) = \frac{2}{(1 + q^-/q^+)} \ M_S(t) \ , \tag{8.75}$$

where the subscripts A and S indicate "asymmetric" and "symmetric" respectively. We note in passing that, for the case $q^+ = q^-$, this simple argument would imply that $M(t) \sim (Dt)^{1/2}$, independent of the rates since the quantity $m_{\rm eq} = 0$. This is indeed the case as described originally.

We now make the approximation that in a coarse-grained model the dynamics of relaxation to this "background magnetization" are the same as the relaxation to zero magnetization in the symmetric model. This amounts to a simple linear shift in the order parameter $\phi(\mathbf{r}, t)$ which appears in the continuum description. We therefore write the analog of (7.15) for asymmetric rates in the form

$$\partial_t \phi(\mathbf{r}, t) = -\lambda [\phi(\mathbf{r}, t) - m_{\rm eq}] \Delta_l(\mathbf{r} - \mathbf{R}(t)) \ . \tag{8.76}$$

We may now use this model to derive results for the average magnetization density and the average global magnetization. Define the field $\delta\phi(\mathbf{r}, t) \equiv \phi(\mathbf{r}, t) - m_{\rm eq}$. Then $\delta\phi(\mathbf{r}, t)$

satisfies the original continuum theory (7.15), but with an initial condition $1 - m_{\rm eq}$. Thus, for any realization of the BA we have the relationship

$$\phi_A(\mathbf{r}, t; 1) - m_{\rm eq} = \phi_S(\mathbf{r}, t; 1 - m_{\rm eq}) \ , \tag{8.77}$$

where we have included the initial value of the field as the final argument. Given that the field is linearly proportional to its initial value, the above relation simplifies further to

$$\phi_A(\mathbf{r}, t; 1) = m_{\rm eq} - (1 - m_{\rm eq})\phi_S(\mathbf{r}, t; 1) \ . \tag{8.78}$$

Thus the average magnetization density relaxes to its equilibrium value with the dynamics of the symmetric system (cf. Eqn. (7.27)), up to a factor of $(1 - m_{\rm eq})$. Integrating this equation over space, and using the definition (7.31) of the average global magnetization, it is easy to see that the relation (8.75) is an exact consequence of this model.

We have tested the validity of (8.78) by measuring the average magnetization density of a patch of spins in a numerical simulation, and have found reasonable agreement. We report on our numerical work in more detail in the next section.

8.3.2 Quenched random rates

We now consider an alternative generalization in which the rates are symmetric, but spatially inhomogeneous. At the microscopic level, this is modeled by attaching to each lattice position $\mathbf{r}$ a quenched random variable $q_{\mathbf{r}} \in (0, 1)$ drawn from some distribution $S(\{q_{\mathbf{r}}\})$. The random variable $q_{\mathbf{r}}$ gives the probability of switching in the event that the BA visits the site $\mathbf{r}$. In the continuum theory, we model these quenched random couplings by a simple extension of Eqn. (7.15). We generalize the coupling parameter λ to a spatially inhomogeneous random function $\lambda(\mathbf{r})$, with a distribution $S[\lambda]$. This does not affect the solvability of the model due to the locality of the continuum theory, so that we have the explicit solution

$$\phi(\mathbf{r}, t; \lambda) = \exp\left[-\lambda(\mathbf{r}) \int_0^t dt' \ \Delta_l(\mathbf{r} - \mathbf{R}(t'))\right] \ , \tag{8.79}$$

where we have emphasized the dependence of ϕ on λ.

There is an enormous variety in the forms of the quenched disorder distribution S that one may study. A comprehensive analysis is beyond the scope of this thesis. In our simulations (to be described in the next section) we have chosen to study switching rates $q_{\mathbf{r}} \in (0, 1)$ which are independent random variables drawn from a uniform distribution. There is more than one way in which such a distribution can manifest itself at the continuum level. Depending on the extent to which one coarse-grains the lattice model, the continuum theory will have a distribution of couplings which is either very similar to the lattice distribution (*i.e.* uncorrelated and uniform), or more Gaussian in nature (due to

the central limit theorem). We expect different physics according to the behavior of the distribution $S[\lambda]$ as $\lambda \to 0$. Roughly speaking, if S has zero weight for small λ we expect the quenched disorder to be irrelevant to the system for large times. Conversely, if S has non-zero weight for small λ, then the disorder will play a role for arbitrarily late times. In order to exemplify this latter case, we consider as an example the distribution

$$S[\lambda] = \prod_{\mathbf{r}} S_{\rm loc}\ (\lambda(\mathbf{r}))\ , \tag{8.80}$$

where $S_{\rm loc}$ is a local (or "on-site") distribution function which we take to be uniform:

$$S_{\rm loc}(\lambda) = (1/\lambda_m)\ H(\lambda_m - \lambda)H(\lambda)\ , \tag{8.81}$$

where $H(x)$ is the Heaviside step function [49]. Henceforth we shall concentrate on $d = 1$ for simplicity.

Due to the way in which the quenched random couplings enter the continuum theory, we can easily generalize our earlier exact results. Let us first concentrate on the magnetization density at the origin, averaged over both the BA trajectories, and the distribution of λ. The first average is performed in the usual way using Laplace transforms (see chapter 7) and we have the analog of Eqn. (7.25)

$$\hat{m}(0, s; \lambda) = \frac{1}{s}\left[\frac{1}{1 + \lambda(0)\hat{g}(0, s)}\right]\ . \tag{8.82}$$

On averaging this density over the distribution of random couplings (8.81) we have

$$\langle \hat{m}(0, s; \lambda)\rangle_S = \left(\frac{2D}{\lambda_m^2 s}\right)^{1/2} \log\left[1 + \left(\frac{\lambda_m^2}{2Ds}\right)^{1/2}\right]\ . \tag{8.83}$$

Inverse Laplace transforming yields the asymptotic result

$$\langle m(0, t; \lambda)\rangle_S = \left(\frac{D}{2\pi\lambda_m^2 t}\right)^{1/2} \log\left(\frac{\lambda_m^2 t}{2D}\right)\ . \tag{8.84}$$

Therefore the decay in the homogeneous case (of $1/\sqrt{t}$ behavior) for the average magnetization density is slowed by a logarithmic factor due to the presence of the quenched random couplings. It is interesting that this logarithmic slowing down does not affect the average of the global magnetization. This quantity may be explicitly calculated using the method of infinite order perturbation theory described in chapter 7. The result is that the leading order term for large times is independent of the coupling, and is unaffected by the average over S. Thus the average over the random couplings will in no way affect the leading order behavior of $M(t) \sim (Dt)^{1/2}$. The average of the global magnetization is a very

robust quantity, and is unaffected by scalings of the homogeneous couplings and by making the couplings quenched random variables. We have performed numerical simulations for systems with quenched random couplings and report our findings toward the end of the following section.

Finally, we briefly discuss the changes that can occur to the probability distribution $\mathcal{P}$ of the local magnetization density at the origin, when quenched random couplings are introduced. We have from the previous chapter the exact result (7.50) for this function in $d = 1$: it is a log-normal distribution. The same form will hold in the present case, but now the parameter λ is to be averaged over $S[\lambda]$. We average over the uncorrelated uniform distribution given above in Eqn. (8.81). Simple integration gives

$$\langle \mathcal{P} \rangle_S = \frac{1}{2(\pi t)^{1/2} \hat{\lambda}_m \phi} \, \mathrm{E}_1 \left(\frac{(\log \phi)^2}{4 \hat{\lambda}_m^2 t} \right) \, , \tag{8.85}$$

where $\hat{\lambda}_m = \lambda_m/(2D)^{1/2}$ and $\mathrm{E}_1(z)$ is the exponential integral [48] . This distribution behaves very much like the pure log-normal distribution for $\phi \ll 1$. However, we have the interesting result that the distribution is singular at $\phi = 1$. Explicitly we have for $\psi \equiv 1 - \phi \ll 1$:

$$\langle \mathcal{P} \rangle_S \sim \frac{\log[\psi^2/4\hat{\lambda}_m^2 t]}{2(\pi t)^{1/2} \hat{\lambda}_m} \, . \tag{8.86}$$

This logarithmic singularity stems from the fact that if $S[\lambda]$ has a non-zero weight for arbitrarily small λ, there will be a non-vanishing subset of systems for which almost no corruption occurs. For large times, this subset will appear as a pronounced "peak" in the distribution $\langle \mathcal{P} \rangle_S$ for $\phi \to 1$.

8.4 Numerical Simulations

In this section we describe the details of our numerical simulations, and present figures of our data to support the various theoretical claims made in the preceding sections. The simulations are performed on a d-dimensional lattice (with d either 1 or 2) and follow the lattice rules. We set the hopping probability $p = 1$, so that in each time step the BA is moved randomly to one of its $2d$ nearest neighbor sites. In doing so, the spin it leaves behind is flipped with probability q (which is set to unity unless otherwise stated). Systems are taken large enough so that the BA never touches the boundary during the lifetime of the simulation. We generally average over between 10^5 and 10^7 realizations, depending on the desired precision of the simulation.

In section 8.1 we calculated the asymptotic form of the average magnetization density at the origin from an exact lattice calculation. As noted, the sub-leading term is not obtainable from the Tauberian theorem. However, it is clear from the various calculations

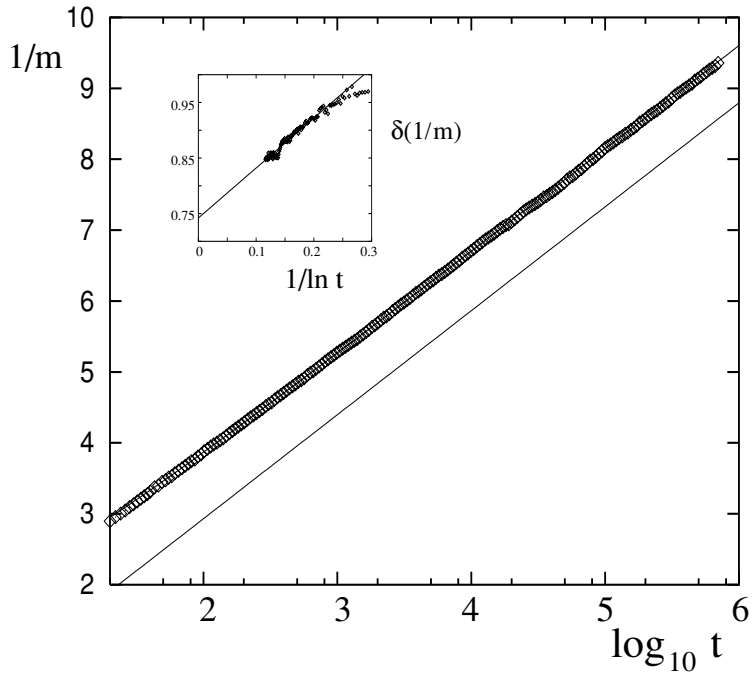

Figure 8.1: *Plot of* $1/m(\mathbf{0}, t)$ *(the inverse of the average magnetization density at the origin), as a function of* $\log t$ *for* $d = 2$*. The lower solid line is the asymptotic prediction, while the upper solid line (which is partially obscured by the data) is the prediction with corrections to scaling included. The inset shows the difference between* $1/m(\mathbf{0}, t)$ *and its asymptotic form, plotted against* $1/\ln t$*. The data may be fitted to a straight line, thereby yielding the corrections to scaling explicitly.*

in section 8.1 that the corrections decay as $1/(\log t)^2$. We have checked this in the following way. From our simulations we measure $m(\mathbf{0}, t) = \sum_{\mathbf{R}} \Theta(\mathbf{0}, \mathbf{R}, n\delta t)$. We take its inverse and subtract the predicted asymptotic result of $(2/\pi) \log n$ (in order to compare with Eqn. (8.9)). The resulting data is plotted against $1/\log n$, which should yield a straight line, the y-intercept of which fixes $C(1)$. As seen in the inset of Fig. 8.1, the data indeed confirms this expectation, and we find $C(1) \simeq -0.742$. In Fig. 8.1, we have plotted the inverse of the data against $\log t$, along with the predicted asymptotic result. The large difference between the curves indicates the strong role of the corrections (which are of order 10% even for $t \sim 10^6$).

We have also attempted to measure the probability distribution $\mathcal{P}(\phi, \mathbf{0}, t)$ in $d = 2$, as calculated in section 8.1.5. In the previous chapter, we attempted to measure this quantity in $d = 1$ and we met with limited success. The difficulty lies in the fact that the distribution only makes sense for a coarse-grained magnetization density (since a single spin always has a bimodal distribution). Thus, to construct $\mathcal{P}$ numerically we must measure

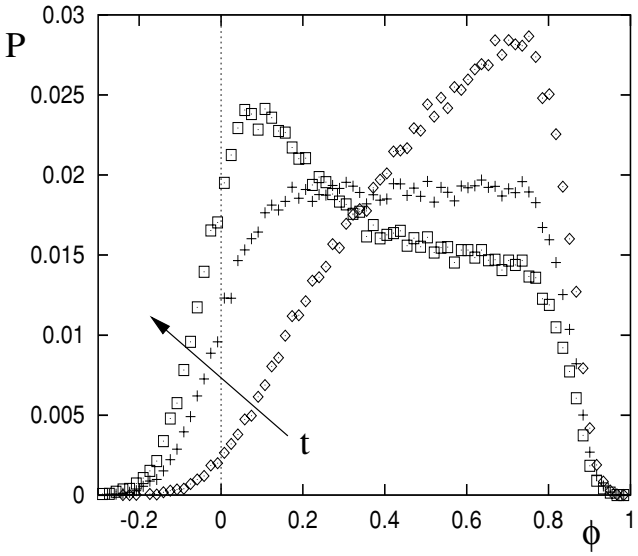

Figure 8.2: *Plot of the probability distribution $\mathcal{P}$ as a function of ϕ for $d = 2$, for times $t = 10^3(\diamondsuit)$, $t = 10^4$ (+), and $t = 10^5(\sqcap)$. Note the qualitative similarity (as time proceeds) between these different histograms, and the theoretical prediction (8.44).*

the magnetization density for a patch of spins. If the patch is too small, the resulting histogram will have too few bins to have any smooth structure; but if the patch is too large, the time scales required to allow the agent to wander far away from the patch and return many times become numerically prohibitive. Thus we must compromise, and we use a square patch of 121 spins. The agent is started on the boundary of the patch to avoid the patch being internally decimated by the transient motion of the agent. The predicted result for $\mathcal{P}$ is given in Eqn. (8.44). It shows three types of behavior set by a cross-over time t^* defined by $\beta(t^*) = 1$. For $t \ll t^*$ the distribution has most weight near $\phi = 1$, and then for $t \sim t^*$ the distribution becomes uniform over the entire interval of ϕ. For late times $t \gg t^*$, the distribution approaches the form $\sim 1/\phi$. Our numerical measurement of $\mathcal{P}$ is shown in Fig. 8.2 for these three time regimes. Good qualitative agreement is found. We note, however, that the measured distribution has non-zero weight for negative ϕ due to the modest patch size, and is also suppressed near $\phi = 1$ due to internal decimation of the patch magnetization.

In section 8.2 we presented an analysis of the continuum theory with N agents. We described the interference between the agents by a number termed the "disordering efficacy" $\sigma_N(d)$. In particular we calculated the exact value for $\sigma_N(1)$ for $N = 2, 3$ and 4, as given in Eqn. (8.56). We also predicted the large-N form of $\sigma_N(1)$, along with the exact form of the strong logarithmic corrections, as shown in Eqn. 8.70). In two dimensions we argued that

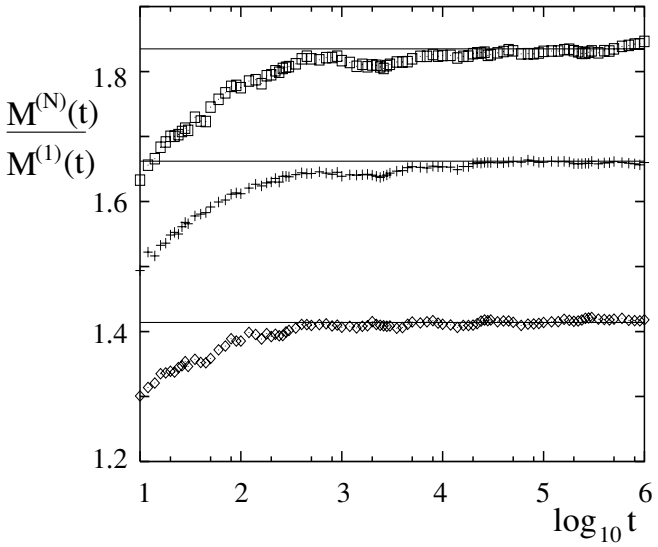

Figure 8.3: *Plot of the ratio of the average global magnetization for N agents as compared to a single agent, for (in ascending order) $N = 2, 3$, and 4, in $d = 1$. The solid lines are the theoretical predictions (8.56) for the disordering efficacies, which are the asymptotes of this ratio.*

$\sigma_N(2) = N$ for all N, but only for times $t \gg e^N$. We have performed numerical simulations of the many agent system in order to test these results. The microscopic rule we use is that there is no hard-core exclusion between the agents, and that for each time step the N agents are in turn moved to a randomly chosen nearest neighbor site. A spin which is occupied by two agents, say, will thus (for $q = 1$) be flipped twice in that time step. In Fig. 8.3 we show the evolution of the ratio of the average global magnetization for N agents as compared to one agent, for $d = 1$. Asymptotically this ratio is the disordering efficacy by definition. Results are shown for $N = 2, 3$ and 4. The curves asymptote to constants as expected, the values of which are compared to the theoretical predictions. Excellent agreement (to within less than 2%) is found. The numerical values are also given in Table 1 in section 8.2. We have measured the disordering efficacy for higher values of N in $d = 1$, and we plot our results on a logarithmic scale in Fig. 8.4. Also shown is the theoretical prediction (8.70) for large-N (where we have included both the leading and sub-leading terms). Again, excellent agreement is found. As argued in section 8.2, the cross-over times in the two-dimensional many agent system are very large, growing exponentially with N. We have attempted to measure $\sigma_N(2)$ numerically, but we have been unable to reach large enough times to see the ratio of the average global magnetizations reach a constant value. However, we may still compare our results to the theoretical prediction, by plotting the predicted value of the asymptote ($= N$) minus the measured ratio, against $1/\log t$. If the

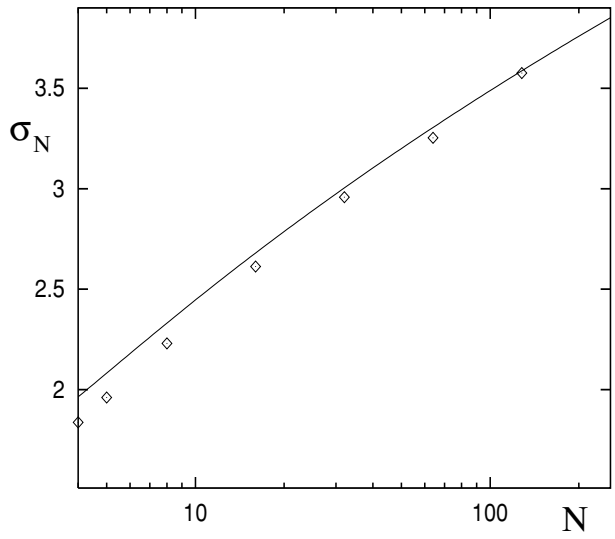

Figure 8.4: *Plot of the disordering efficacy σ_N as a function of N in $d = 1$. The solid line is the theoretical prediction (8.70) (including the strong logarithmic corrections).*

predicted asymptote is correct, the data so plotted should converge to the origin. In Fig. 8.5 we present such a plot for $N = 2, 3$ and 4. The resulting curves appear to be heading for the origin, and therefore constitute numerical support for the prediction $\sigma_N(2) = N$.

In the first part of section 8.3 we considered a system with asymmetric switching rates, and argued for the very simple phenomenological description given by the equation of motion (8.76). This equation may be solved and one obtains the simple relationship (8.78) between the magnetization density for asymmetric rates and that for symmetric rates. In particular, this result may be used to derive the intuitive result (8.75) for the proportionality of the average global magnetization for the asymmetric and symmetric cases ($M_A(t)$ and $M_S(t)$ respectively). We have performed simulations of the system with asymmetric rates in $d = 1$. In Fig. 8.6 we show the ratio of $M_A(t)/M_S(t)$ for different choices of the rates q^+ and q^-. It is seen that the ratio gradually tends to a constant, and that the constant is in agreement with the theoretical prediction (8.75). We have also tried to test Eqn. 8.78) at the level of the average magnetization density. We have found that the ratio of the densities is constant for all but the shortest times, which already indicates that the form of the time decay of $m(0, t)$ (relative to its equilibrium value) is insensitive to the asymmetry in the rates. However, we have found that this constant is sensitive to whether we measure the densities for an individual spin, or for a patch. The value of the constant decreases as we increase the patch size. In Fig. 8.7 we plot the ratio of magnetization densities for asymmetric and symmetric systems, for various patch sizes with the rates $q^+ = 0.8$ and $q^- = 0.2$. As we see, the ratio seems to be approximately

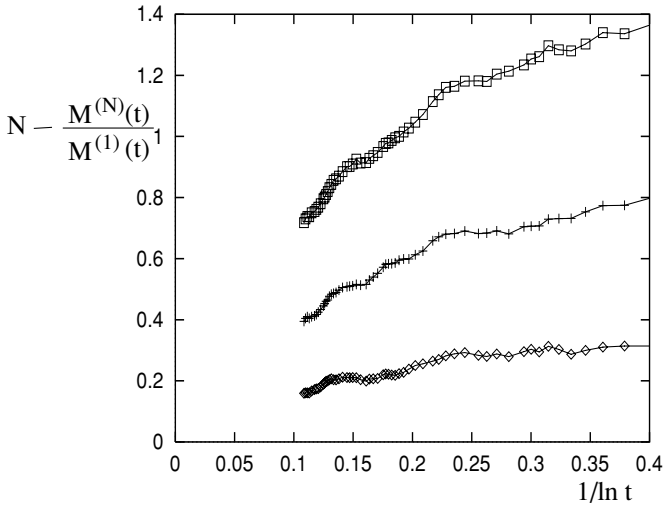

Figure 8.5: *Plot of the ratio of the average global magnetization for N agents as compared to a single agent, subtracted from N, as a function of $1/\log t$ for (in ascending order) $N = 2, 3,$ and 4, in $d = 2$. The data in each case is apparently heading for the origin, thus supporting the theoretical prediction $\sigma_N = N$.*

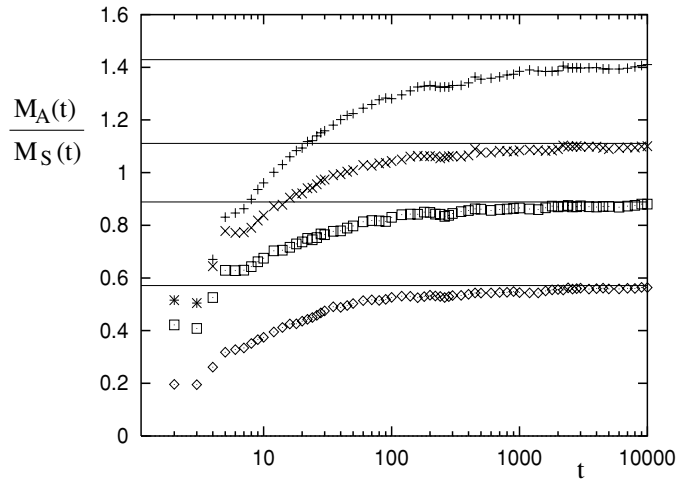

Figure 8.6: *Plot of the ratio $M_A(t)/M_S(t)$ versus time for systems in $d = 1$ with asymmetric rates. In ascending order, the values of the rates are $(q^-, q^+) = (0.5, 0.2),\ (0.5, 0.4),\ (0.4, 0.5),\ (0.2, 0.5)$. The solid lines are the theoretical predictions obtained from (8.75).*

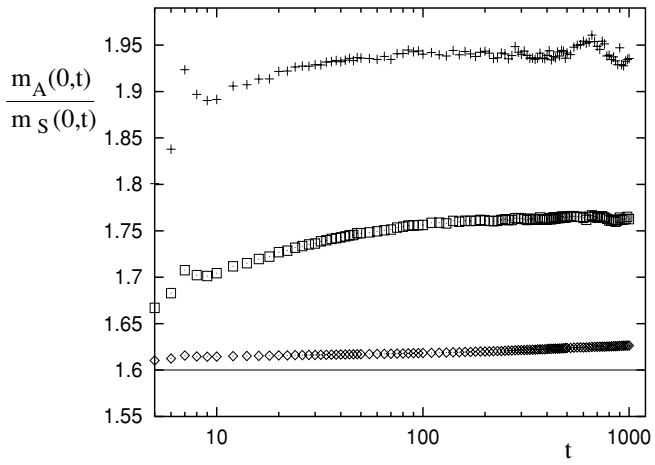

Figure 8.7: *Plot of the ratio of magnetization densities $m_A(0,t)/m_S(0,t)$ for $d = 1$ with asymmetric rates $q^- = 0.2$ and $q^+ = 0.8$. The ratio is measured for different patch sizes, the patches having from top to bottom 9, 19, and 101 spins respectively. The solid line is the theoretical prediction from Eqn. 8.78).*

constant, and the value decreases as the patch size is increased. Reasonable agreement is found with the prediction of Eqn. 8.78) for the largest patch of 101 spins. This indicates that (8.78) is likely to be correct, but only after a large degree of coarse-graining.

Finally we turn to the predictions of section 8.3.2, which concern the system with symmetric quenched random rates. We investigated this situation numerically in $d = 1$ by measuring the global magnetization, and the magnetization density. We perform the averaging in batches; namely, we use the same set of quenched rates for a batch of 1000 systems, which are then averaged over their different BA histories. Then we repeat this for N_b batches (with $N_b \sim 10^3$), thus averaging over different realizations of the quenched rates. We choose the quenched couplings $\{q_{\mathbf{r}}\}$ to be uncorrelated random variables drawn from a uniform distribution in the range $[0, 1]$. In Fig. 8.8 we show the average of the global magnetization in a system with quenched rates, and compare it to the same quantity in a "pure" system. The two curves become identical for late times (following a power law growth $\sim \sqrt{t}$) indicating that the average global magnetization is insensitive to the quenched rates, as predicted. Turning to the average magnetization density, we found at first that our results could not be fitted to the theoretical prediction (8.84). However, a closer analysis revealed that great care must be taken in making the comparison. The point is that one wishes to compare theory and simulation for long times (when the asymptotic form given in (8.84) becomes valid). However, it turns out that there is a new cross-over time t_f within the numerical simulations, beyond which the theoretical prediction is expected to break down. This cross-over time emerges due to insufficient averaging over

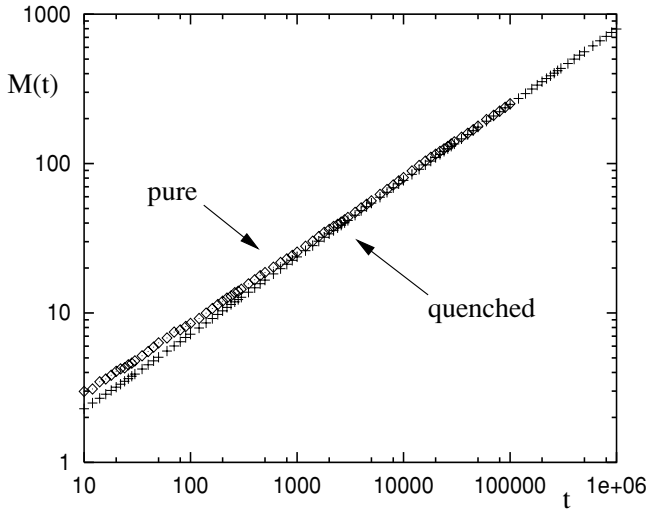

Figure 8.8: *Plot of the average global magnetization versus time for systems with quenched and pure (homogeneous) switching rates. For long times the functions become identical, growing* $\sim \sqrt{t}$.

batches. In the simulation we average over N_b batches, and thus select N_b couplings from the uniform distribution. There will be a smallest selected value $q_f \sim 1/N_b$ of the coupling, and thus from this finite sampling of S, we cannot discern if we are really using a uniform distribution with non-zero weight all the way down to $q = 0$, or a distribution with non-zero weight only down to $q = q_f$. In the latter case, one can shown (from either the lattice or continuum theories) that the logarithmic slowing down will vanish after a time $t_f \sim 1/q_f^2$. Thus, in our simulations we can only expect to see the logarithmic slowing down for times much less than $t_f \sim N_b^2$. So, in order to makes this time-window as large as possible it is important to perform as many batch averages as possible, at the expense of averaging over BA histories within a given batch. To make a quantitative comparison to theory, we have calculated the exact form of the logarithmic slowing down from the lattice theory, using the methods described in section 8.3.1. After averaging over a uniform distribution of the rates, we have from the Tauberian theorem the exact asymptotic result

$$\left\langle \sum_R \Theta(0, R, n\delta t) \right\rangle_S \sim \frac{\log(n)}{2(2\pi n)^{1/2}} \left[1 + O\left(\frac{1}{\log n} \right) \right] . \tag{8.87}$$

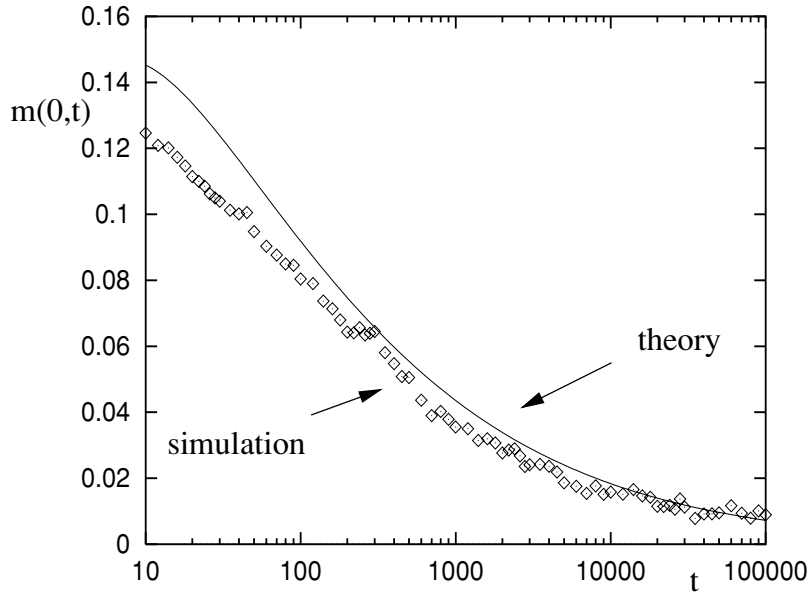

Figure 8.9: *Plot of the magnetization density at the origin (averaged over both BA histories and the quenched rates) versus time. The solid line is the asymptotic form of the theoretical prediction Eqn. 8.87) with no free parameters.*

We plot in Fig. 8.9 the average magnetization density, and the above asymptotic result. Good agreement is found, and the difference may be well fitted against the slow logarithmic corrections. Note, for times longer than those shown on the plot, the data fails to agree with the predicted result due to cross-over into the regime $t \gg t_f$ in which finite sampling effects dominate.

Chapter 9

Summary, discussion and conclusion

In the first half of this part, we have introduced and analyzed a simple model of data corruption due to a Brownian agent (BA). In section 7.1 we introduced a discrete version of the model, which consists of a BA flipping bits (or spins) on a lattice. The model is non-trivial since the value of a given spin depends very sensitively on the path of the BA (*i.e.* whether the spin has been visited an odd or even number of times). We presented a master equation formulation of the model and derived an equation of motion for the marginal average of the magnetization density. In the continuum limit, this quantity was seen to satisfy an imaginary-time Schrödinger equation (ITSE) for a particle in a repulsive δ-function potential. Higher-order marginal averages also satisfy ITSE's with an additional repulsive δ-function potential for each spin being averaged. We also proved that there is an exact proportionality between the rate of change of the mean global magnetization $M(t)$ (as defined in Eq.(7.8)) and the mean magnetization density at the origin, thus revealing a non-trivial statistical relation between a global and a local quantity.

In section 7.2 we recast the discrete model as a stochastic cellular automaton (SCA). From the local rules of the SCA, we postulated a particularly simple continuum theory written in terms of a coarse-grained magnetization density $\phi(\mathbf{r}, t)$ (which is a functional of the walk $\mathbf{R}(t)$ of the BA). We showed that averages of this stochastic field may be recast as integrals over the final BA position, the integrands of which are imaginary-time path integrals (ITPI's). These ITPI's were shown to describe quantum systems of repulsive δ-function potentials identical to those revealed through the ITSE formulation of the master equation. In this way we have confirmed that the continuum theory is a good representation of the underlying discrete model. It is worth mentioning that averages of $1/\phi$ correspond to the quantum mechanics of an *attractive* δ-function potential. In this case there is the possibility of a sharp transition in behavior for $d > 2$ as one varies λ, since bound states only exist for a sufficiently attractive well.

In section 7.3 we thoroughly examined the properties of the continuum theory for $d = 1$. First, we derived an exact expression for the evolution of the magnetization density

$m(x,t)$, and found its spatial variation for small and large x. In particular we found $m(0,t) \sim 1/\lambda\sqrt{t}$ for large times; and also the existence of both a diffusive and a ballistic scale in $m(x,t)$. Using the exact result for $m(x,t)$ enabled us to prove that the rate of change of $M(t)$ is proportional to $m(0,t)$ for all times (with proportionality constant λ) which is the continuum analog of the global/local relation that was proved in section 7.1. We then studied the two-point correlation function $C(x,t)$. An exact expression was found for the Laplace transform of this quantity, from which we were able to extract its long-time behavior, which is expressed in terms of a Jacobi theta function as shown in Eq.(7.43). The correlation function has an asymptotic scaling form; namely the ratio $C(x,t)/m(0,t)$ depends only on $x/\sqrt{t}$. Finally, we examined the probability density $\mathcal{P}$ of the magnetization density. Using a fortuitous property of the original continuum theory which enables us to represent the n^{th} moment of the magnetization density in terms of $m(x,t)$, along with our exact expression for this latter quantity, we were able to derive an exact expression for $\mathcal{P}(\phi,x,t)$ as shown in Eq.(7.49). In particular, setting $x = 0$ reveals that $\mathcal{P}(\phi,0,t)$ is a pure log-normal distribution. This last result emphasizes the importance of extreme fluctuations in this system. For instance, $m(0,t)$ decays as $1/\sqrt{t}$, whilst the typical value of the magnetization density at the origin (i.e. the mode of $\mathcal{P}$) decays as $\exp(-\lambda^2 t/D)$.

In section 7.4 we presented our results from extensive numerical simulations of the original lattice model. We measured the spatial and temporal variation of the mean magnetization density, the mean global magnetization, and the two-point correlation function $C_x(t)$. In all cases we found excellent agreement between our data and the theoretical predictions arising from the continuum model. In particular, the agreement between the theoretical form for $C(x,t)$ and the numerical data is very satisfying, as there are no free parameters to adjust. We also measured $m_{\mathbf{0}}(t)$ in two dimensional simulations, and found good agreement with the predicted logarithmic decay. Finally we attempted to measure the probability distribution of the magnetization density, by binning the magnetization of a spin patch (containing 21 spins) from 10^8 realizations. The results are not of high enough quality to directly compare with the derived log-normal distribution; however, we do see clear evidence of a long robust tail of the histogram for values of ϕ near unity, which is a clear signature of the importance of extreme fluctuations.

In the second half of these studies, we pursue a continuation of our previous chapter. In order to make closer contact to potential physical realizations of this process we have extended our original study in three directions: i) a careful examination of two dimensions, which is the critical dimension for the model, ii) the competition induced by more than one agent, and iii) the case of generalized couplings between the BA and its environment.

Section 8.1 was devoted to a careful examination of two dimensions, which, because of the recurrent properties of random walks, is the critical dimension for this process. Thus, naive dimensional arguments are modified by logarithmic corrections, and there are also strong corrections to the leading order results. For these reasons it is difficult to obtain controlled analytic results and to compare them meaningfully to numerical data. In an

attempt to overcome these obstacles we presented four different methods of calculation for the average magnetization density at the origin $m(\mathbf{0}, t)$, using both discrete and continuum models. We found agreement in all cases for the leading behavior $m(\mathbf{0}, t) \sim 2\pi D/\lambda \log t$. We also gained insight into the non-universal nature of the sub-leading terms, which in all cases depends on the type of regularization used. However it is clear from the various forms of $m(\mathbf{0}, t)$ that the leading corrections decay as $1/(\log t)^2$. This allowed us to analyze our data in a quantitative way, and excellent agreement was found with our numerical simulations for both the leading term, and for the nature of the logarithmic corrections. Furthermore, given the explicit functional forms derived for $m(\mathbf{0}, t)$ we were able to derive approximate forms for the probability distribution $\mathcal{P}$ of the magnetization density at the origin. The precise form is again non-universal as the shape of $\mathcal{P}$ depends sensitively on the sub-leading terms of $m(\mathbf{0}, t)$. However, we compared the simplest form (8.44) with simulation and found good qualitative agreement.

In section 8.2 we generalized the model to a process with N agents, which although non-interacting, produce statistical interference in the corruption of the system due to the overlap of their histories. We described their effect via the "disordering efficacy" $\sigma_N(d)$ defined as the ratio of the average global magnetization due to N agents, as compared to that of one agent. After deriving a general form for $\sigma_N(d)$ (for $d < 2$), we first studied the case $d = 1$. We were able to derive exact values for $\sigma_N(1)$ for $N = 2, 3$ and 4 which are in excellent agreement with simulations. Returning to general $d < 2$ we found that $\sigma_2(d) = 2^{d/2}$, which assuming smooth continuation to two dimensions implies $\sigma_2(2) = 2$, meaning that the two agents are statistically independent. We then formulated a large-N analysis of the disordering efficacy, and found for $d < 2$ that $\sigma_N(d) \sim [\log N]^{d/2}$. Thus in dimensions less than two, the agents interfere very strongly with one another. The precise logarithmic dependence (with the accompanying strong logarithmic corrections) are supported by excellent quantitative agreement with simulations in $d = 1$. We found that the large-N analysis fails on continuation to $d = 2$. An alternative analysis for $d = 2$ yielded the result $\sigma_N(2) = N$ which is satisfied in the deep asymptotic regime $t \gg e^N$. This result is also supported by numerical simulation in $d = 2$ for modest values of N. Thus, the disordering efficacy is extremely sensitive to the dimensionality of the system, and is strongly discontinuous as $d \to 2$.

We moved on to a study of generalized couplings in section 8.3. First we considered homogeneous couplings (between the BA and the environment) which are asymmetric. In the context of data corruption, this means that the agent has a probability of switching $0 \to 1$ which is different to the probability of switching $1 \to 0$. We proposed to model this effect by a simple extension of the original continuum model, based on the idea that the dynamics of the asymmetric process may be described relative to the non-zero background magnetization, using the relaxational dynamics of the symmetric process. This idea leads to several simple predictions for the average (local and global) magnetization which are supported by simulation. Second, we considered symmetric but inhomogeneous couplings.

Thus, the probability for the agent to switch a given element is given by a quenched random variable. We incorporated this new effect into the continuum model by generalizing the constant parameter λ to a quenched random field $\lambda(\mathbf{r})$ described by a distribution $S[\lambda]$. We investigated the simple case in which S is spatially uncorrelated, with a uniform on-site distribution function. We found that the average magnetization density at the origin decays more slowly than in the homogeneous case, by a factor $\sim \log t$. However, the average global magnetization is asymptotically insensitive to the quenched couplings. The probability density for the magnetization density at the origin $\mathcal{P}(\phi, 0, t)$ is dramatically altered for values of ϕ close to unity, where it suffers a logarithmic divergence; this is due to a non-vanishing subset of systems for which the coupling $\lambda(x = 0)$ is very small, such that barely any corruption occurs. The main features of corruption in the presence of quenched random couplings were supported by numerical simulation. Finally in section 8.4 we described the details of our numerical simulations, and presented figures supporting the different analytic predictions from the previous sections.

In conclusion, we have introduced and solved a model in which a BA interacts with a bimodal environment (*i.e.* a medium containing two types of particles, spins, bits, etc.). Our primary application has been an environment composed of bits of data, which the BA steadily corrupts. We have been interested in the statistical correlations and fluctuations of the disordered medium, and our exact results (arising from a simple continuum model) reveal the correlations to be non-trivial and the fluctuations to be extreme in nature. These statements are made quantitative by the form of the two-point correlation function, and the probability distribution of the density of corrupted bits. Then we have presented three important extensions of our investigation.

The most important fact to emerge from this investigation is the robustness of the phenomenological model (7.15) in accounting for the properties of the data corruption process under a wide range of conditions. The fact that this process may be modeled by such a simple continuum theory gives one confidence in applying similar phenomenological models to more complicated physical situations involving Brownian agents.

The model may also be seen to be a very simplified version of other systems. For instance the bistable medium can be taken to be composed of two chemical species A and B (with vanishingly low mobility) and the BA to be a high mobility catalyst, inducing a reversible reaction between A and B (and *vice versa*). Alternatively we can think of the BA as a wandering impurity in an ionic crystal (such as an anion or cation vacancy in $NaCl$) or a semiconductor compound (such as Zn in $GaAs$), which has a small probability of reordering the local bi-atomic structure as it passes through a given unit cell [50]. The data corruption process appears to us the most interesting application, as well as being the most potentially relevant. This is especially true given the enormous efforts dedicated to creating memory storage devices of ever-decreasing size. Such miniaturization will lead to new causes of soft error production [41], amongst which will inevitably be found the Brownian agent.

It remains to be seen whether one can find a solid application of the models. By having explored more challenging situations such as two dimensions, many agents, and asymmetric and quenched random couplings, we are able to seriously address the practical issues involved in making the connection between the rich statistical properties of our model, and their potential existence in the real world.

Appendix

APPENDIX IA

In this Appendix, we add a few details of the Poisson resummation procedure. Our starting point is Eqn. (3.11). Dropping the constant prefactor, we focus on the expression in the brackets, with $\zeta \equiv \epsilon t$:

$$F(\zeta) \equiv 1 - \frac{8}{\pi^2} \sum_{n=1}^{\infty} e^{-\zeta(2n-1)^2}/(2n-1)^2 \tag{1}$$

This sum converges rapidly in the limit $\zeta \to \infty$. We seek a form which converges equally well in the limit $\zeta \to 0$. We first recast this sum in terms of a much simpler one, namely,

$$S(\lambda) \equiv \sum_{n=1}^{\infty} e^{-(\lambda n)^2}. \tag{2}$$

We begin by noting that $\sum_1^\infty 1/(2n-1)^2 = \pi^2/8$ so that

$$\begin{aligned} F(\zeta) &= \frac{8}{\pi^2} \sum_{n=1}^{\infty} \frac{1 - e^{-\zeta(2n-1)^2}}{(2n-1)^2} \\ &= \frac{8}{\pi^2} \zeta \int_0^1 ds \sum_{n=1}^{\infty} e^{-\zeta(2n-1)^2 s} \end{aligned} \tag{3}$$

It is easy to recognize the sum in this expression as the "odd" terms in $S(\lambda)$, with $\lambda = \sqrt{s\zeta}$. This suggests that we should recast $S(\lambda)$ in the form

$$\begin{aligned} S(\lambda) &= \sum_{n=1}^{\infty} e^{-(2\lambda n)^2} + \sum_{n=1}^{\infty} e^{-(\lambda(2n-1))^2} \\ &\equiv S_e(\lambda) + S_o(\lambda) \end{aligned}$$

where the "even" terms just reproduce $S(\lambda)$, via $S_e(\lambda) = S(2\lambda)$. Summarizing so far, we obtain

$$F(\zeta) \equiv \frac{8}{\pi^2} \zeta \int_0^1 ds \; S_o(\sqrt{\zeta s}) \tag{4}$$

$$= \frac{8}{\pi^2} \zeta \int_0^1 ds \; \left[S(\sqrt{\zeta s}) - S(2\sqrt{\zeta s}) \right] \tag{5}$$

Thus, it is sufficient for us to resum $S(\lambda)$. We recall the Poisson resummation formula [33], for a function $f\,(x)$, defined on $0 \leq x < \infty$ with $\lim_{x\to\infty} f(x) = 0$ and $\int_0^\infty dx\ f(x)$ finite:

$$\frac{1}{2}f(0) + \sum_{n=1}^{\infty} f(n\lambda) = \lambda^{-1}\left[\frac{1}{2}\tilde{f}(0) + \sum_{m=1}^{\infty}\tilde{f}(\frac{2\pi m}{\lambda})\right] \tag{6}$$

where $\tilde{f}$ is the Fourier cosine transform of f:

$$\tilde{f}(\alpha) \equiv 2\int_0^\infty dx\ f(x)\cos(\alpha x)\ .$$

From Eqns. (2), we can immediately read off $f(x) = \exp(-x^2)$ for our case whence

$$\tilde{f}(\alpha) = \sqrt{\pi}\exp(-\alpha^2/4)\ .$$

Thus, we obtain

$$S(\lambda) = -\frac{1}{2} + \lambda^{-1}\left\{\frac{\sqrt{\pi}}{2} + \sqrt{\pi}\sum_{m=1}^{\infty} e^{-(m\pi/\lambda)^2}\right\} \tag{7}$$

Clearly, the original form of $S(\lambda)$, Eqn. (2) converges rapidly for large λ, while the alternate form presented here converges rapidly for $\lambda \to 0$. Inserting our result into Eqn. (5) and performing the integration results in

$$F(\zeta) = \frac{4}{\pi^{3/2}}\sqrt{\zeta}\left\{1 + 2\sum_{m=1}^{\infty}(-1)^m\left[e^{-u_m^2} - u_m\Gamma(\frac{1}{2}, u_m)\right]\right\} \tag{8}$$

where $u_m \equiv \pi m/\sqrt{8\epsilon t}$. This leads immediately to our result for the disorder parameter, Eqn. (3.12).

The Poisson resummation of the magnetization profile, Eqn. (4.12), is a little more involved, but follows an analogous series of steps. In this case, the problem can be reduced to resumming

$$\Sigma(\tilde{y}, \zeta) \equiv \sum_{n=1}^{\infty}\frac{\sin(n\tilde{y})}{n}e^{-\zeta n^2},$$

where $\tilde{y} \equiv 2\pi y/L$, since we can rewrite

$$\psi(\mathbf{r}, t) = \frac{4}{\pi}\left[\Sigma(\tilde{y}, \zeta) - \frac{1}{2}\Sigma(2\tilde{y}, 4\zeta)\right]\ .$$

The resummation leads to

$$\Sigma(\tilde{y}, \zeta) = -\frac{\tilde{y}}{2} + \frac{\pi}{2}\,\mathrm{erf}\left(\frac{\tilde{y}}{2\sqrt{\zeta}}\right) + \frac{\pi}{2}\sum_{m=1}^{\infty}\left[\mathrm{erf}\left(\frac{\tilde{y} + 2\pi m}{2\sqrt{\zeta}}\right) + \mathrm{erf}\left(\frac{\tilde{y} - 2\pi m}{2\sqrt{\zeta}}\right)\right]$$

so that we finally arrive at Eqn. (3.13).

APPENDIX IB

In this appendix, we present the mathematical details of solving Eqn. (4.10) for brick-wall boundary conditions, restricted to the intermediate and late stages of the disordering process, i.e., $O(L^2) \ll t$. Thus, in the following, "early" refers to times at the onset of the intermediate regime while "late" times are deeply within the saturation region. To recall, we seek a solution, $\psi(y,t)$, to the partial differential equation

$$\partial_t \psi(y,t) = \partial[\phi_o(y)\partial\psi(y,t)] \tag{9}$$

where

$$\phi_o(y) = \frac{EL}{2L^d \sinh(EL/2)} \exp(Ey)$$

subject to the initial and boundary condition $\psi(y,0) = 2\theta(y) - 1$ and $\partial\psi(\pm\frac{L}{2},t) = 0$. First, we introduce the new variable

$$x \equiv \int_y^\infty dy' \frac{1}{\phi_o(y')} = \frac{1}{E\phi_o(y)} \ , \tag{10}$$

which is strictly positive. This reduces Eqn. (9) to a diffusion equation with a spatially varying diffusion coefficient:

$$\partial_t \psi(x,t) = Ex\partial_x^2 \psi(x,t). \tag{11}$$

subject to the boundary condition $\partial_x \psi(x_\pm,t) = 0$ at $x_\pm \equiv [E\phi_o(\pm L/2)]^{-1}$. We note that the definition (10) implies $0 < x_+ < x_-$. Next, we separate variables, according to the ansatz

$$\psi(x,t) = T(t)f(x). \tag{12}$$

whence we obtain two ordinary differential equations:

$$\frac{dT}{dt} + \kappa T = 0 \tag{13}$$

$$\frac{d^2 f}{dx^2} + \frac{\kappa}{Ex} f = 0 \ , \tag{14}$$

The constant κ must be positive in order to be consistent with the steady state solution, $\lim_{t\to\infty} \psi(y,t) = \psi_o(y) = 0$. The first of these equations describes a simple exponential decay. The second constitutes a well-defined Hermitean eigenvalue problem, with eigenvalues κ and eigenfunctions f. For convenience, we define $\kappa/E \equiv \alpha^2/4$ and transform (14) into the differential equation for the *Bessel functions* [48], via $u \equiv \alpha\sqrt{x}$. The solutions are

$$T(t) = \exp(-\kappa t) \tag{15}$$

$$f(x) = A\alpha\sqrt{x}J_1(\alpha\sqrt{x}) + B\alpha\sqrt{x}N_1(\alpha\sqrt{x}). \tag{16}$$

Here, A and B are integration constants. We have two boundary conditions, one at each end of the system. Using the recursion relations for the Bessel functions, we can eliminate one of the integration constants, e.g.,

$$B = -A\frac{J_0(\alpha\sqrt{x_-})}{N_0(\alpha\sqrt{x_-})} \tag{17}$$

and specify the allowed eigenvalues α_n as the solutions of the implicit equation

$$\begin{aligned} 0 &= N_0(\alpha_n\sqrt{x_-})J_0(\alpha_n\sqrt{x_+}) - N_0(\alpha_n\sqrt{x_+})J_0(\alpha_n\sqrt{x_-}) &(18)\\ &\equiv N_0(\lambda z_n)J_0(z_n) - N_0(z_n)J_0(\lambda z_n) &(19)\end{aligned}$$

The second line, with $z_n \equiv \alpha_n\sqrt{x_+}$ and $\lambda \equiv \sqrt{\frac{x_-}{x_+}} = \exp(LE/2) > 1$, is a more standard form of the eigenvalue equation [48]. Since both J_0 and N_0 oscillate, this equation has infinitely many solutions. The eigenvalues are real, non-degenerate and discrete; they increase monotonically with n. The lowest ones are easily determined numerically for different λ. For large $n\pi/(\lambda-1)$, there is an asymptotic expansion,

$$z_n = \frac{n\pi}{\lambda-1}\left\{1 - \frac{1}{8\lambda}\left(\frac{\lambda-1}{n\pi}\right)^2 + O\left[\left(\frac{\lambda-1}{n\pi}\right)^4\right]\right\} \tag{20}$$

To find the eigenfunctions $\{U_n(x)\}$, we need to normalize the f's. For convenience, we introduce the auxiliary function

$$F(s) \equiv s[N_0(\alpha_n\sqrt{x_-})J_1(s) - J_0(\alpha_n\sqrt{x_-})N_1(s)] \tag{21}$$

and define the normalization constants

$$c_n \equiv \frac{\alpha_n}{\left[F^2(\alpha_n\sqrt{x_-}) - F^2(\alpha_n\sqrt{x_+})\right]^{1/2}} = \frac{\alpha_n}{\left[F^2(\lambda z_n) - F^2(z_n)\right]^{1/2}}\ . \tag{22}$$

Then, the eigenfunctions take the form:

$$\begin{aligned} U_n(x) &= \frac{c_n}{\alpha_n}F(\alpha_n\sqrt{x})\\ &= c_n\sqrt{x}\left[N_0(\alpha_n\sqrt{x_-})J_1(\alpha_n\sqrt{x}) - J_0(\alpha_n\sqrt{x_-})N_1(\alpha_n\sqrt{x})\right]\ . &(23)\end{aligned}$$

They are real and orthonormal:

$$\delta_{nm} = \int_{x_+}^{x_-} dx\, x^{-1}U_n(x)U_m(x) = E\int_{-L/2}^{+L/2} dy\, U_n(y)U_m(y)$$

where the second equality expresses the orthonormality condition in terms of the original variable y. They form a complete set so that the full solution for the magnetization density can be written as an expansion:

$$\psi(x,t) = \sum_{n=1}^{\infty} A_n U_n(x) \exp(-\kappa_n t) \ , \tag{24}$$

where $\kappa_n = E\alpha_n^2/4$, and $x = [E\phi_o(y)]^{-1}$. The expansion coefficients A_n are chosen such that the initial condition is satisfied. With $x_o \equiv [E\phi_o(0)]^{-1}$, this yields:

$$A_n = \frac{4c_n}{\alpha_n} \left[N_0(\alpha_n\sqrt{x_o}) J_0(\alpha_n\sqrt{x_-}) - N_0(\alpha_n\sqrt{x_-}) J_0(\alpha_n\sqrt{x_o}) \right] \tag{25}$$

$$= \frac{4}{\left[F^2(\lambda z_n) - F^2(z_n)\right]^{1/2}} \left[N_0(\sqrt{\lambda} z_n) J_0(\lambda z_n) - N_0(\lambda z_n) J_0(\sqrt{\lambda} z_n) \right] \tag{26}$$

This completes the solution. Of course, it is given rather implicitly in terms of the eigenvalues.

APPENDIX IC

In this appendix, we investigate how our expressions depend on the key system parameters, L and E. We first establish the scaling properties of the eigenvalues, κ_n. Beginning with Eqn. (19), we conclude that the z_n's are functions of λ alone. Since $\lambda = \exp(LE/2)$, each z_n depends only on the scaling parameter LE. To obtain a similar conclusion for $\kappa_n = E\alpha_n^2/4 = Ez_n^2/(4x_+)$, we recall that

$$1/x_+ = E\phi_o(+L/2) = \frac{(EL)^2 \exp(EL/2)}{2L^{d+1}\sinh(EL/2)}$$

Thus, the desired scaling form for the eigenvalues is

$$\kappa_n = L^{-(d+2)} g_n(LE) \tag{27}$$

where the scaling function $g_n(x)$, with $x \equiv LE$, is given by

$$g_n(x) \equiv z_n^2(x) \frac{x^3 \exp(x/2)}{8\sinh(x/2)} \tag{28}$$

Its limits for small and large argument are easily found from Eqn. (19) and the asymptotic form (20):

$$\lim_{x\to 0} g_n(x) = (n\pi)^2 \left[1 + O(x)\right] \quad \textit{and} \quad \lim_{x\to\infty} g_n(x) \simeq x_n \exp(-x/2) \ , \tag{29}$$

where x_n denotes the n-th zero of the Bessel function J_0.

In particular, we are interested in the *late crossover time*, Eqn. (4.18), defined as the inverse of the first eigenvalue,

$$t_c(L,E) \equiv \kappa_1^{-1} \equiv L^{d+2}\tau_c(LE) \ . \tag{30}$$

This characteristic time is a measure for when the crossover from the intermediate to the saturation regime occurs. The behavior of its scaling function, $\tau_c(x) \equiv g_1^{-1}(x)$, follows immediately from Eqn. (29): $\lim_{x\to 0}\tau_c(x) = \pi^{-2}\left[1 + O(x)\right]$ and $\lim_{x\to\infty}\tau_c(x) \simeq (0.1729.../x^3)\exp(x)$.

Finally, we will need the scaling behavior of the expansion coefficients A_n. From Eqn. (26), it is immediately apparent that these coefficients depend only on the *combination* LE so that $A_n = A_n(LE)$.

APPENDIX ID

While Eqn. (4.14) for $\mathcal{A}(L,E;t)$ is of course completely exact within our mean-field theory, it converges rapidly only for late times, $\kappa_n t \gg 1$. There, keeping only the $n=1$ term in the sum already results in an excellent approximation. In contrast, Eqn. (4.14) is not very practical if we wish to extract the observed power law at early times. Fortunately, a *Poisson resummation* [33] of Eqn. (4.14) allows us to recast the disorder parameter in a form that converges rapidly in the short-time limit. Some details of this procedure form the content of this section.

We recall Eqn. (4.14):

$$\mathcal{A}_R(L,E;t) = \frac{d}{2}L^d\left[1-\frac{1}{EL}\sum_{n=1}^{\infty}A_n^2\exp(-2\kappa_n t)\right] \ , \tag{31}$$

where both A_n and κ_n depend on the summation index via the eigenvalues z_n. The key to the Poisson resummation resides in the following three statements:
First, from the discussion below Eqn. (4.13), we recall the initial condition on the disorder parameter, namely $\mathcal{A}_R(L,E;0)=0$. This implies [54]

$$\frac{1}{EL}\sum_{n=1}^{\infty}A_n^2 = 1 \ , \tag{32}$$

so that there is no constant term in the short-time expansion of $\mathcal{A}_R$.
Second, considering any *finite* number of terms in Eqn. (31) can only generate a *linear* time dependence, $\mathcal{A}_R(L,E;t)\propto t$. Therefore, the *anticipated* short-time behavior $\mathcal{A}_R\propto\sqrt{t}$ must be controlled by the *large* n contributions to the sum. Hence, these are crucial for our purposes.
Third, for sufficiently large $n>n_o$, we can always approximate the eigenvalues z_n by their explicit asymptotic form, Eqn. (20). Since the latter holds provided $n\pi/[\lambda-1]\gg 1$, the critical $n_o\sim\lambda\equiv\exp(LE/2)$ increases rapidly with LE. However, this presents no problem since only finite values of LE are of interest to us.

In summary, to obtain the short-time behavior of $\mathcal{A}_R$ it is sufficient to replace the eigenvalues z_n by their asymptotic form *everywhere*. Any errors generated in this way are at most linear in t. In this manner, the dependence on the summation index n becomes explicit, and we can apply the Poisson resummation formula [33], which holds for any continuous, bounded function $f(x)$, provided its Fourier transform $F(\omega)\equiv 2\int dx f(x)\cos(\omega x)$ is well-defined:

$$\frac{1}{2}f(0)+\sum_{n=1}^{\infty}f(n\varsigma) = \frac{1}{\varsigma}\left\{\frac{1}{2}F(0)+\sum_{m=1}^{\infty}F(\frac{2\pi m}{\varsigma})\right\} \ . \tag{33}$$

Here, ς is the parameter that controls the convergence of the sums. In our case, we identify

$$\varsigma \equiv \sqrt{\frac{4\pi^2(\ln\lambda)^3\lambda^2}{(\lambda-1)^3(\lambda+1)}L^{-(d+2)}t} \tag{34}$$

The resummation is now straightforward and results in

$$\begin{aligned}\mathcal{A}_R(L,E;t) &= \frac{d}{2}L^d\frac{4(\lambda-1)}{\pi^{3/2}\sqrt{\lambda}\ln\lambda}\zeta\left\{1+O\left[\exp(-\pi^2/\zeta^2)\right]\right\} \\ &\simeq \frac{d}{2}L^d\frac{8}{\sqrt{\pi}}\sqrt{t/t_s}\left\{1+O\left[\exp(-\pi^2/\zeta^2)\right]\right\}\end{aligned}$$

where the *scale factor* for the short-time scaling is given by

$$t_s(L,E) \equiv L^{d+2}\frac{4\sinh(LE/2)}{LE\exp(LE/2)}. \tag{35}$$

While this characteristic scale obeys the same scaling form as the late crossover time, (30),

$$t_s(L,E) = L^{d+2}\tau_s(LE) \quad with \quad \tau_s(x) \equiv \frac{x\exp(x/2)}{4\sinh(x/2)}$$

we note that the scaling function $\tau_s(x)$ is different from $\tau_c(x)$.

APPENDIX IIA

In this appendix we outline the solution to the discrete equation (7.3) for the marginal average $\Theta(\mathbf{r}, \mathbf{R}, t)$. This is achieved by use of discrete Fourier and Laplace transforms defined via

$$\mathcal{F}_{k|R}[\mathcal{L}_{z|t}[\Theta(\mathbf{r}, \mathbf{R}, t)]] = \sum_{n=0}^{\infty} z^n \sum_{\mathbf{R}} \Theta(\mathbf{r}, \mathbf{R}, n\delta t) \exp(i\mathbf{k} \cdot \mathbf{R}) \ , \tag{36}$$

(with $t = n\delta t$). By self-consistently determining the function $\Theta(\mathbf{r}, \mathbf{r}, t)$, one can explicitly solve for the double transform of Θ. Inverting the discrete Fourier transform and summing over $\mathbf{R}$ one finds (with the particular choice of initial condition (7.6))

$$\sum_{\mathbf{R}} \mathcal{L}_{z|t}[\Theta(\mathbf{R}, \mathbf{R}, t)] = \frac{1}{(1-z)} \left\{ \frac{1 - 2(1-z) \int_{\mathrm{BZ}} d^d k \ E(\mathbf{k}, z)}{1 + \frac{zq}{d} \int_{\mathrm{BZ}} d^d k \ E(\mathbf{k}, z) \ \sum_{\mathbf{l}} e^{-i\mathbf{k}\cdot\mathbf{l}}} \right\} \ , \tag{37}$$

where $\int_{\mathrm{BZ}}$ indicates integration over the first Brillouin zone, and

$$E(\mathbf{k}, z) = \left\{ 1 - z + \frac{qz}{2d} \sum_{\mathbf{l}} [1 - \exp(-i\mathbf{k} \cdot \mathbf{l})] \right\}^{-1} \ . \tag{38}$$

Similarly one can find an explicit expression for $\sum_{\mathbf{R}} \mathcal{L}_{z|t}[\Theta(\mathbf{0}, \mathbf{R}, t)]$. The expressions can be shown to be equal thus proving the relation (7.7) as given in the main text.

APPENDIX IIB

In this appendix we outline the procedure for averaging the expression in Eqn. (7.22). First, we time order the integrals, thereby absorbing the factor of $1/n!$. Then, making an integral representation of each Dirac δ-function, we have

$$\begin{aligned}\chi_n(x,t) &= \int_0^t d\tau_1 \int_0^{\tau_1} d\tau_2 \cdots \int_0^{\tau_{n-1}} d\tau_n \int dk_1 e^{ik_1 x} \cdots \int dk_n e^{ik_n x} \\ &\times \left\langle \exp\left[-ik_1 R(\tau_1) - \cdots - ik_n R(\tau_n)\right] \right\rangle . \end{aligned} \tag{39}$$

Using the solution of Eqn. (7.14), we may rewrite the average in (39) as

$$\left\langle \exp\left[-ik_1 \int_{\tau_2}^{\tau_1} d\tau \xi(\tau) - i(k_1+k_2) \int_{\tau_3}^{\tau_2} d\tau \xi(\tau) - \cdots - i(k_1+\cdots+k_n) \int_0^{\tau_n} d\tau \xi(\tau)\right]\right\rangle . \tag{40}$$

The Gaussian average over the noise may now be performed, and the above expression reduces to

$$\exp\left\{-\frac{D}{2}[k_1^2(\tau_1-\tau_2) + (k_1+k_2)^2(\tau_2-\tau_3) + \cdots + (k_1+\cdots+k_n)^2\tau_n]\right\} . \tag{41}$$

We now insert this expression back into Eqn. (39), and make the change of variables $k_1' = k_1,\ k_2' = k_1+k_2, \cdots, k_n' = k_1+\cdots+k_n$. The integrals over $\{k_j'\}$ are easily performed and we arrive at Eqn. (7.23) in the main text.

APPENDIX IIC

In this appendix we outline the evaluation of the $2n$-fold integral for $c_n(x,t)$ given in Eqn. (7.37). We note first that the time integrals have the form of a n-fold convolution. Thus, we can Laplace transform the expression to find

$$\begin{aligned}\hat{c}_n(x,s) &= \frac{1}{s}\int\frac{dk_1}{2\pi}\,(1+e^{-ik_1x})\cdots\int\frac{dk_n}{2\pi}\,(1+e^{-ik_nx}) \\ &\qquad\times\prod_{m=1}^{n}\frac{1}{[s+(D/2)(k_1+\cdots+k_m)^2]}\ . \end{aligned} \tag{42}$$

We make the change of variable $k_1'=k_1,\ k_2'=k_1+k_2,\cdots,k_n'=k_1+\cdots+k_n$, and rearrange the integrals to give

$$\begin{aligned}\hat{c}_n(x,s) &= \frac{1}{s}\int\frac{dk_1'}{2\pi}\,[s+(D/2){k_1'}^2]^{-1}\cdots\int\frac{dk_n'}{2\pi}\,[s+(D/2){k_n'}^2]^{-1} \\ &\qquad\times\prod_{m=1}^{n}\Big[1+\exp[-i(k_m'-k_{m-1}')x]\Big]\ , \end{aligned} \tag{43}$$

with the understanding that $k_0'\equiv 0$. We now multiply out the product which gives us 2^n terms. These are grouped into $n+1$ sets, the m^{th} set containing C_m^n terms which are equal after integration. Thus each term in the m^{th} set (within the integrals) may be taken to contain m factors of e^{ik_jx} (where $j=1,\cdots,m$) and $(n-m)$ factors of unity. Using the integral

$$\int_{-\infty}^{\infty}\frac{dk}{2\pi}\ \frac{e^{ikx}}{[s+(D/2)k^2]}=\frac{1}{(2sD)^{1/2}}\exp\left[-\left(\frac{2s}{D}\right)^{1/2}|x|\right]\ , \tag{44}$$

we can reduce Eqn. (43) to the form

$$\hat{c}_n(x,s)=\frac{1}{s}\sum_{m=0}^{n}C_m^n\left[\frac{1}{(2sD)^{1/2}}\right]^n\exp\left[-m\left(\frac{2s}{D}\right)^{1/2}|x|\right]\ . \tag{45}$$

Performing the binomial sum gives Eqn. (7.38) in the main text.

APPENDIX IID

In this appendix we outline the derivation of Eqn. (7.47) from Eqns. (7.45) and (7.46). The only non-trivial aspect of the derivation is the frequency integral and sum (over n) of the second term in Eqn. (7.46). Ignoring the prefactor of that term (namely $\hat{g}(x,s)/s\hat{g}(0,s)$) we must evaluate a quantity $Q(s,\phi)$, which has the form

$$Q(s,\phi) \equiv \int_{-\infty}^{\infty} \frac{d\omega}{2\pi} e^{-i\omega\phi} \sum_{n=0}^{\infty} \frac{(i\omega)^n}{n!} \frac{1}{(1+n\lambda\hat{g}(0,s))} \ . \tag{46}$$

In order to perform the sum, we introduce the integral representation

$$\frac{1}{(1+n\lambda\hat{g}(0,s))} = \int_0^{\infty} du \ \exp\Big[-u(1+n\lambda\hat{g}(0,s))\Big] \ . \tag{47}$$

The sum over n now reconstitutes an exponential function, and we have

$$Q(s,\phi) = \int_0^{\infty} du \ e^{-u} \int_{-\infty}^{\infty} \frac{d\omega}{2\pi} e^{-i\omega\phi} \exp\left(i\omega e^{-u\lambda\hat{g}}\right) \ . \tag{48}$$

The integral over ω is easily done to give

$$Q(s,\phi) = \int_0^{\infty} du \ e^{-u} \ \delta\left(\phi - e^{-u\lambda\hat{g}}\right) \ . \tag{49}$$

Finally, changing variables to $v = e^{-u\lambda\hat{g}}$ we have

$$Q(s,\phi) = \frac{1}{\lambda\hat{g}(0,s)\phi} \exp\left[-\frac{1}{\lambda\hat{g}(0,s)} \log\left(\frac{1}{\phi}\right)\right] \ . \tag{50}$$

Using this result for Q in conjunction with Eqns. (7.45) and (7.46) we have (7.47) in the main text.

APPENDIX IIE

In this appendix we outline the procedure of taking the inverse Laplace transform of Eqn. (8.16). Consider the function $H(t)$, the Laplace transform of which has the form

$$\hat{H}(s) = \frac{1}{s[a - b\log s]} \ , \tag{51}$$

for sufficiently small Re(s) such that the apparent pole at $s = e^{a/b}$ may be disregarded (a and b are positive constants). The inverse Laplace transform is given by the Bromwich integral[49]

$$H(t) = \int_C \frac{ds}{2\pi i} \ \frac{e^{st}}{s[a - b\log s]} \ , \tag{52}$$

where the contour C is to be taken up the imaginary axis (note the integration around the simple pole at the origin gives a contribution of zero). The important singularity is the branch point at the origin. We take the cut along the negative real axis and deform the contour around this cut. Integrating across the cut then gives us

$$H(t) = \frac{1}{b}\int_0^\infty \frac{dx}{x} \ \left[\frac{e^{-xt}}{(\log x - a/b)^2 + \pi^2}\right] \ . \tag{53}$$

We are interested in the asymptotic form of this integral for large t. In this limit the integral is dominated by small x. We therefore expand the denominator to give

$$H(t) = \frac{1}{b}\int_0^\infty \frac{dx}{x} \ \frac{e^{-xt}}{(\log x)^2} \ \left[1 + \frac{2a}{b\log x} + O\left(\frac{1}{(\log x)^2}\right)\right] \ . \tag{54}$$

By splitting the range of integration into two pieces ($x \in (0, 1/t)$ and $x \in (1/t, \infty)$) we systematically evaluate the terms in the above expansion to find

$$H(t) = \frac{1}{b\log t} - \frac{(a + \gamma b)}{(b\log t)^2} + O\left(\frac{1}{(\log t)^3}\right) \ , \tag{55}$$

where $\gamma = 0.57721...$ is Euler's constant. Using the appropriate form for the constants a and b we arrive at Eqn. (8.17) correct up to $O(1/(\log t)^3)$.

APPENDIX IIF

In this appendix we indicate the steps leading from Eqn. (8.53) to Eqn. (8.54). First we factorize the integrand to give

$$\sigma_N(d) = d\Gamma(1-d/2)\sum_{n=0}^{N-1} J_n(d) \ , \tag{56}$$

where

$$J_n(d) = \int_0^\infty dr \ r^{d-1} \ f(r)m(r)^n \ , \tag{57}$$

with $f(r) \equiv 1 - m(r)$. We then integrate the above expression by parts using

$$\int^r du \ u^{d-1} f(u) = \frac{r^d f(r)}{d} - \frac{e^{-r^2}}{d\Gamma(1-d/2)} + \text{constant} \ . \tag{58}$$

The resulting integral contains a factor of re^{-r^2} which allows one to integrate by parts a second time, thus yielding after some algebra (for $n > 0$)

$$J_n(d) = -\frac{\delta_{n,1}}{d\Gamma(1-d/2)} + K_n(d) - K_{n-1}(d) \ , \tag{59}$$

with

$$K_n(d) = \frac{2n(n+1)}{d\Gamma(1-d/2)^2}\int_0^\infty dr \ r^{1-d} \ e^{-2r^2} \ m(r)^{n-1} \ . \tag{60}$$

Substitution of Eqn. (59) into (56) yields the result (8.54) as shown in the main text.

APPENDIX IIG

In this appendix we indicate the evaluation of $\sigma_N(1)$ as given by Eqn. (8.55) for $N = 3$ and $N = 4$. For $N = 3$ we require

$$\sigma_3(1) = \frac{12}{\pi^{1/2}} \int_0^\infty dx \; e^{-2x^2} \; \mathrm{erf}(x) \; . \tag{61}$$

We introduce the integral

$$I(\beta) \equiv \pi^{1/2} \int_0^\infty dx \; e^{-\beta x^2} \; \mathrm{erf}(x) \; . \tag{62}$$

Using integration by parts it is straightforward to show that $I(\beta)$ satisfies the differential equation

$$2\beta \frac{dI}{d\beta} + I = -\frac{1}{(1+\beta)} \; . \tag{63}$$

This differential equation may then be integrated (using the boundary condition $I(\infty) = 0$) to give

$$I(\beta) = \frac{1}{2\beta^{1/2}} \int_\beta^\infty d\beta' \frac{1}{\beta'^{1/2}(1+\beta')} = \frac{1}{\beta^{1/2}} \sin^{-1}\left(\frac{1}{(1+\beta)^{1/2}}\right) \; . \tag{64}$$

Using this result along with the fact that $\sigma_3(1) = (12/\pi)I(2)$, we have the leftmost result of Eqn. (8.56) as shown in the main text.

The evaluation of $\sigma_4(1)$ proceeds along similar grounds. We define a function

$$L(\beta) \equiv \pi^{1/2} \int_0^\infty dx \; e^{-\beta x^2} \; \mathrm{erf}(x)^2 \; , \tag{65}$$

which may be shown to satisfy the differential equation

$$2\beta \frac{dL}{d\beta} + L = -\frac{2}{(1+\beta)(2+\beta)^{1/2}} \; . \tag{66}$$

This equation may be integrated, and the resulting integral may be calculated by elementary methods to yield

$$L(\beta) = \frac{1}{\beta^{1/2}} \sin^{-1}\left(\frac{1}{1+\beta}\right) \; . \tag{67}$$

Using this result along with the fact that $\sigma_4(1) = (24/\pi)L(2)$, we have the rightmost result of Eqn. (8.56) as shown in the main text.

A similar method may be used to simplify the integrals for higher N, but we have been unable to evaluate these integrals in closed form. Naturally, the integral in Eqn. (8.55) may be evaluated numerically for a given N to any desired precision.

Bibliography

[1] R. Brown, Philos. Mag. Ann. of Philos. New Ser. **4**, 161 (1823).

[2] A. Einstein, Ann. der Physik **17**, 549 (1905).

[3] B. D. Hughes, *Random Walks and Random Environments*, Vol. 1: *Random Walks* (Clarendon Press, Oxford, 1995).

[4] J-P. Bouchaud and A. Georges, Phys. Rep., **195**, 127 (1990).

[5] J. Bernasconi, H. Beyeler, S. Strässler and S. Alexander, Phys. Rev. Lett., **42**, 819 (1979).

[6] J. R. Manning, *Diffusion Kinetics for Atoms in Crystals*, (Van Nostrand, Princeton N.J., 1968).

[7] M. J. A. M. Brummelhuis and H. J. Hilhorst, J. Stat. Phys. **53**, 249 (1988). See also Z. Toroczkai, Int. J. Mod. Phys. **B11**, 3343 (1997).

[8] T. J. Newman, Phys. Rev. B , **59**, 13754 (1999).

[9] Z. Toroczkai, G. Korniss, B. Schmittmann and R. K. P. Zia, Europhys Lett. **40**, 281 (1997).

[10] J.D. Gunton, M. San Miguel and P.S. Sahni, in: *Phase Transitions and Critical Phenomena*, Vol. 8, eds. C. Domb and J.L. Lebowitz (Academic, New York, 1983); H. Furukawa, Adv. Phys. **34**, 703 (1985); K. Binder, Rep. Prog. Phys. **50**, 783 (1987), and in: *Phase Transition of Materials*, eds. R.W. Cahn, P. Haasen and E.J. Kramer (VCH, Weinheim, 1991); J. S. Langer, in *Solids far from Equilibrium*, ed. C. Godrèche (Cambridge University Press, 1992); A. J. Bray, Adv. Phys. **43**, 357 (1994).

[11] see, e.g., W.D. Callister Jr., *Material Science and Engineering: An Introduction* (Wiley, 1994).

[12] M. Blume, V.J. Emery and R.B. Griffiths, Phys. Rev. **A4**, 1071 (1971); R.B. Potts, Proc. Camb. Phil. Soc. **48**, 106 (1952); F.Y. Wu, Rev. Mod. Phys. **54**, 235 (1982).

[13] O.G. Mouritsen and P.J. Shah, Phys. Rev. **B40**, 11445 (1989); P.J. Shah and O.G. Mouritsen, Phys. Rev. **B41**, 7003 (1990); K. Yaldram and K. Binder, Z. Phys. **B82**, 405 (1991) and references therein; K. Yaldram, G.K. Khalil and A. Sadiq, Solid State Comm. **87**, 1045 (1993); C. Frontera, E. Vives, T. Castan and A. Planes, Phys. Rev. **B51**, 11369 (1995) and references therein; S. Puri, Phys. Rev. **E55**, 1752 (1997); P. Fratzl and O. Penrose, Phys. Rev. **B50**, 3477 (1994) and Phys. Rev. **B55**, R6101 (1997); S. Puri and R. Sharma, Phys. Rev. **E57**, 1873 (1998).

[14] S. Puri, Phys. Rev. **E55**, 1752 (1997); S. Puri and R. Sharma, Phys. Rev. **E57**, 1873 (1998).

[15] K.W. Kehr, K. Binder, and S.M. Reulein, Phys. Rev. **B39**, 4891 (1989).

[16] S. Alexander, Y. Rabin, and R. Zeitak, J. Chem. Phys. 95, 2012 (1991).

[17] O.G. Mouritsen and P.J. Shah, Phys. Rev. **B40**, 11445 (1989); P.J. Shah and O.G. Mouritsen, Phys. Rev. **B41**, 7003 (1990); E. Vives and A. Planes, Phys. Rev. Lett. **68**, 812 (1992) and Phys. Rev. **B47**, 2557 (1993); C. Frontera, E. Vives, and A. Planes, Phys. Rev. **B48**, 9321 (1993); C. Frontera, E. Vives, T. Castan and A. Planes, Phys. Rev. **B51**, 11369 (1995) and Phys. Rev. **B55**, 212 (1997); M. Porta, C. Frontera, E. Vives, and T. Castan, Phys. Rev. **B56**, 5261 (1997); C. Frontera and E. Vives, Phys. Rev. **B59**, 11121 (1999); M. Porta, E. Vives, and T. Castan, Phys. Rev. **B60**, 3920 (1999).

[18] M. Plapp and J.-F. Gouyet, Phys. Rev. Lett. **78**, 4970 (1997).

[19] H-F. Meng and E.D.G. Cohen, Phys. Rev. E**51**, 3417 (1995); J. Krug and P. Meakin, Phys. Rev. Lett. **66**, 703 (1991); R. Cuerno, H.A. Makse, S. Tomassone, S. Harrington and H.E. Stanley, Phys. Rev. Lett. **75**, 4464 (1995) and references therein; S. G. Corcoran, to appear in: *Proceedings of the Electrochemical Society*, Symposium on Critical Factors in Localized Corrosion III, 1998.

[20] I. Žižak, P. Fratzl, and O. Penrose, Phys. Rev. **B55**, 12121 (1997).

[21] D. Drouin, J. Beauvais, R. Lemire, E. Lavallée, R. Gauvin, and M. Caron, Appl. Phys. Lett. **70**, 3020 (1997).

[22] M. N. Baibich, J. M. Broto, A. Fert, F. Nguyen Van Dau, F. Petroff, P. Etienne, G. Creuzet, A. Friederich, and J. Chazelas, Phys. Rev. Lett. **61**, 2472 (1988); G. Binasch, P. Grünberg, F. Saurenbach, and W. Zinn, Phys. Rev. **B39**, 4828 (1989).

[23] S. Sanvito, C.J. Lambert, and J.H. Jefferson, cond-mat/9903381, (1999).

[24] R.K.P. Zia and Z. Toroczkai, J. Phys. **A31**, 9667 (1998).

[25] T. Aspelmeier, B. Schmittmann, and R.K.P. Zia, to be published.

[26] L. Onsager, Phys. Rev. **65**, 117 (1944).

[27] N. Metropolis, A.W. Rosenbluth, M.M. Rosenbluth, A.H. Teller and E. Teller, J. Chem. Phys. **21**, 1087 (1953).

[28] B.M. McCoy and T.T. Wu, *The Two-Dimensional Ising Model* (Harvard University Press, 1973).

[29] S.T. Chui and J.D. Weeks, Phys. Rev. Lett. **40**, 733 (1978); S.F. Edwards and D. R. Wilkinson, Proc. Roy. Soc. London, Ser. **A381**, 17 (1982).

[30] M. Kardar, G. Parisi, and Y.-C. Zhang, Phys. Rev. Lett. **56**, 889 (1986).

[31] B. Schmittmann, K. Hwang, and R.K.P. Zia, Europhys. Lett. **19**, 19 (1992).

[32] D.J. Amit, *Field Theory, the Renormalization Group, and Critical Phenomena* (World Scientific, 1984).

[33] D.S. Jones, *The Theory of Generalised Functions* (Cambridge University Press, 1982).

[34] H. van Beijeren and I. Nolden, in: *Structure and Dynamics of Surfaces II*, eds. W. Schommers and P. von Blanckenhagen; Vol. 43 of *Topics in Current Physics* (Springer Verlag, Berlin 1987).

[35] J.S. Rowlinson and B. Widom, *Molecular Theory of Capillarity* (Oxford University Press 1982).

[36] B. Schmittmann, unpublished.

[37] This equation is strictly correct only for systems with an odd number of sites. For a system with an even number of sites, the exact relation is $N^+ = N^- + 1 = \frac{N}{2}$, i.e., $N^+ = N^- + O(L^{-2})$. However, this correction will be neglected in the following: even for our smallest system (20×20), it is below 1%.

[38] F. Spitzer, Adv. Math. **5**, 246 (1970).

[39] Ref. [9] uses a slightly different normalization.

[40] S. Middelhoek, P. K. George and P. Dekker, *Physics of Computer Memory Devices* (Academic Press, London, 1976).

[41] A. K. Sharma, *Semiconductor Memories* (IEEE Press, Piscataway NJ, 1996).

[42] For more diverse examples see I. S. Herschberg and R. Paans, Informatie, **28**, 10 (1986); F. B. Cohen, in *Information Security - the Next Decade*, eds. J. H. P. Eloff and S. H. von Solms (Chapman and Hall, London, 1995).

[43] C. W. Gardiner, *Handbook of Stochastic Processes*, 2nd ed. (Springer-Verlag, Berlin, 1985).

[44] L. D. Landau and E. M. Lifschitz, *Quantum Mechanics* (Pergamon Press, London 1958).

[45] *Theory and Applications of Cellular Automata*, ed. S. Wolfram, (World Scientific, Singapore, 1987); F. Bagnoli in *Dynamical Modelling in Biotechnologies*, eds. F. Bagnoli, P. Lio and S. Ruffo, (World Scientific, Singapore, 1998)

[46] H. E. Stanley, *Introduction to Phase Transitions and Critical Phenomena*, (Oxford University Press, 1971).

[47] R. P. Feynman and A. Hibbs, Quantum Mechanics and Path Integrals (McGraw-Hill, New York, 1965); L. S. Schulman, *Techniques and Applications of Path Integration* (Wiley, New York, 1981).

[48] *Handbook of Mathematical Functions* 10th Edition, M. Abramowitz and I. A. Stegun Eds. (Dover, NY, 1972).

[49] H. Jeffreys and B. Jeffreys, *Methods of Mathematical Physics* 3rd Edition (Cambridge University Press, Cambridge, 1980).

[50] *Point Defects in Solids*, eds. J. H. Crawford and L. M. Slifkin (Plenum Press, New York, 1976); F. Agullo-Lopez, C. R. A. Catlow and P. D. Townsend, *Point Defects in Materials* (Academic Press, London, 1988).

[51] J. Magnin and B. Schmittmann, to be published.

[52] H. Larralde, P. Trunfio, S. Havlin, H. E. Stanley, and G. H. Weiss, Phys. Rev. A, **45**, 7128 (1992).

[53] B. Schmittmann, W. Triampo and R.K.P. Zia, Braz. J . Phys , **30**, 139 (2000).

[54] To the best of our knowledge, this is a new sum rule for Bessel functions.

[55] W. Triampo, T. Aspelmeier, and B. Schmittmann, Phys. Rev. E , **61**, 2386 (2000).

[56] T. J. Newman and Wannapong Triampo, Phys. Rev. E, **59**, 5172 (1999).

[57] Wannapong Triampo and T. J. Newman, Phys. Rev. E, **60**, 1450 (1999).

Vita

Birthdate/Place : November 22, 1970; Nakonratchasima, Thailand

Sex : Male

Nationality: Thai.

Education:

1989-93	B.Sc.(Physics) at Mahidol University, Bangkok, Thailand,
1993-95	M.Sc.(Applied Mathematics) at Mahidol University, Bangkok, Thailand,
1995-01	M.Sc.(Physics) at Virginia Polytechnic Institute & State University,
	Ph.D.(Physics) at Virginia Polytechnic Institute & State University USA

Experience :

1990-94	Physics and Math tutor at RAC company and Mahidol University, Bangkok, Thailand,
1994-95	Instructor at Mahidol University, Bangkok, Thailand,
1997-01	Teaching Assistant at Virginia Polytechnic Institute & State University.

Research Interests:

- Non-equilibrium statistical mechanics
- Random walks
- Driven-diffusive systems
- Monte-Carlo simulation techniques
- Biological and Medical Physics

Publications:

- ◇ *The propagator corresponding to a model with quadratic action*,
  J. Poulter and Wannapong Triampo , J. Sci. Soc. Thailand, **24** (1995) 253,

- ◇ *Binary data corruption due to a Brownian agent*,
  T.J. Newman and Wannapong Triampo, Phys. Rev. **E59** (1999) 5172,

- ◇ *Binary data corruption due to a Brownian agent. II. Two dimensions, competing agents*,
  Wannapong Triampo and T.J. Newman, Phys. Rev. **E60** (1999) 1450,

- ◇ *Universal aspects of vacancy-mediated disordering dynamics: The effect of external fields*,
  Wannapong Triampo, T. Aspelmeier and B. Schmittmann, Phys. Rev. **E61** (2000) 2386,

- ◇ *Dynamic scaling in vacancy-mediated disordering*,
  B. Schmittmann, R.K.P. Zia and Wannapong Triampo. Braz. J. Phys. **30** (2000) 139